Year : 2012

Tumor-host interactions
Part 1 : Stromal signatures of breast and prostate cancer
Part 2 : GLG1 and the control of the secretory pathway in tumor cells

Anne PLANCHE

UNIL | Université de Lausanne

Faculté de biologie et de médecine

Tumor-host interactions
Part 1: Stromal signatures of breast and prostate cancer
Part 2: GLG1 and the control of the secretory pathway in tumor cells

Thèse de doctorat ès sciences de la vie (PhD)

Conduite au sein de l'Institut Universitaire de Pathologie
Centre Hospitalier Universitaire Vaudois (CHUV)

Présentée à la Faculté de Biologie et de Médecine de l'Université de Lausanne

par

Anne PLANCHE

Master en Sciences et Technologies du Vivant
Ecole Polytechnique Fédérale de Lausanne (EPFL)

Jury

Prof. Michel MONOD , Président
Prof. Ivan STAMENKOVIC, Directeur de thèse
Prof. Tatiana PETROVA, Représentante du comité du *International PhD Program*
Prof. Michel AGUET, Expert
Prof. Pedro ROMERO, Expert
Prof. Gisou VAN DER GOOT, Experte

Lausanne, 2012

UNIL | Université de Lausanne
Faculté de biologie
et de médecine

Ecole Doctorale

Doctorat ès sciences de la vie

Imprimatur

Vu le rapport présenté par le jury d'examen, composé de

Président	Monsieur	Prof. Michel **Monod**
Directeur de thèse	Monsieur	Prof. Ivan **Stamenkovic**
Experts	Madame	Prof. Tatiana **Petrova**
	Madame	Prof. Gisou **Van der Goot**
	Monsieur	Prof. Michel **Aguet**
	Monsieur	Prof. Pedro **Romero**

le Conseil de Faculté autorise l'impression de la thèse de

Madame Anne Planche

Master of Science de l'Ecole Polytechnique de Lausanne

intitulée

Tumor-host interactions
Part 1: Stromal signatures of breast and prostate cancer
Part 2 : GLG1 and the control of the secretory pathway in tumor cells

Lausanne, le 21 décembre 2012

pour Le Doyen
de la Faculté de Biologie et de Médecine

Prof. Michel Monod

TABLE OF CONTENTS

ACKNOWLEDGEMENTS

Je tiens tout d'abord à remercier le Professeur Stamenkovic de m'avoir ouvert les portes de son laboratoire afin d'y effectuer mon projet de master et de m'avoir ensuite offert la possibilité d'y réaliser ma thèse de doctorat.

J'aimerais remercier les membres passés et présents du laboratoire. Merci à Mario Suvà, Nicola Riggi, Claudio De Vito, Michalina Janiszewska, Ruzanna Leemann-Zakaryan pour leur disponibilité et leur contribution à une agréable atmosphère au sein du laboratoire. J'adresse des remerciements tout particuliers à Marie-Aude Le Bitoux, Cynthia Dayer et Aurélie Formey pour leur soutien et leur amitié qui m'ont précieusement accompagnés au quotidien.

J'adresse aussi mes remerciements à Paolo Provero pour son aide avec les analyses bioinformatiques et statistiques, à Janine Horlbeck et Jean-Christophe Stehle pour les nombreuses lames d'immunohistochimie, à Marlène Maire pour sa patience et son travail irréprochable, à Phil Shaw pour ses nombreux conseils et discussions aux accents chantants, ainsi qu'à toutes les personnes, plus ou moins de l'ombre, qui participent au bon fonctionnement de l'institut, je pense notamment à Pierre Audisio, à Alvaro Baptista et aux femmes et aux hommes d'entretien.

Merci à mes amis, à ma famille et principalement à mes parents sans qui je n'en serais pas là aujourd'hui, et qui continuent à me soutenir inconditionnellement et à me servir d'exemple jour après jour.

Finalement, *last but not least*, je suis infiniment reconnaissante envers Sigismond pour son amour et son soutien indéfectible et absolu. Je le remercie de vouloir encore passer sa vie avec moi, même après ma thèse ☺.

CURRICULUM VITAE

Anne PLANCHE

Chemin du Noirmont 5
1004 Lausanne

Switzerland

+41(0)79 7471310

anneplanche@gmail.com

12th of December 1983
Swiss

Education

November 2008 - December 2012	**PhD in Life Sciences**, International PhD Program in Cancer and Immunology University of Lausanne, Switzerland
October 2006 - July 2008	**Master of Science (MSc) in Life Sciences and Technology**, specialization in Molecular Medicine and Oncology Swiss Federal Institute of Technology Lausanne (EPFL), Switzerland Master Project: *Gene expression profiling of the stromal reaction to invasive human breast and prostate cancer*, accepted with summa cum laude and awarded with prize from the Société Académique du Valais
October 2003 - July 2006	**Bachelor of Science (BSc) in Life Sciences and Technology**, orientation in Life Sciences and Technology Swiss Federal Institute of Technology Lausanne (EPFL), Switzerland Bachelor Project in Neurosciences: *How RGS2 modulates the G-protein signalling*
August 1998 - June 2003	**Federal "Maturité" (Baccalaureate equivalent)** College of Saint-Maurice Abbey, Switzerland Prize of the best "Maturité" in the literary section "Maturité" Project: *Naissance, principes et implications de la physique quantique*, accepted with summa cum laude and awarded with prize of the best "Maturité" Project

Professional Experience

November 2008 - December 2012	**Centre Hospitalier Universitaire Vaudois (CHUV), University of Lausanne** **Experimental Pathology Division of Institute of Pathology, Stamenkovic laboratory** PhD in Life Sciences
September 2007 - July 2008	**CHUV, University of Lausanne** **Experimental Pathology Division of Institute of Pathology, Stamenkovic laboratory** Master Project
September 2007 - December 2007	**EPFL** **Laboratoire d'Optique Biomédicale, Lasser laboratory** Assistant for biomicroscopy exercise sessions
March 2006 - June 2006	**EPFL** **Laboratory of Functional Neurogenomics, Luthi-Carter laboratory** Bachelor Project

Technical expertise

Laboratory	Cell culture, standard biochemistry and molecular biology techniques including protein analysis, bacterial cultures, cloning, plasmid construction, qRT-PCR, co-immunoprecipitation, mass spectrometry analysis, sh and siRNA techniques, microarray technology Laser capture microdissection Flow cytometry Animal experimentation including subcutaneous, intravenous and orthotopic injection of tumor cells Imaging and microscopy including confocal and time-lapse microscopy
Informatics	R, ImageJ, Photoshop, C, C^{++} and utilization of usual tools in office software

Publications

Research papers	Bacac M, Fusco C, **Planche A**, Santodomingo J, Demaurex N, Leemann-Zakaryan R, Provero P, Stamenkovic I. Securin and separase modulate membrane traffic by affecting endosomal acidification. Traffic 2011;12(5):615-626.
	Planche A, Bacac M, Provero P, Fusco C, Delorenzi M, Stehle JC, Stamenkovic I. Identification of prognostic molecular features in the reactive stroma of human breast and prostate cancer. PLoS One 2011;6(5):e18640.
	Planche A, Stamenkovic I., The Golgi protein GLG1 coordinates ARF3 activation by recruiting the guanine nucleotide-exchange factor BIG1 to the Golgi membrane. Manuscript in preparation.
Posters	**Planche A**, Bacac M, Stamenkovic I. The Golgi protein GLG1 participates in tumor progression. Presented at:
	• EPFL Life Science Symposium, Lausanne (Switzerland), 2011
	• AACR (American Association for Cancer Research) Annual Meeting, Chicago (IL, USA), 2012
	• FBM (Faculty of Biology and Medicine), Lausanne (Switzerland), 2012

Languages

French	Mother tongue
English	Fluent
German	High school level

Hobbies

Sports	Basketball (16 years, including 4 years in Swiss National League, first division), skiing, hiking
Others	Reading, music, photography

SUMMARY

Tumor-host interaction is a key determinant during cancer progression, from primary tumor growth to metastatic dissemination. At each step, tumor cells have to adapt to and subvert different types of microenvironment, leading to major phenotypic and genotypic alterations that affect both tumor and surrounding stromal compartments. Understanding the molecular mechanisms that govern tumor-host interplay may be essential for better comprehension of tumorigenesis in an effort to improve current anti-cancer therapies. The present work is composed of two projects that address tumor-host interactions from two different perspectives, the first focusing on the characterization of tumor-associated stroma and the second on membrane trafficking in tumor cells.

Part 1. To selectively address stromal gene expression changes during cancer progression, oligonucleotide-based Affymetrix microarray technology was used to analyze the transcriptomes of laser-microdissected stromal cells derived from invasive human breast and prostate carcinoma. Comparison showed that invasive breast and prostate cancer elicit distinct, tumor-specific stromal responses, with a limited panel of shared induced and/or repressed genes. Both breast and prostate tumor-specific deregulated stromal gene sets displayed statistically significant survival-predictive ability for their respective tumor type. By contrast, a stromal gene signature common to both tumor types did not display prognostic value, although expression of two individual genes within this common signature was found to be associated with patient survival.

Part 2. GLG1 is known as an E-selectin ligand and an intracellular FGF receptor, depending on cell type and context. Immunohistochemical and immunofluorescence analyses showed that GLG1 is primarily localized in the Golgi of human tumor cells, a central location in the biosynthetic/secretory pathways. GLG1 has been shown to interact with and to recruit the ARF GEF BIG1 to the Golgi membrane. Depletion of GLG1 or BIG1 markedly reduced ARF3 membrane localization and activation, and altered the Golgi structure. Interestingly, these perturbations did not impair constitutive secretion in general, but rather seemed to impair secretion of a specific subset of proteins that includes MMP-9. Thus, GLG1 coordinates ARF3 activation by recruiting BIG1 to the Golgi membrane, thereby affecting secretion of specific molecules.

RÉSUMÉ

Les interactions tumeur-hôte constituent un élément essentiel à la progression tumorale, de la croissance de la tumeur primaire à la dissémination des métastases. A chaque étape, les cellules tumorales doivent s'adapter à différents types de microenvironnement et les détourner à leur propre avantage, donnant lieu à des altérations phénotypiques et génotypiques majeures qui affectent aussi bien la tumeur elle-même que le compartiment stromal environnant. L'étude des mécanismes moléculaires qui régissent les interactions tumeur-hôte constitue une étape essentielle pour une meilleure compréhension du processus de tumorigenèse dans le but d'améliorer les thérapies anti cancer existantes. Le travail présenté ici est composé de deux projets qui abordent la problématique des interactions tumeur-hôte selon différentes perspectives, le premier se concentrant sur la caractérisation du stroma tumoral et le second sur le trafic intracellulaire des cellules tumorales.

Partie 1. Pour examiner les changements d'expression des gènes dans le stroma en réponse à la progression du cancer, des puces à ADN Affymetrix ont été utilisées afin d'analyser les transcriptomes des cellules stromales issues de carcinomes invasifs du sein et de la prostate et collectées par microdissection au laser. L'analyse comparative a montré que les cancers invasifs du sein et de la prostate provoquent des réponses stromales spécifiques à chaque type de tumeur, et présentent peu de gènes induits ou réprimés de façon similaire. L'ensemble des gènes dérégulés dans le stroma associé au cancer du sein, ou à celui de la prostate, présente une valeur pronostique pour les patients atteints d'un cancer du sein, respectivement de la prostate. En revanche, la signature stromale commune aux deux types de cancer n'a aucune valeur prédictive, malgré le fait que l'expression de deux gènes présents dans cette liste soit liée à la survie des patients.

Partie 2. GLG1 est connu comme un ligand des sélectines E ainsi que comme récepteur intracellulaire pour des facteurs de croissances FGFs selon le type de cellule dans lequel il est exprimé. Des analyses immunohistochimiques et d'immunofluorescence ont montré que dans les cellules tumorales, GLG1 est principalement localisé au niveau de l'appareil de Golgi, une place centrale dans la voie biosynthétique et sécrétoire. Nous avons montré que GLG1 interagit avec la protéine BIG1 et participe à son recrutement à la membrane du Golgi. L'absence de GLG1 ou de BIG1 réduit drastiquement le pool d'ARF3 associé aux membranes

ainsi que la quantité d'ARF3 activés, et modifie la structure de l'appareil de Golgi. Il est particulièrement intéressant de constater que ces perturbations n'ont pas d'effet sur la sécrétion constitutive en général, mais semblent plutôt affecter la sécrétion spécifique d'un sous-groupe défini de protéines comprenant MMP-9. GLG1 coordonne donc l'activation de ARF3 en recrutant BIG1 à la membrane du Golgi, agissant par ce moyen sur la sécrétion de molécules spécifiques.

GENERAL INTRODUCTION

Cancer is a leading cause of death worldwide, accounting for 13% of all the deaths in 2008[1]. There are approximately 110 distinct types of human cancer [1] that can affect every part of the body. Clearly, understanding the biology of cancer in a way that is conducive to novel and effective therapies is crucial.

Carcinogenesis is a multistep process initiated and driven by the accumulation of genetic mutations that alter the physiology of normal cells and promote tumor formation and growth. Key alterations consist primarily of the acquisition of self-sufficiency in growth signals, insensitivity to antigrowth signals, resistance to apoptosis, the capacity to induce angiogenesis and limitless replicative potential. Additional properties such as anchorage-free survival capacity, a more motile and migratory phenotype, and the ability to degrade basement membrane allow the formation of distant colonies, known as metastases. Acquisition of these hallmark capabilities is facilitated by at least two characteristics of neoplasia that include the genomic instability, and thus mutability, and tumor-promoting inflammation. Increasing evidence suggests that additional attributes of cancer cells might be functionally important for the pathogenesis of many tumor types and might be added to the list of core hallmarks. Two such emerging hallmarks are noteworthy: the ability to modify/reprogram cellular energy metabolism and to evade immune destruction [2, 3].

Successful metastatic spread depends on the cumulative ability of cancer cells to adapt to different microenvironments at each step of the metastatic process: the primary site, the systemic circulation and the final metastatic niche (Figure 1). Indeed, after having overcome the constraints imposed by the microenvironment at the primary tumor site, some cancer cells can intravasate into blood or lymphatic vessels where they have to adapt to an entirely different microenvironment. Before becoming a clinical relevant metastatic colony, these circulating tumor cells have to survive within the circulation and grow in a potentially inhospitable tissue. The combination of these rate-limiting steps determines the ability of cancer cells to establish secondary tumors within the metastatic site.

[1] http://www.who.int

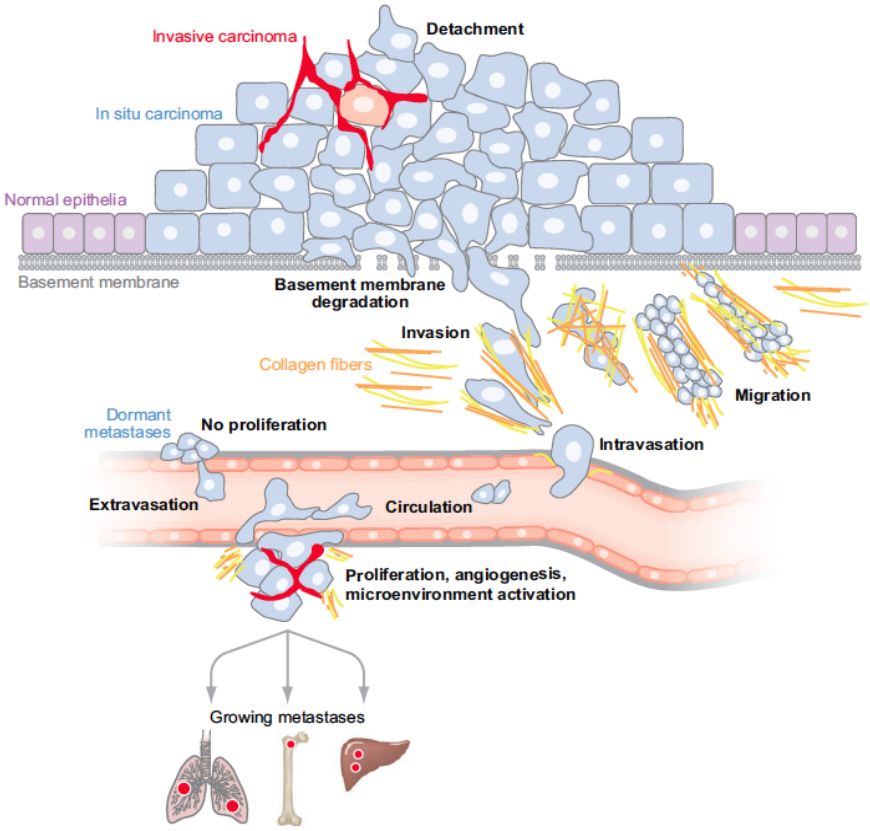

Figure 1. Principal steps of metastatic progression. Transformation of normal epithelial cells leads to carcinoma *in situ*, which may then acquire an invasive profile. Following basement membrane degradation, tumor cells invade the surrounding stroma, migrate and intravasate into blood or lymph vessels. Thereafter, surviving cells have to extravasate and colonize distant organs to form metastasis [3].

A major obstacle toward the management of cancer resides in its complex nature and its ability to draw on physiological functions of tissues at each step of disease progression. In fact, the network of interactions between cancer cells and the surrounding tissues is similar to that required for normal functions of an organ. The complex nature of interactions between tumor cells and their host tissue environment plays a central role in determining the evolution of the disease toward invasion and metastasis, which are the principal causes of death from cancer [3].

The microenvironment, that surrounds both normal and tumor tissues, is composed of cells of mesenchymal origin (fibroblasts, endothelial cells, immune cells) and of extracellular matrix (ECM), which is mainly composed of collagens, fibronectin, laminin and various proteoglycans [4]. In parallel to the evolution of tumor cells, the cells that compose the microenvironment undergo genotypic and phenotypic alterations in response to tumor progression resulting in the formation of activated or tumor-associated stroma [4, 5]. The activated stroma is characterized by robust ECM protein deposition, increased numbers of

inflammatory cells, enhanced capillary density, and release of active proteases. The stromal reaction also includes increased proliferation of fibroblasts that differentiate toward myofibroblasts, also called carcinoma-associated fibroblasts (CAFs) [4, 6, 7]. Similar to tumor cells, tumor stromal cells, and principally CAFs, can display genomic instability and alterations [8-10], epigenetic changes [11], morphological modifications [4] as well as alterations in their gene expression profile [12-15] throughout tumor progression. Thus, during disease progression, the host stroma, which normally contributes to the preservation of stable tissue structure, evolves toward a tumor growth-promoting microenvironment.

In addition to synchronous evolution, numerous signals are exchanged between the epithelial and the stromal compartments that can promote, or inhibit, tumor progression. As mentioned above, normal cells undergo major phenotypic changes during transformation that affect cell surface receptor expression, cytoskeletal function, growth factor and cytokine secretion, proteolytic enzyme production and secretion, and glycosyltransferase as well as glycosidase repertoires [3]. These changes have an important impact on the way in which the transformed cell communicates with its microenvironment. In particular, the biosynthetic/secretory pathways are of special relevance to tumor-host interactions. Indeed, propensity of tumor cells to disrupt their signaling and their adhesion receptors through derailed endocytosis has recently emerged as a key event to which some of the hallmarks of cancer could be attributed, especially the ability to invade tissues. In addition to material uptake, endocytosis regulates signal transduction and morphogenetic aspects of the cell that include adhesion and migration. Under normal conditions, there is a tightly controlled balance between endocytic and exocytic cycles and between the lysosomal pathway and the recycling route to allow appropriate cell motility and survival. But intracellular trafficking displays multiple abnormalities in human tumors that contribute to their progression. For instance, dissolution of cell-cell junctions, loss of morphological polarity, enhanced recycling of adhesion molecules such as integrins and delayed receptor downregulation, among others, strongly contribute to malignant transformation by conferring self-sufficiency and highly dynamic features to tumor cells [16].

The secretory aspect of the membrane trafficking pathway, particularly the secretion of microvesicles and exosomes, has attracted increasing interest in cancer research. Tumor-derived microvesicles are small membrane particles that are shed from the surface of tumor

cells into the extracellular environment. They carry a broad variety of molecules that include proteases, adhesion receptors, proangiogenic regulators and miRNAs able to significantly modulate the tumor microenvironment [17-19]. Exosomes, which originate from multivesicular bodies, are smaller than tumor-derived microvesicles and contain a distinct set of proteins including specific tetraspanins and heat shock proteins. They can influence a variety of cellular processes, particularly inflammatory responses [20, 21]. By their effect on the surrounding environment through mediation of intercellular communication, microvesicles may influence many steps of cancer progression. In addition, as mentioned before, tumor and stromal cells secrete soluble molecules including growth factors, proteases and cytokines that are important for tumor progression. Analysis of material released by tumor and stromal cells is thus of major interest and several studies have focused on the secretome of tumor cells in order to identify candidate biomarkers and to provide new insights into the molecular mechanisms of tumorigenesis [22-24]. Furthermore, analysis of molecular events implicated in the process of secretion itself should be performed in tumor and tumor-associated stromal cells to try identifying candidate alterations that may indirectly influence tumor progression.

As a consequence of phenotypic and genotypic alterations of both tumor and stromal cells, the homeostatic equilibrium found in normal tissues is disrupted and is substituted by a new balance driven by pathological intercellular communication between tumor cells and the stromal compartment that not only enhances primary tumor growth, but also facilitates metastatic dissemination to distant organs, which defines malignant tumors (Figure 2). Understanding tumor-stroma crosstalk at the molecular level and from different angles will constitute a key step toward better global comprehension of the process of tumor invasion in an effort to design rational, mechanism-based anticancer therapies.

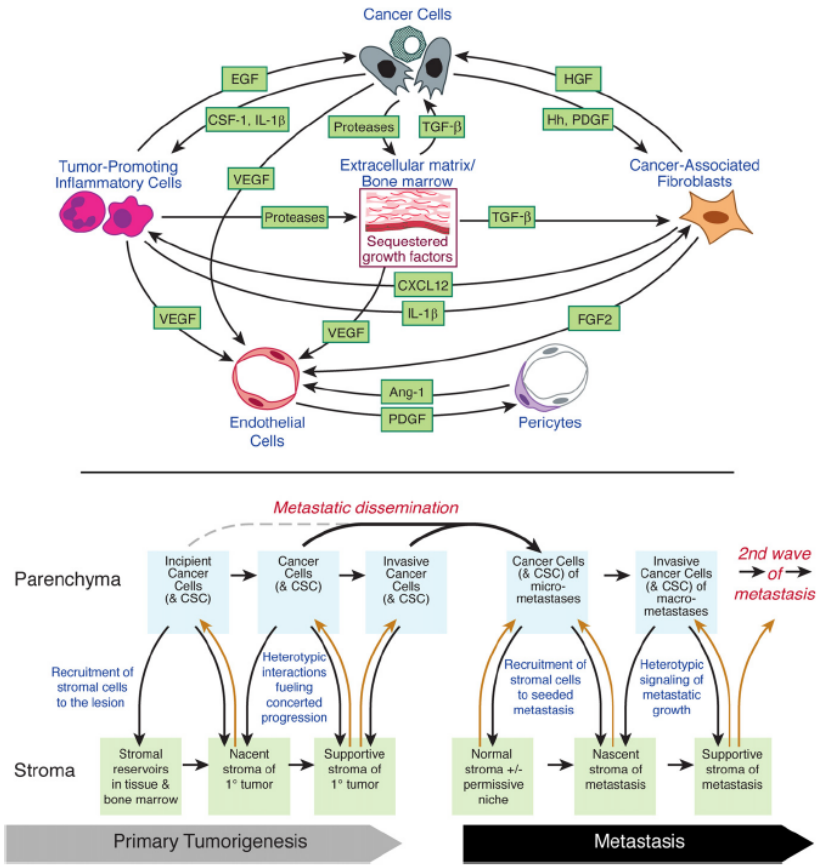

Figure 2. Crosstalk between cancer cells and tumor microenvironment during malignant progression. Adapted from [2].

This thesis addresses tumor-host interactions from two different perspectives, using two different approaches. The first project aims at characterizing tumor-associated stroma by gene expression profiling, which constitutes a broad, "horizontal" approach. The work was published in the open access journal PLOS ONE on May 18th 2011 under the title "Identification of prognostic molecular features in the reactive stroma of human breast and prostate cancer". The second project is a "vertical", in depth analysis of one particular molecule, GLG1, implicated in intracellular trafficking and thus secretion of key molecules, resulting in a manuscript entitled "The Golgi protein GLG1 coordinates ARF3 activation by recruiting the guanine nucleotide-exchange factor BIG1 to the Golgi membrane".

PART 1: STROMAL SIGNATURES OF BREAST AND PROSTATE CANCER

Introduction

In normal epithelial tissues, the epithelium is separated from the stromal compartment by the basement membrane that helps maintain tissue integrity. During tumor invasion, the basement membrane is degraded and tumor and stromal cells enter into physical contact for the first time, allowing both cell types to influence each other in an abnormal way. The homeostatic equilibrium found in normal tissue is substituted by pathological communication between tumor and stromal compartments. The overall process of tumorigenesis shares molecular mechanisms with the physiological processes of wound healing and early embryogenesis [2]. However, contrary to the latter, the pathological process of tumor invasion persists, leading to the notion that invasive cancers behave as "wounds that never heal" [25].

Tumor-host interactions are determining for local tumor growth and tumor cell dissemination. Cytokines, chemokines and proteolytic enzymes secreted by tumor cells induce the activation, proliferation and recruitment of diverse stromal cells culminating in the formation of an activated stroma (Figure 3). As mentioned before, stromal activation in the tumor context is primarily associated with changes in ECM composition and increased proliferation of CAFs, which undergo epigenetic changes and genetic mutations during tumor progression that distinguish them from normal fibroblasts. The activated microenvironment secretes a plethora of angiogenic, inflammatory and growth factors that act in paracrine (on tumor cells) or autocrine (on stromal cells themselves) fashion. Whereas tumor-derived factors mainly stimulate the proliferation and differentiation of fibroblasts, as well as basement membrane degradation, activated stroma-derived factors provide pro-survival, pro-invasive and anti-anoikis signals to cancer cells and reinforce stroma remodeling that further sustains tumor growth and invasion [4, 6, 26, 27].

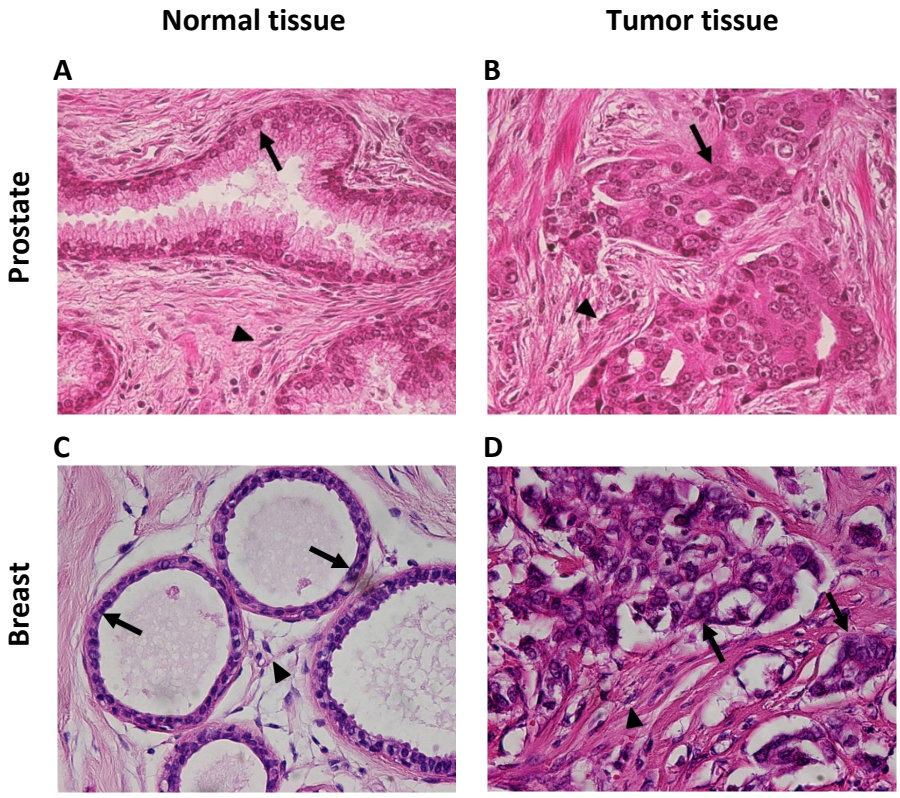

Figure 3. Tissue morphology of normal and tumor samples from breast and prostate patients. In normal tissues (A, C), arrows point to normal epithelial glands surrounded by the supportive stroma (arrowheads). Tumor tissues (B, D) present disorganized clusters of tumor cells (arrows) invading the activated stroma (arrowheads) characterized by dense cellularity, disorganized appearance and increased deposition of ECM components, as indicated by more intense Eosin staining (pink). Staining: H&E, magnification: 400x.

Several studies have demonstrated the active role played by the stroma, and more specifically by CAFs, in the initiation and progression of cancer. CAFs stimulate tumor formation when co-injected with transformed epithelial cells, whereas normal fibroblasts do not, suggesting that abnormal signaling from CAFs participates in tumor formation and progression [28-30]. Moreover, normalization of cancer-associated stroma was shown to slow down or reverse tumor progression, reinforcing the notion that activated stroma is essential for the tumor development [6] and should be targeted in addition to tumor cells by anticancer therapeutic design.

The first data concerning tumor-host interaction were obtained from tumor cell-fibroblast co-culture system and tumor xenograft models in immunocompromised mice [7, 31]. Although useful, these systems may not completely reflect what happens in human tissues *in vivo*, the tumor-stroma interplay remaining more complex than any *in vitro* model and the mouse microenvironment not necessarily mimicking the response of its human counterpart. Other approaches to study the microenvironment of tumors in a more real setting include, among others, gene expression profile analysis of microdissected reactive stroma and gene

expression analysis in defined FACS-sorted cancer stromal cell subsets. To address the stromal response to tumor growth in a natural situation, our laboratory examined the molecular events in the stromal cell compartment during cancer progression in a transgenic mouse model of multistage prostate carcinogenesis using laser capture microdissection (LCM) [15]. This work allowed the identification of genes found to be induced specifically in invasive tumor stroma compared to stroma associated with prostate intraepithelial neoplasia (PIN). Functional gene ontology (GO) annotation analysis of the stromal signature revealed several over represented functional families, including ones annotated to the terms *endopeptidase activity* and *extracellular region*, consistent with tissue remodeling. Remarkably, a subset of genes observed to be up-regulated in the tumor stroma was found to have prognostic value in human prostate and breast cancer.

This study, similar to most such studies in the field, analyzed the stromal reaction of one particular tumor type. Although it allowed the identification of a mouse stromal gene set with prognostic significance for two different human tumors, it could not provide information about the degree of similarity among stromal reactions to different tumor types. Indeed, it remained unclear whether the tumor stroma displays distinct features according to tumor type or whether there is a general stromal signature common to invasive cancers of different origins.

The aim of the present project was to carry out stromal gene expression profiling of human breast and prostate cancer, two types of carcinoma known to be associated with a prominent stromal reaction, in order to determine their degree of similarity and to assess their survival-predictive value for patients.

Results summary

In order to characterize the stromal reaction to human breast and prostate carcinoma, LCM was performed on fresh frozen primary tumor specimens for selective isolation of stromal cells *in vivo*. To limit variability among samples, breast and prostate patients selected for the study did not undergo chemotherapy and/or radiotherapy and presented comparable inflammatory reaction, as assessed by histological analysis. In addition, both tumor and normal tissue were available for each patient. Total RNA was extracted from microdissected stromal cells and subjected to amplification prior to hybridization on Affymetrix microarrays.

Global gene expression profile of normal and tumor stroma from breast and prostate specimens was first analyzed using Principal Component (PCA), revealing that breast and prostate cancer display a tumor-specific stromal response (Figure 4 A). This analysis showed also a clear distinction between tumor and normal samples of each tissue type. In addition, gene sets containing differentially expressed genes between tumor stroma and corresponding normal stroma were defined. Pearson correlation analysis showed higher correlation of the genes of the breast stromal gene set with breast data than with prostate data and vice versa, underscoring the specificity of stromal reaction to each tumor types (Figure 4 B).

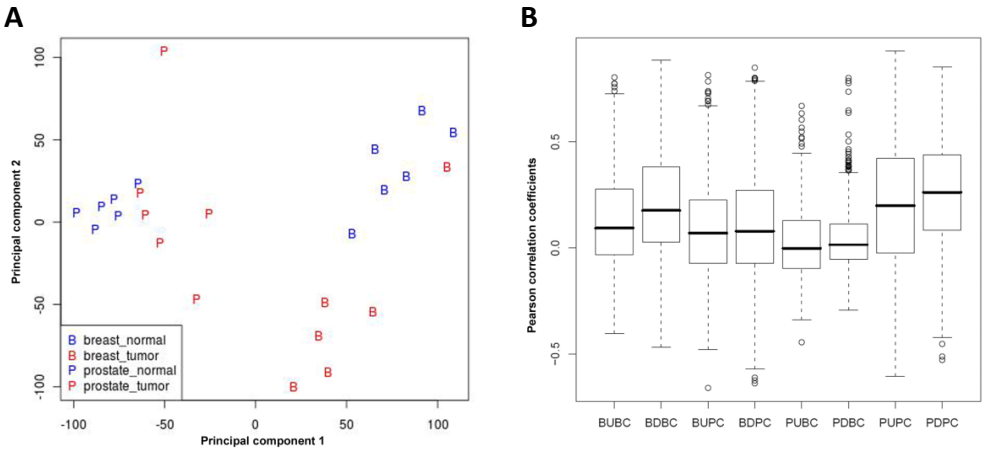

Figure 4. Tumor-specific stromal responses displayed by breast and prostate cancer. (A) PCA shows that breast and prostate tumors have a distinct stromal reaction to tumor invasion and suggests that overall stromal response in breast cancer is stronger than in prostate cancer. (B) Pairwise correlation analysis showing a higher correlation of breast stromal genes with breast data than with prostate data and vice versa.

A high proportion of genes of the breast stromal gene set encodes ECM components, proteolytic enzymes and adhesion receptors, including *COL11A1*, *MMP9*, *COMP* and *FN1*,

consistent with the pronounced stroma remodeling observed by histology. By contrast, the prostate stromal reaction displayed fewer genes involved in tissue remodeling but was associated with deregulated expression of homeobox genes including NKX3-1, HOXC6 and HOXD11, implicated in developmental differentiation processes.

Although PCA showed a clear distinction between breast and prostate stromal responses, suggesting limited overlap between the two signatures, a short list of genes common to stromal reaction of both tumor types could be identified. This common stromal signature, as well as the specific breast and prostate stromal signatures, were assessed for their survival-predictive ability using publicly available datasets of human cancer patients. Both breast and prostate tumor-specific stromal genes were observed to cluster breast and prostate cancer patients, respectively, into two distinct groups. Kaplan-Meier survival analysis and log-rank test revealed that the two groups defined by stromal gene expression profile in both tumor types differ significantly in their overall survival (Figure 5 A and B). By contrast, the list of genes common to breast and prostate stromal reaction did not display statistically significant prognostic value.

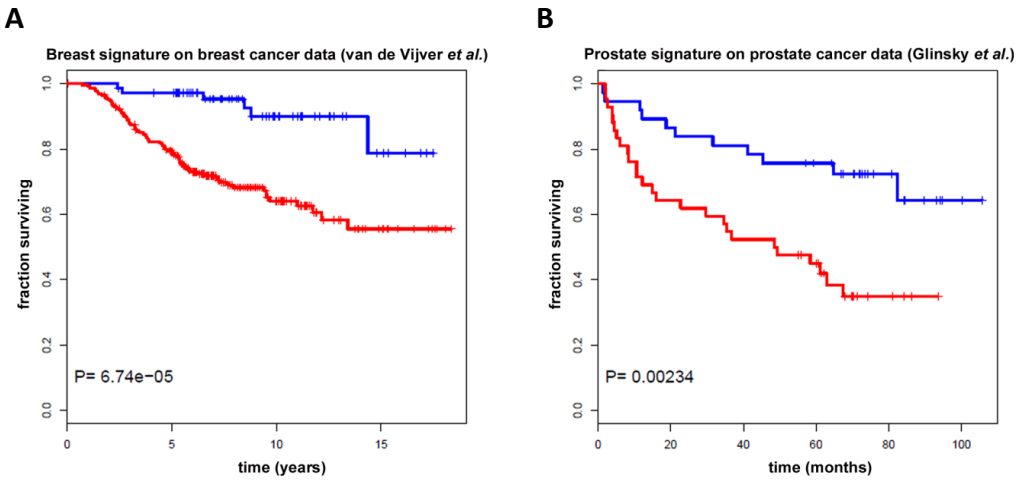

Figure 5. Kaplan-Meier survival analysis. (A) Kaplan-Meier survival analysis of early-breast carcinoma patients (van de Vijver *et al.*) and (B) prostate carcinoma patients (Glinsky *et al.*) performed using breast and prostate stromal genes respectively (FDR 15%) shows that the two groups of patients obtained after hierarchical clustering differ significantly in their overall survival. Red, poor prognosis group; blue, good prognosis group.

Whereas Kaplan-Meier survival analysis denoted a prognostic value for the overall lists of breast and prostate cancer stromal genes, univariate Cox analysis was performed to identify genes whose expression correlates most strongly with patient survival. This analysis identified a list of genes associated with poor and good prognosis for breast and prostate cancer (Table 1). Interestingly, although the common gene signature did not exhibit any

survival-predictive value, two individual genes present in the common signature, *POSTN* and *RUNX1* were associated with survival of patients with both tumor types. POSTN expression was validated by immunohistochemistry in a panel of human tumors known to be associated with a marked stromal reaction and was shown to be stroma-specific.

Table 1. Cox analysis. Selection of breast and prostate stromal genes strongly associated with breast cancer patient survival (van de Vijver *et al.*) and prostate cancer patient survival (Glinsky *et al.*), respectively. Positive Z values indicate that the expression level of the gene is associated with poor prognosis, whereas negative Z values indicate correlation with good prognosis.

Gene symbol	Gene description	Z value
Breast stromal genes		
YARS	Tyrosyl-tRNA synthetase	4.4
ADAM19	ADAM metallopeptidase domain 19 (meltrin beta)	3.6
BMP2	Bone morphogenetic protein 2	3.5
SPP1	Secreted phosphoprotein 1	3.3
TNXB	Tenascin XB	2.5
EGFR	Epidermal growth factor receptor (erythroblastic leukemia viral (v-erb-b) oncogene homolog, avian)	2.4
NOVA1	Neuro-oncological ventral antigen 1	-3.2
XIST	X (inactive)-specific transcript (non-protein coding)	-2.4
INHBA	Inhibin, beta A	-2.4
POSTN	Periostin, osteoblast specific factor	-2.2
TGFBR3	Transforming growth factor, beta receptor III	-2.2
RUNX1	Runt-related transcription factor 1	-2.0
Prostate stromal genes		
HOXC6	Homeobox C6	3.9
SERP1	Stress-associated endoplasmic reticulum protein 1	3.3
CDH11	Cadherin 11, type 2, OB-cadherin (osteoblast)	2.5
BMPR1B	Bone morphogenetic protein receptor, typeIB	2.4
POSTN	Periostin, osteoblast specific factor	2.2
GREM1	Gremlin 1, cysteine knot superfamily, homolog (Xenopus laevis)	2.1
HOXD13	Homeobox D13	-3.8
GRIA1	Glutamate receptor, ionotropic, AMPA 1	-3.5
RUNX1	Runt-related transcription factor 1	-3.4
PTGDS	Prostaglandin D2 synthase 21kDa (brain)	-3.0
GARNL3	GTPase activating Rap/RanGAP domain-like 3	-2.2
ESR1	Estrogen receptor 1	-2.0

Thus, it appears that the tumor-specificity of the stromal reaction, rather than the common features, is a key element in survival.

The main findings of this work can be summarized as follows:

- Expression profile of stromal genes is sufficient to discriminate tumor from normal samples
- Breast and prostate cancer elicit distinct stromal responses
- Tumor-specific stromal signatures carry survival-predictive value

Discussion and perspectives

Stroma activation associated with tumor is now widely accepted to be a determining factor for primary tumor growth, cancer cell migration and establishment of distant metastases, and must therefore be taken into account when developing new therapeutical strategies. In an effort to effectively target the tumor-associated microenvironment, better comprehension of the molecular features of stroma activation and remodeling is required.

There is an abundance of significant results regarding the molecular characterization of the tumor microenvironment, most of them derived from studies that focused on the stromal reaction of a particular tumor type. Such analyses proved to be instructive by identifying stromal gene expression signatures that showed prognostic value to the tumors they are associated with [12-15, 32] but they do not give an indication as to whether different tumor types elicit distinct or common stromal reactions that vary only in amplitude among tumors. Our study was designed in a way that allows the comparison of the stromal gene expression signature of human breast and prostate carcinoma in order to determine their degree of similarity and identify common candidate deregulated genes.

The global gene expression profile of microdissected stroma was sufficient to distinguish breast from prostate patients and also normal from tumor samples, underscoring the notion that tumor-associated stroma is distinct from corresponding normal stroma. Both breast and prostate tumor-specific deregulated stromal gene sets displayed statistically significant survival-predictive ability for their respective tumor type. Although the two stromal reactions present distinct transcriptomes, a common stromal gene signature was identified but did not have survival predictive value. In addition, comparison of upregulated breast and prostate stromal genes with published stroma datasets from studies on various human and murine cancers uncovered significant similarities. Closer examination of the signatures revealed that similitude resided primarily among genes implicated in tissue remodeling.

Tissue remodeling constitutes a general common feature shared by every tumor stromal reaction. Interestingly, we showed that specific gene sets, rather than common signature, have predictive value for patients with related tumor types. This absence of prognostic value for common stromal molecular characteristics might be due precisely to the broad character of stroma remodeling that concerns every tumor type and every stage of the disease, making it inappropriate for patient clustering and survival prediction. Remodeling is certainly

a necessary aspect of tumor-associated stroma but is probably not sufficient to promote tumor progression. In addition to a rather common stromal activation, each tumor has specific requirements for successful invasion related to its nature and localization. For instance, the needs of breast tumor cells present in a fatty environment are not necessarily similar to those of colon tumor cells that have to deal with an environment rich in proteases. Thus, tumor cells, depending on their nature and their differentiation status, display distinct secretory repertoires, which may elicit quantitative and qualitative differences in tissue remodeling and immune infiltration that will impact tumor invasion. Tumor transcriptomes differ among different tumor types because the cells are intrinsically different - a breast tumor cell is different in its nature from a prostate tumor cell. By contrast, the stromal compartment that is primarily composed of mesenchymal cells, including fibroblasts, may display greater similarity among different organs. However, interactions with cells from a specific tumor type may induce morphological and genotypic alterations in the stroma that distinguish it from its normal counterpart and from stroma associated with other, unrelated, tumor types. Stromal remodeling may also be important for the establishment and maintenance of a niche for cancer stem cells that require a specific microenvironment to self-renew and sustain tumor bulk formation. Therefore, acquisition of tumor-specific traits by the stroma reflects properties of each tumor type and may account for the capacity of tumor cells to survive, proliferate and disseminate.

Whereas Kaplan-Meier analysis allowed the evaluation of the survival-predictive value of the overall lists of stromal genes, univariate Cox analysis correlated the level of individual gene expression with patient survival. This analysis identified two genes within the common signature, *POSTN* and *RUNX1* that were strongly associated with survival of patients with both tumor types, suggesting that deregulated expression of these two genes may be relevant for the stromal reaction and survival of different tumor types.

Overexpression of RUNX1 was shown to be associated with favorable prognosis in both breast and prostate cancer patients. RUNX1, also known as acute myeloid leukemia 1 protein (AML1), is a transcription factor involved in normal hematopoiesis and chromosomal translocations involving RUNX1 have been associated with several types of leukemia [33]. RUNX1 overexpression was also shown to be associated with various solid tumors including human ovarian cancer, skin and oral squamous cell carcinoma (SCC) [34] and colorectal

cancer [35], suggesting that RUNX1 may act as a tumor promoter. However, RUNX1 was also shown to exhibit tumor suppressor functions in the mouse intestine [36] and to present tumor subtype-specific functions in human breast cancer [37, 38]. RUNX1 is suggested to regulate cancer development by repressing p21 [39], promoting STAT3 activation [40], activating MMP transcription [41] and affecting WNT and NOTCH signaling [36]. Its expression in breast and prostate cancer-associated stroma may therefore contribute to the proliferation of stromal cells and ECM remodeling. However, its association with good prognosis in both breast and prostate cancer patients would argue rather for a tumor suppressor function. RUNX1 is known to play an important role in normal adult hematopoietic stem cell homeostasis [42]. Stromal expression of RUNX1 could therefore potentially restrict cancer stem cell proliferation by modulating their environment [34].

POSTN overexpression was associated with good prognosis in breast cancer patients but with poor prognosis in prostate cancer patients, underlying once again the tumor specificity of each stromal reaction. POSTN is a component of the extracellular matrix whose binding to various integrins has been reported to promote invasion of tumor cells [43-45]. POSTN was also found to be overexpressed in several human cancers [43-50]. In the present study, in addition to being associated with breast and prostate cancer patient survival, POSTN was found to be upregulated in tumor but not in normal samples and its expression was observed exclusively in the stromal compartment. POSTN was recently shown to be highly relevant for metastatic colonization and stromal POSTN expression induced by infiltrating tumor cells was shown to be necessary to initiate colonization in the secondary target organ. POSTN was identified as a stromal factor of stem cell niches that participates in stem cell maintenance by increasing WNT signaling and whose absence prevents metastasis [51]. These data may support the association of POSTN with poor prognosis in prostate cancer patients. By contrast, they do not explain the discrepancy observed with breast cancer patients in whom POSTN is associated with more favorable prognosis. This divergence is possibly related to the level of POSTN expression that could be relevant to its effect on the tumor. Strong overexpression, as observed in prostate tumor-associated stroma in the present study, may promote pro-tumorigenic ECM remodeling, whereas lower expression, as observed in breast cancer stroma, may be insufficient to elicit phenotypic alterations that would negatively impact patient outcome. But overall, these data, and particularly the

determination of its stroma-restricted expression, encourage considering POSTN as an attractive potential therapeutic target.

Based on these considerations and the notion that stromal cells are thought to be more stable genetically than tumor cells, thereby presenting a lower risk of becoming resistant to drugs, targeting the microenvironment to support and improve conventional therapies directed against tumor cells may be relevant at each step of tumor progression, from primary tumor growth to distant metastasis. Moreover, targeting specifically the metastatic niche, which is a specialized microenvironment, could interfere not only with metastatic colonization but also with survival and activation of disseminated, dormant cancer cells, thereby offering promising perspectives [51]. Research efforts to identify pertinent stromal therapeutic target are therefore worthy to be pursued.

Original article

OPEN ACCESS Freely available online

PLoS one

Identification of Prognostic Molecular Features in the Reactive Stroma of Human Breast and Prostate Cancer

Anne Planche[1☯], Marina Bacac[1☯], Paolo Provero[2], Carlo Fusco[1], Mauro Delorenzi[3], Jean-Christophe Stehle[1], Ivan Stamenkovic[1]*

1 Institute of Pathology, CHUV, and Faculty of Biology and Medicine, University of Lausanne, Lausanne, Switzerland, **2** Department of Genetics, Biology and Biochemistry, University of Turin, Turin, Italy, **3** Swiss Institute of Bioinformatics, Lausanne, Switzerland

Abstract

Primary tumor growth induces host tissue responses that are believed to support and promote tumor progression. Identification of the molecular characteristics of the tumor microenvironment and elucidation of its crosstalk with tumor cells may therefore be crucial for improving our understanding of the processes implicated in cancer progression, identifying potential therapeutic targets, and uncovering stromal gene expression signatures that may predict clinical outcome. A key issue to resolve, therefore, is whether the stromal response to tumor growth is largely a generic phenomenon, irrespective of the tumor type or whether the response reflects tumor-specific properties. To address similarity or distinction of stromal gene expression changes during cancer progression, oligonucleotide-based Affymetrix microarray technology was used to compare the transcriptomes of laser-microdissected stromal cells derived from invasive human breast and prostate carcinoma. Invasive breast and prostate cancer-associated stroma was observed to display distinct transcriptomes, with a limited number of shared genes. Interestingly, both breast and prostate tumor-specific dysregulated stromal genes were observed to cluster breast and prostate cancer patients, respectively, into two distinct groups with statistically different clinical outcomes. By contrast, a gene signature that was common to the reactive stroma of both tumor types did not have survival predictive value. Univariate Cox analysis identified genes whose expression level was most strongly associated with patient survival. Taken together, these observations suggest that the tumor microenvironment displays distinct features according to the tumor type that provides survival-predictive value.

Citation: Planche A, Bacac M, Provero P, Fusco C, Delorenzi M, et al. (2011) Identification of Prognostic Molecular Features in the Reactive Stroma of Human Breast and Prostate Cancer. PLoS ONE 6(5): e18640. doi:10.1371/journal.pone.0018640

Editor: Francesco Falciani, University of Birmingham, United Kingdom

Received October 27, 2010; **Accepted** March 14, 2011; **Published** May 18, 2011

Funding: This work was supported by the Swiss Fonds National pour la Recherche Scientifique (FNRS) grant No. 310030-130350 and the NCCR Molecular Oncology. P.P. gratefully acknowledges support from the Italian Association for Cancer Research under grant IG9408. The funders had no role in study design, data collection and analysis, decision to publish or preparation of the manuscript.

Competing Interests: The authors have declared that no competing interests exist.

* E-mail: Ivan.Stamenkovic@chuv.ch

☯ These authors contributed equally to this work.

Introduction

It is widely recognized that tumor progression and metastasis are intimately linked to tissue remodeling resulting from tumor cell interactions with the host tissue stroma. In normal epithelial tissues, the basement membrane provides a natural barrier between epithelial cells and the stroma. Proliferation of transformed epithelial cells is therefore initially confined to the epithelial compartment, leading to the development of a *carcinoma in situ*. Invasion is heralded by degradation of the tumor cell basement membrane, recently shown to be mediated primarily by membrane-bound matrix metalloproteinases (MT-MMPs) [1]. Subsequent to penetration of the basement membrane, tumor cells engage for the first time in physical contact with the extracellular matrix (ECM) and stromal cells, including fibroblasts, leukocytes, dendritic cells and endothelial cells, triggering crosstalk between tumor and stromal cells that has profound consequences on local tumor growth and tumor cell dissemination [2,3,4].

The sequence of events that occur following tumor cell irruption into the host tissue stroma is difficult to define because several events are likely to occur simultaneously. However, evidence suggests that cytokines, chemokines and proteolytic enzymes secreted by tumor cells participate in local macrophage, fibroblasts and endothelial cell activation and recruitment of a variety of leukocyte subsets [5,6]. Activated macrophages and recruited leukocytes in turn secrete their own repertoire of cytokines, chemokines and proteolytic enzymes, leading to ECM degradation, which results in the release of a host of sequestered growth factors [7,8,9]. Some of these growth factors participate in promoting angiogenesis whereas others stimulate fibroblasts and myofibroblasts to synthesize and secrete ECM proteins [2,5,6]. The overall process is virtually indistinguishable from the remodeling that characterizes tissue repair following injury [10]. However, the released growth factors and ECM degradation products provide resources that ensure tumor cell survival, proliferation and migration, which in turn perpetuate tissue remodeling, leading to the notion that invasive tumors behave as "wounds that never heal" [11].

Tumor-associated stromal reactions vary both in amplitude and composition according, at least in part, to the tumor type. Most carcinomas display some degree of stromal reaction, which in

some tumors, particularly breast, prostate and pancreatic carcinoma, can be associated with massive ECM deposition, referred to as desmoplasia. Because tissue remodeling provides a means for tumor cells to grow and disseminate, it is widely held that rational anticancer therapeutic design should target not only tumor cells but the reactive stroma as well [3,4,12]. It follows that understanding tumor-stroma cross-talk at the molecular level and identification of molecular events whose disruption may destabilize tumor growth will constitute key steps toward therapeutic control of cancer growth. Several approaches have been used to address the stromal response to invasive cancer growth, including gene expression profile analysis of microdissected reactive stroma in human [13,14,15] and murine [16] tumors; gene expression analysis in defined FACS-sorted breast cancer stromal cell subsets [17]; development of new bioinformatics methods that decompose the gene expression signal originating from the entire tumor into multiple independent signatures allowing identification of those emanating from the stroma [18]; and modeling inducible tumor development to study tumor-host interactions as a function of time during tumor progression. Together, these studies have identified several candidate stroma-derived molecules that compose gene expression signatures relevant to cancer progression and metastases [3,13,14,15,16,18,19]. However, all of these studies have focused on the stromal reaction of a particular tumor type, and although the identified reactive stromal gene expression signatures are reported to bear prognostic significance to the tumors they are associated with, it is unclear whether different tumor types share reactive stromal gene expression signatures or whether they elicit distinct responses.

In the present work we focused on the analysis of gene expression signatures of human breast and prostate cancer stroma in an effort to determine the degree of similarity among stromal reactions to different invasive cancer types and identify candidate deregulated genes common to tumor invasion irrespective of tumor origin. Our results reveal distinct stromal gene expression signatures in human breast and prostate cancer, each of which is predictive of poor prognosis of its respective tumor type, and identify a small deregulated gene set common to both tumor types that, by contrast, is not predictive of patient survival.

Results

Patient sample selection

Breast and prostate cancer patients were selected according to the following criteria: availability of both tumor and normal tissue for each patient; presence of an adequate amount of stroma in both normal and tumor tissues for efficient microdissection; absence of chemotherapy and/or radiotherapy and presence of a comparable inflammatory reaction, as assessed by histological analysis, to limit variability among samples. To ensure reliable statistical analysis at least six patients per cancer type with defined histopathological characteristics were included (Table S1). All breast cancer patients had primary tumors with an invasive component that was at least 0.5 cm in the greatest dimension and five out of six patients presented lymph node metastasis and were estrogen receptor (ER)-positive (90–100%). All prostate cancer patients presented primary invasive tumors involving both lobes of the prostate, with a Gleason score$\geq$7 and no lymph node metastasis (pN0), thus constituting a homogeneous group. Both normal and tumor tissues were hematoxylin-eosin (H&E)-stained to assess tissue morphology prior to microdissection.

The selected candidate samples were subsequently stained using an anti-multi-cytokeratin antibody to identify tumor cells within tissue sections (Figure S1, panels A and B) and an anti-vimentin antibody to identify the stromal compartment (Figure S1 panel C). Extensive stromal areas within tumor tissue sections were found to be free of invading tumor cells and were thus amenable to microdissection. Normal and tumor tissue sections of the breast and prostate patients were subjected to laser capture microdissection (LCM) for selective analysis of the stromal compartment (Figure S2). Generally, 20 to 100 ng of total RNA were extracted from microdissected samples and subjected to mRNA amplification prior to hybridization to Affymetrix microarrays.

Breast and prostate cancer display distinct stromal responses

The global gene expression profile of microdissected stroma obtained from breast and prostate specimens was first analyzed using Principal Component Analysis (PCA). The projection of the stromal expression profiles on the two first components is shown in Figure 1A. Notwithstanding some outliers, the figure demonstrates a clear distinction in stromal expression profiles between breast and prostate tumors and also between tumor and normal samples of each tissue type. The figure also suggests that the overall stromal response in breast cancer is stronger than in prostate cancer. We concluded that breast and prostate tumors have a distinct stromal reaction to tumor invasion that may be successfully used for classifying cancer patients. In addition, we defined genes sets labeled BU, BD, PU and PD containing the genes represented by probesets that are up or downregulated in breast and prostate tumor stroma compared to the corresponding normal stroma at FDR 5% and 10% cutoffs, respectively, and at least a 2-fold change in expression level. We used different FDR cutoffs for breast and stroma to obtain lists of differentially expressed genes of comparable size. The fact that we had to use a higher FDR in the case of prostate cancer confirms that the overall stromal response is weaker than in breast cancer. Pearson correlation between any pair of different genes in each of these stromal gene sets calculated in the ExpO consortium breast and prostate subsets shows a better correlation of the breast stromal genes with breast data (BU: 0.09/BD: 0.18) than with prostate data (BU: 0.07/BD: 0.08). Similarly, prostate stromal genes show better correlation with prostate data (PU: 0.20/PD: 0.26) than with breast data (PU: 0.00/PD: 0.01) (Figure 1B).

Differentially expressed genes between tumor and normal stroma

The genes sets BU, BD, PU and PD defined above contained 181 and 462 statistically relevant probes for BU and BD, respectively, (FDR 5%, Table S2), and 154 and 165 for PU and PD, respectively, (FDR 10%, Table S3). Fourteen randomly chosen genes within the lists were validated by quantitative real-time PCR (Figure S3).

Genes specific to the stromal reaction of breast tumors

A selection of genes found to be differentially expressed between tumor and normal stroma of breast cancer patients are listed in Table 1. Stromal reaction to invasive breast carcinoma was associated with increased expression of genes encoding ECM components, proteolytic enzymes and adhesion receptors, including *COL11A1*, *COL10A1*, *COMP*, *MMP11*, *FN1* and *MFAP2*, consistent with the abundant stromal remodeling observed by histology. Genes encoding components of the ECM, including *TNXB* and *MATN2* were identified among downregulated transcripts, together with other participants in tumor progression, including growth factors, such as *FIGF* and growth factor receptors, such as *TGFBR3*.

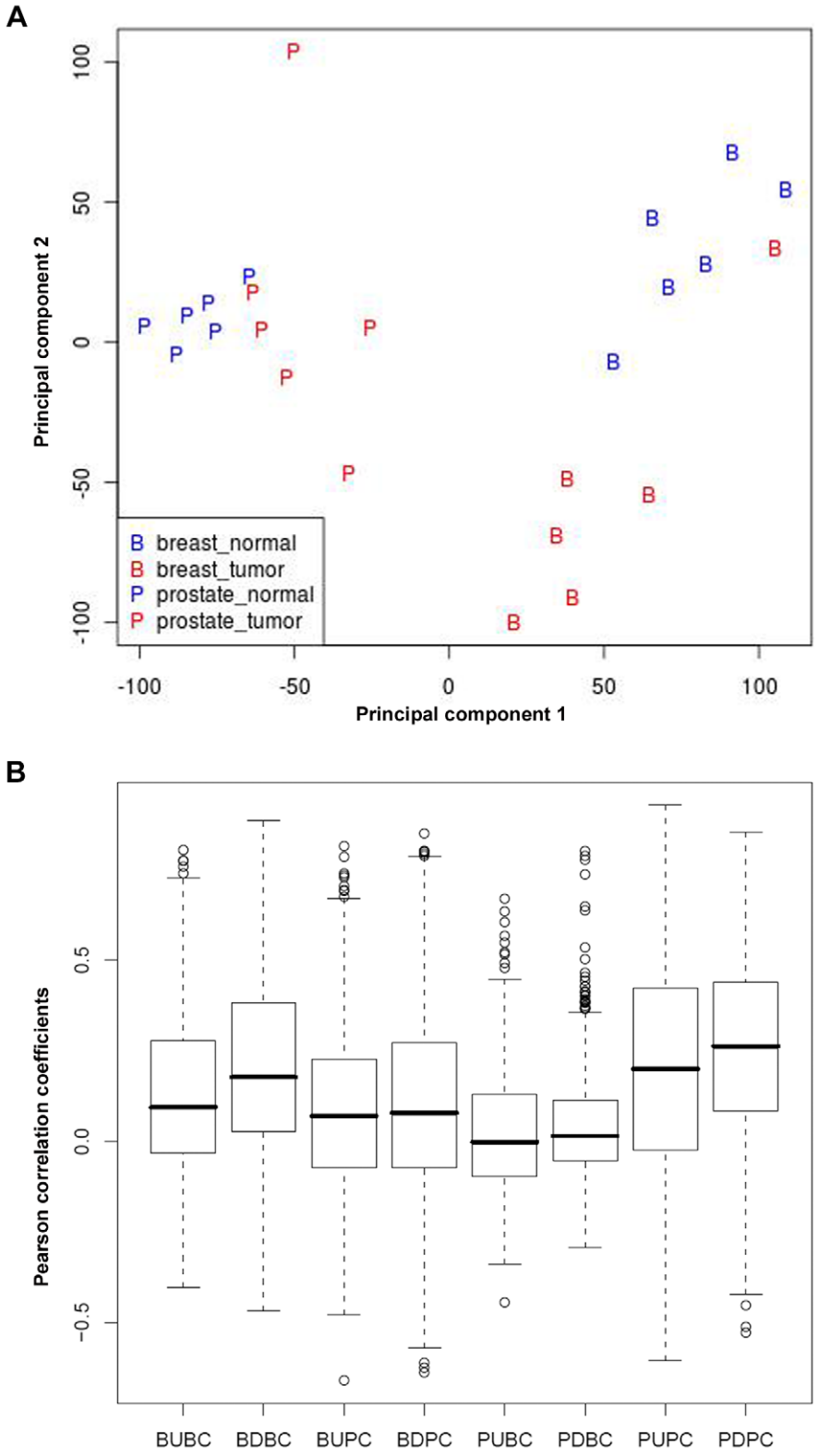

Figure 1. Tumor-specific stromal responses displayed by breast and prostate cancer. A, PCA shows that breast and prostate tumors have a distinct stromal reaction to tumor invasion that can be used to classify cancer patients. B, pairwise correlation analysis showing a higher correlation of breast stromal genes with breast data than with prostate data and vice versa.
doi:10.1371/journal.pone.0018640.g001

Table 1. Selection of differentially expressed genes between tumor and normal breast stroma (FDR<0.05, |M|≥2).

Gene symbol	Gene description	logFC	Adjusted P-value
Upregulated genes in tumor stroma			
COL11A1	Collagen, type XI, alpha 1	7.3	6.0E-03
COL10A1	Collagen, type X, alpha 1(Schmid metaphyseal chondrodysplasia)	6.0	1.2E-02
COMP	Cartilage oligomeric matrix protein	4.9	1.6E-02
INHBA	Inhibin, beta A	4.8	8.0E-03
CXCL10	chemokine (C-X-C motif) ligand 10	3.9	4.8E-02
SULF1	Sulfatase 1	3.7	2.4E-02
SDC1	Syndecan 1	3.4	2.4E-02
MMP11	Matrix metallopeptidase 11 (stromelysin 3)	3.2	2.6E-02
F2RL1	Coagulation factor II (thrombin) receptor-like 1	3.1	3.1E-02
CDKN2B	Cyclin-dependent kinase inhibitor 2B (p15, inhibits CDK4)	3.1	2.3E-02
RUNX2	Runt-related transcription factor 2	2.7	4.7E-02
CDKN2A	Cyclin-dependent kinase inhibitor 2A (melanoma, p16, inhibits CDK4)	2.6	3.1E-02
CADM1	Cell adhesion molecule 1	2.5	6.0E-03
P4HA3	Procollagen-proline, 2-oxoglutarate 4-dioxygenase (proline 4-hydroxylase), alpha polypeptide III	2.4	3.8E-02
FN1	Fibronectin 1	2.4	3.8E-02
NRG1	Neuregulin 1	2.2	4.7E-02
MFAP2	Microfibrillar-associated protein 2	2.2	4.9E-02
RUNX1	runt-related transcription factor 1 (acute myeloid leukemia 1; aml1 oncogene)	2.1	1.6E-02
Downregulated genes in tumor stroma			
CD36	CD36 molecule (thrombospondin receptor)	−4.9	3.2E-03
FIGF	C-fos induced growth factor (vascular endothelial growth factor D)	−4.8	1.0E-02
KLF4	Kruppel-like factor 4 (gut)	−3.9	2.4E-02
MATN2	Matrilin 2	−3.7	2.5E-02
LIFR	Leukemia inhibitory factor receptor alpha	−3.5	1.2E-02
EMCN	Endomucin	−3.3	2.7E-02
GPC3	Glypican 3	−3.2	1.1E-02
FOSB	FBJ murine osteosarcoma viral oncogene homolog B	−3.2	1.9E-02
IL33	Interleukin 33	−3.1	4.9E-02
MEG3	Maternally expressed 3	−3.1	7.4E-03
TGFBR3	Transforming growth factor, beta receptor III	−3.1	6.1E-03
RHOJ	Ras homolog gene family, member J	−3.1	2.6E-02
DLC1	Deleted in liver cancer 1	−3.0	3.1E-02
TNXB	Tenascin XB	−2.9	5.0E-03
ANK2	Ankyrin 2, neuronal	−2.8	4.3E-02
NOVA1	neuro-oncological ventral antigen 1	−2.6	1.6E-02
ENPP2	Ectonucleotide pyrophosphatase/phosphodiesterase 2 (autotaxin)	−2.6	3.8E-02
LEPR	Leptin receptor	−2.6	6.0E-03

doi:10.1371/journal.pone.0018640.t001

Genes specific to the stromal reaction of prostate cancer

A distinct selection of genes found to be differentially expressed in the tumor stroma of prostate cancer patients compared to their normal tissue counterparts is shown in Table 2. In contrast to breast tumor stroma, the stromal reaction to invasive prostate cancer displayed fewer genes involved in tissue remodeling but a higher number of genes belonging to defined signaling pathways, including members of the Wnt signaling pathway (*SFRP1*, *RSPO3*). Several transcription factors, including *NKX3-1*, *HOXB13*, *HOXC6*, *HOXD11* and *HOXD13*, were also found to have deregulated expression in the stromal reaction to invasive prostate tumors.

Genes common to the stromal reaction of both tumor types

Although PCA showed a clear separation of breast and prostate patients, suggesting a limited overlap between the lists of breast and prostate stromal genes, we nevertheless attempted to compare the two lists in order to identify genes that might be common to the stromal reaction of both tumor types. Using an FDR of 15%

Table 2. Selection of differentially expressed genes between tumor and normal prostate stroma (FDR<0.10, |M|≥2).

Gene symbol	Gene description	logFC	Adjusted P-value
Upregulated genes in tumor stroma			
PRAC	Prostate cancer susceptibility candidate	4	1.4E-02
ASPN	Asporin	3.8	2.5E-02
CTHRC1	Collagen triple helix repeat containing 1	3.7	7.5E-02
TARP	TCR gamma alternate reading frame protein	3.4	1.1E-02
AGR2	Anterior gradient homolog 2 (Xenopus laevis)	3.2	5.3E-02
POSTN	Periostin, osteoblast specific factor	3.2	9.8E-02
ESR1	estrogen receptor 1	3.2	6.6E-02
NKX3-1	NK3 homeobox 1	3.2	4.1E-02
HOXB13	Homeobox B13	2.8	4.6E-02
SFRP1	Secreted frizzled-related protein 1	2.8	6.3E-02
BMPR1B	Bone morphogenetic protein receptor, type IB	2.7	4.8E-02
FOLH1	Folate hydrolase (prostate-specific membrane antigen) 1	2.7	9.9E-02
RSPO3	R-spondin 3 homolog (Xenopus laevis)	2.3	5.7E-02
PKP2	Plakophilin 2	2.3	6.9E-02
ERG	V-ets erythroblastosis virus E26 oncogene homolog (avian)	2.3	5.3E-02
TSPAN1	Tetraspanin 1	2.2	3.2E-02
HOXC6	Homeobox C6	2	3.0E-02
GREB1	GREB1 protein	2.0	6.9E-02
Downregulated genes in tumor stroma			
NELL2	NEL-like 2 (chicken)	−4.6	6.2E-02
BMP5	Bone morphogenetic protein 5	−4.5	2.9E-02
PENK	Proenkephalin	−4.2	5.4E-02
GPM6A	Glycoprotein M6A	−4.1	1.2E-02
DKK1	Dickkopf homolog 1 (Xenopus laevis)	−3.4	9.8E-02
PTGS1	Prostaglandin-endoperoxide synthase 1 (prostaglandin G/H synthase and cyclooxygenase)	−3.1	9.4E-02
SEMA3E	Sema domain, immunoglobulin domain (Ig), short basic domain, secreted, (semaphorin) 3^E	−2.8	3.0E-02
FOXQ1	Forkhead box Q1	−2.8	5.3E-02
DPT	Dermatopontin	−2.7	9.4E-02
ARHGAP28	Rho GTPase activating protein 28	−2.7	8.8E-02
HOXD13	homeobox D13	−2.7	6.6E-02
TSLP	Thymic stromal lymphopoietin	−2.4	2.4E-02
PRKCB1	Protein kinase C, beta 1	−2.4	2.9E-02
PTGDS	Prostaglandin D2 synthase 21 kDa (brain)	−2.3	9.8E-02
HAPLN1	Hyaluronan and proteoglycan link protein 1	−2.3	8.6E-02
GPR133	G protein-coupled receptor 133	−2.1	8.0E-02
PGF	Placental growth factor	−2.0	8.8E-02
HOXD11	Homeobox D11	−2.0	8.8E-02

doi:10.1371/journal.pone.0018640.t002

for both breast and prostate analyses, we identified 20 upregulated (P = 1.3E-03, Fisher's exact test) and 28 downregulated (P = 2.4E-05) common genes (Table 3). Several of the upregulated genes encoded adhesion receptors, secreted proteins and cytoskeletal components, including *CDH11*, *POSTN* and *MYO5B*, along with *RUNX1*, a master regulator of differentiation processes in different tissues implicated in cell transformation and tumor progression [20,21]. Several of the downregulated genes encoded enzymes implicated in metabolic processes including *BCO2*, *GLT25D2*, *GSTM5*, *ASPA* and *PTGDS*. Interestingly, the hepatic leukemia factor (*HLF*), a member of bZIP transcription factor family known to regulate the expression of *RUNX1*, was also found to be downregulated.

Comparison to datasets from studies on human breast and pancreatic and murine prostate cancer revealed a high degree of similarity between upregulated genes in our breast cancer patient stroma and upregulated genes in the Ma et al. [13] and Bauer et al. study of breast tumors [22] as well as in the Binkley et al. study

Table 3. Genes common to the stromal reaction of breast and prostate cancer patients (FDR 15%).

Gene symbol	Gene description
Upregulated genes in the tumor stroma	
ABCC4	ATP-binding cassette, sub-family C (CFTR/MRP), member 4
C11orf75	chromosome 11 open reading frame 75
CDH11	cadherin 11, type 2, OB-cadherin (osteoblast)
ENC1	ectodermal-neural cortex (with BTB-like domain)
ESRP2	epithelial splicing regulatory protein 2
GOLM1	golgi membrane protein 1
KIAA0101	KIAA0101
MYO5B	myosin VB
NDUFS8	NADH dehydrogenase (ubiquinone) Fe-S protein 8, 23 kDa (NADH-coenzyme Q reductase)
NNMT	nicotinamide N-methyltransferase
NTM	neurotrimin
PBRM1	polybromo 1
PDLIM5	PDZ and LIM domain 5
POSTN	periostin, osteoblast specific factor
RUNX1	runt-related transcription factor 1
SERP1	stress-associated endoplasmic reticulum protein 1
SORD	sorbitol dehydrogenase
SPATS2L	spermatogenesis associated, serine-rich 2-like
VOPP1	vesicular, overexpressed in cancer, prosurvival protein 1
YARS	tyrosyl-tRNA synthetase
Downregulated genes in the tumor stroma	
ADAMTS5	ADAM metallopeptidase with thrombospondin type 1 motif, 5
ADCYAP1R1	adenylate cyclase activating polypeptide 1 (pituitary) receptor type I
ANKDD1A	ankyrin repeat and death domain containing 1A
ASPA	aspartoacylase (Canavan disease)
BCO2	beta-carotene oxygenase 2
C16orf89	chromosome 16 open reading frame 89
CFD	complement factor D (adipsin)
CLEC3B	C-type lectin domain family 3, member B
ETS2	v-ets erythroblastosis virus E26 oncogene homolog 2 (avian)
GARNL3	GTPase activating Rap/RanGAP domain-like 3
GLT25D2	glycosyltransferase 25 domain containing 2
GPM6A	glycoprotein M6A
GPR133	G protein-coupled receptor 133
GSTM5	glutathione S-transferase mu 5
HLF	hepatic leukemia factor
ITM2A	integral membrane protein 2A
KIAA1377	KIAA1377
NAP1L5	nucleosome assembly protein 1-like 5
PENK	proenkephalin
PHACTR2	phosphatase and actin regulator 2
PPARG	peroxisome proliferator-activated receptor gamma
PPL	periplakin
PTGDS	prostaglandin D2 synthase 21kDa (brain)
PTGFR	prostaglandin F receptor (FP)
THSD7A	thrombospondin, type I, domain containing 7A
TJP2	tight junction protein 2 (zona occludens 2)
TRERF1	transcriptional regulating factor 1
ZNF10	zinc finger protein 10

Common upregulated genes: P = 0.0013, common downregulated genes: P = 2.4E-05.
doi:10.1371/journal.pone.0018640.t003

of the stromal response to pancreatic cancer [15] (Table 4). Significant similarity was also found with the mouse stromal response to neuroendocrine prostate cancer growth [16]. The prostate cancer stromal signature was also significantly related to these four datasets, albeit to a lesser degree than the breast cancer signature (Table 4). As expected, our breast cancer stromal signature was more closely related to the two breast signatures than our prostate cancer stromal signature. In addition, both our breast and prostate cancer stromal signatures displayed similarity with pancreatic cancer and mouse neuroendocrine prostate cancer stroma signatures. Closer examination of the signatures, however, revealed that the similarity resided primarily among genes implicated in tissue remodeling.

Periostin (POSTN), found to be upregulated in both breast and prostate cancer stroma, was selected for immunohistochemical validation in a panel of human tumors known to be associated with a prominent stromal reaction (breast, prostate, ovary, colon and lung carcinoma). Representative images shown in Figure 2 confirm the increase of POSTN expression in the stromal compartment of breast and prostate tumor samples (panels B and D, respectively), compared to their normal counterparts (panels A and C, respectively). Intense POSTN expression was also observed in the stroma of ovarian carcinoma (panel E), as well as in lung and colon carcinoma where it was concentrated at the interface between the tumor epithelial cells and the stromal compartment that presented a robust inflammatory reaction (panels F and G, respectively). It is noteworthy that POSTN was not expressed in the tumor cells of the samples analyzed.

Prognostic value of specific and common stromal signatures

Genes identified in breast and prostate stromal reactions (FDR 15%) were assessed for their survival-predictive ability using publicly available datasets of human cancer patients. For each dataset, Pearson correlation-based hierarchical clustering was first used to divide patients into two groups based only on the expression profiles of breast and prostate stromal genes. Kaplan-Meier analysis and log-rank test were then used to determine whether the two groups of patients thus defined showed statistically significant differences in terms of survival. Figure 3A represents the results of Kaplan-Meier survival analysis obtained using breast stromal genes (FDR 15%) on 295 early-stage breast carcinoma patients [23]. The two groups of patients, obtained after hierarchical cluster analysis using stromal genes, differed significantly in their overall survival ($P = 6.74e-05$), indicating that the breast stromal genes had survival-predictive value for breast cancer patients.

Similarly to breast stroma, prostate stromal genes also displayed statistically significant survival-predictive ability ($P = 0.002$) on 79 prostate carcinoma patients [24], (Figure 3B) if only genes with base 2 logarithmic fold change $|M|>2$ are included in the signature. By contrast, genes common to breast and prostate cancer stroma did not display statistically significant prognostic value for breast (23) ($P = 0.773$) or prostate (24) ($P = 0.106$) cancer.

Univariate Cox analysis: identification of genes whose expression correlates most strongly with patient survival

Kaplan-Meier survival analysis indicated that the overall lists of breast and prostate cancer stromal genes had high prognostic value in human breast and prostate cancer datasets, respectively, but did not allow the identification of genes whose expression level is most strongly associated with patient survival. To address this issue, univariate Cox analysis was performed to correlate the level of gene expression with patient survival. For each gene, a z value was obtained, indicating the strength of the correlation between the level of gene expression and patient survival. Positive z values indicated that the expression level of a gene was associated with poor prognosis, while negative z values indicated correlation with good prognosis. A selection of genes associated with poor and good prognosis for breast ([23], Table 5) and prostate ([24], Table 5) cancer are shown. It is noteworthy that although the gene expression signature that was common to the stromal reaction of both breast and prostate carcinoma did not have any survival-predictive value, two individual genes within the common signature, *POSTN* and *RUNX1*, were associated with survival of patients with both tumor types. Interestingly, whereas periostin was associated with good survival in breast cancer patients, its overexpression was associated with poor prognosis in prostate cancer patients (Table 5).

Discussion

Breast and prostate cancer are the most common invasive cancers in women and men, respectively. Although these tumors arise in organs that are widely divergent in terms of anatomic localization, structure and physiological function, both organs require gonadal hormones for normal development. Accordingly, the corresponding tumors are hormone-dependent and display remarkable biological similarity. Based on this notion and the observation that both tumor types are usually accompanied by robust tissue remodeling, it is of interest to determine whether the elicited stromal response displays similar or distinct hallmarks. PCA performed using gene expression profiles of the analyzed samples revealed that the two tumor types had a distinct stromal reaction (Figure 1A). Breast cancer stroma was associated with genes encoding matrix components, including *COL11A1*, *COL10A1*, *COMP*, *MMP11*, *FN1*, *MFAP2*, *TNXB* and *MATN2*, consistent with the robust ECM remodeling frequently observed within breast tumors, whereas prostate cancer stroma was associated with deregulated expression of homeobox genes including *NKX3-1*, *HOXB13 HOXC6*, *HOXD11* and *HOXD13*, implicated in differentiation processes during development. Enhanced expression of these genes raises the interesting possibility that reactivation of developmental programs by prostate

Table 4. Comparison of upregulated breast and prostate genes identified in the present study with published stromal signatures.

	Stroma-related gene expression studies			
Present study (FDR 15%)	**Ma *et al.* (breast carcinoma)**	**Bauer *et al.* (breast carcinoma)**	**Binkley *et al.* (pancreatic carcinoma)**	**Bacac *et al.* (prostate carcinoma, mouse)**
Breast stromal genes	8.1E-22	2.4E-04	9.8E-16	1.3E-07
Prostate stromal genes	0.086	0.02	3.8E-03	8.3E-03

doi:10.1371/journal.pone.0018640.t004

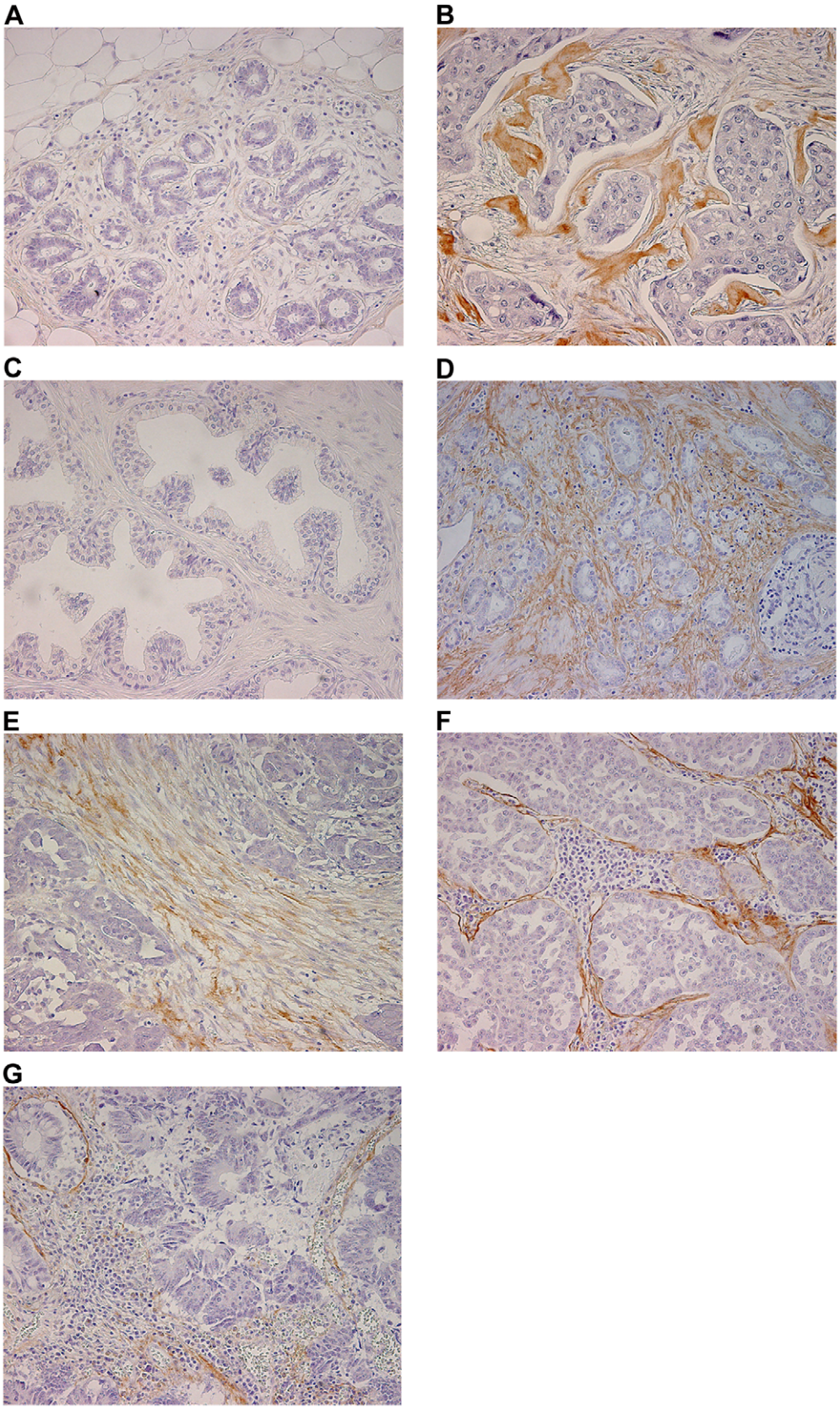

Figure 2. Representative images of periostin expression in normal and tumor tissues. A, normal breast tissue. B, breast carcinoma. C, normal prostate tissue. D, prostate carcinoma. E, ovarian carcinoma. F, lung carcinoma. G, colon carcinoma. Magnification: 200×.
doi:10.1371/journal.pone.0018640.g002

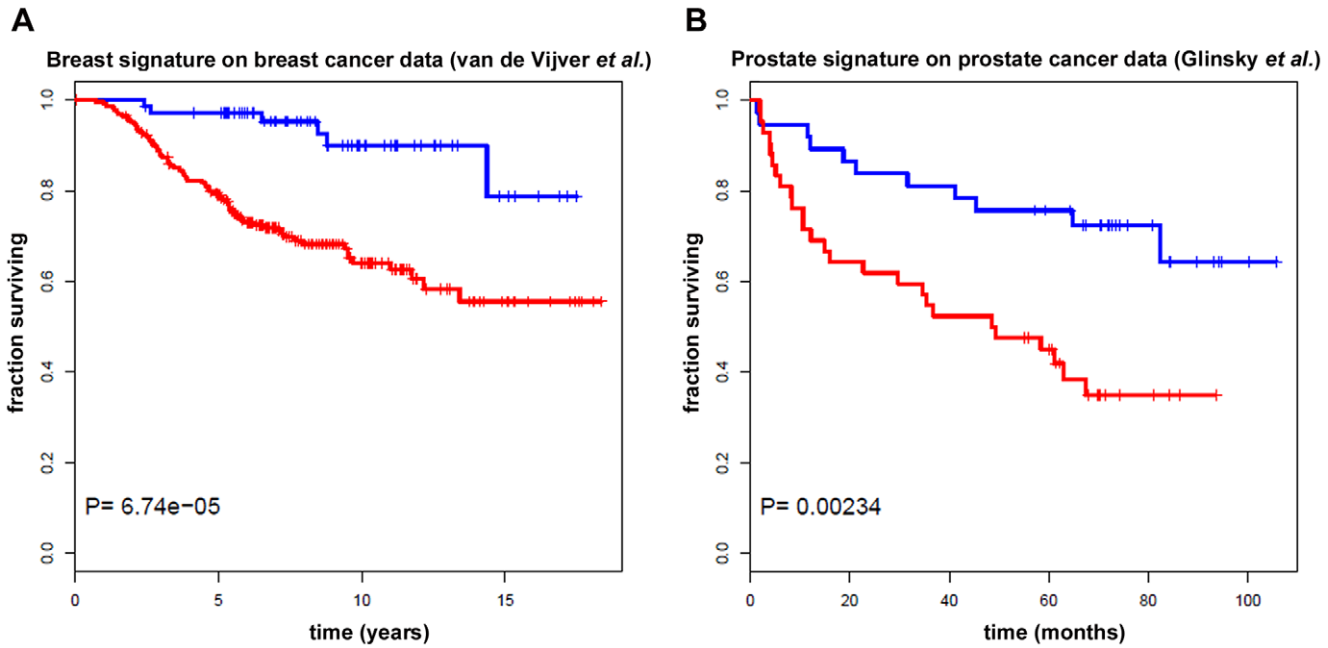

Figure 3. Kaplan-Meier survival analysis. A, Kaplan-Meier survival analysis of early-breast carcinoma patients (van de Vijver et al.) and B, prostate carcinoma patients (Glinsky et al.) obtained using breast and prostate stromal genes respectively (FDR 15%), showing that the two groups of patients differ significantly in their overall survival. Red, poor prognosis group; blue, good prognosis group.
doi:10.1371/journal.pone.0018640.g003

tumor stromal cells may contribute to the establishment of a more permissive microenvironment for tumor growth and progression.

Interestingly, a small subset of genes was found to be common to the stromal reaction of both tumor types and included, among others, genes encoding adhesion and cytoskeletal proteins (*CDH11*, *MYO5B*), a master regulator of differentiation processes, cell transformation, and tumor progression (*RUNX1*), as well as the osteoblast-specific factor periostin (*POSTN*). Several of the up and downregulated genes identified by microarray analysis were validated using *q*Real-time RT-PCR. Further validation of the relevance of the stromal genes was obtained from survival analysis using publicly available breast and prostate cancer patient datasets. Kaplan-Meier survival analysis revealed that the stromal genes identified in the present study clustered the cancer patients into two groups that differed significantly in their overall survival, underscoring their survival-predictive ability. It is noteworthy that the gene expression signature common to the stromal reaction of breast and prostate tumors did not carry prognostic value, suggesting that the "common" remodeling observed in several tumor types is not a key element in survival. Rather, tumor-specificity of the stromal reaction appears to be implicated in predicting evolution and survival.

Univariate Cox analysis further highlighted genes whose expression was most strongly associated with patient survival including, *POSTN* and *RUNX1* that were found to be common to the stromal reaction of both tumor types. Periostin was originally isolated as an osteoblast specific factor, and most of its physiologic functions take place at the epithelial-mesenchymal interface [25]. It is highly homologous to human β Ig-H3, a transforming growth factor β (TGF-β)-induced protein that promotes adhesion and spreading of fibroblasts [26]. Binding of periostin to $\alpha_V\beta_3$, $\alpha_V\beta_5$ or $\alpha_6\beta_4$ integrins has been reported to promote invasion of tumor cells by enhancing cell survival via the Akt/PKB pathway [27,28,29]. POSTN was found to be overexpressed in several human cancers including ovarian [28,30], colon [29], pancreatic [25,27], breast [31,32], lung cancer [33], and melanoma [34], with contradictory data concerning the identity of periostin-expressing cells (i.e. stroma, tumor cells or both).

In the present study, periostin was found to be upregulated and specifically localized to the breast and prostate tumor stroma compared to the normal stroma by immunohistochemistry. The presence of the periostin protein was also shown in the stroma of ovarian, colon and lung carcinoma.

The correlation between periostin expression and poor prostate cancer patient outcome is consistent with previous studies that identified periostin overexpression in several invasive tumor types [25,28,29,34]. Recently, periostin was found to promote invasiveness of esophageal carcinoma [35]. However, another study reported a downregulation of POSTN in lung cancer tissues indicating a potential context-dependent tumor suppressor activity of POSTN [33] that could be in line with the association of POSTN overexpression with good prognosis in breast cancer patients observed in the present study.

Although the notion that tissue remodeling associated with tumor invasion facilitates subsequent tumor progression is widely accepted, the precise molecular features of the remodeling require elucidation if the stromal reaction is to be targeted by therapeutic means. It is therefore important to determine whether tumor invasion in and of itself induces a standard stromal reaction that varies only in amplitude among tumors or whether different tumor types induce distinct stromal reactions whose features are likely to have a bearing on the choice of therapeutic arsenal. The present study reveals that the stromal reaction to invasion by two unrelated tumor types bears distinctive features that are relevant to the prognosis of the respective tumors. By contrast, the gene signature found to be common to breast and prostate stromal reactions failed to show survival-predictive value. However, when Cox analysis was performed, two genes within the common signature, *RUNX1* and *POSTN*, were found to be associated with patient survival, providing potential therapeutic targets of interest. Periostin in particular seems

Table 5. Cox analysis.

Gene symbol	Gene description	Z value
Breast stromal genes		
YARS	Tyrosyl-tRNA synthetase	4.4
ADAM19	ADAM metallopeptidase domain 19 (meltrin beta)	3.6
BMP2	Bone morphogenetic protein 2	3.5
SPP1	Secreted phosphoprotein 1	3.3
TNXB	Tenascin XB	2.5
EGFR	Epidermal growth factor receptor (erythroblastic leukemia viral (v-erb-b) oncogene homolog, avian)	2.4
NOVA1	Neuro-oncological ventral antigen 1	−3.2
XIST	X (inactive)-specific transcript (non-protein coding)	−2.4
INHBA	Inhibin, beta A	−2.4
POSTN	Periostin, osteoblast specific factor	−2.2
TGFBR3	Transforming growth factor, beta receptor III	−2.2
RUNX1	Runt-related transcription factor 1	−2.0
Prostate stromal genes		
HOXC6	Homeobox C6	3.9
SERP1	Stress-associated endoplasmic reticulum protein 1	3.3
CDH11	Cadherin 11, type 2, OB-cadherin (osteoblast)	2.5
BMPR1B	Bone morphogenetic protein receptor, typeIB	2.4
POSTN	Periostin, osteoblast specific factor	2.2
GREM1	Gremlin 1, cysteine knot superfamily, homolog (Xenopus laevis)	2.1
HOXD13	Homeobox D13	−3.8
GRIA1	Glutamate receptor, ionotropic, AMPA 1	−3.5
RUNX1	Runt-related transcription factor 1	−3.4
PTGDS	Prostaglandin D2 synthase 21 kDa (brain)	−3.0
GARNL3	GTPase activating Rap/RanGAP domain-like 3	−2.2
ESR1	Estrogen receptor 1	−2.0

Selection of breast and prostate stromal genes strongly associated with breast cancer patient survival (van de Vijver *et al.*) and prostate cancer patient survival (Glinsky *et al.*), respectively. Positive Z values indicate that the expression level of the gene is associated with poor prognosis, while negative Z values indicate correlation with good prognosis.

doi:10.1371/journal.pone.0018640.t005

to offer attractive therapeutic possibilities, as it is secreted and expressed selectively in tumor but not in normal stroma. Our study proposes periostin to be a novel stromal candidate marker of tumor prognosis that may also constitute potential therapeutic target in a broad range of carcinomas.

Materials and Methods

Patients and sample collection

Fresh frozen samples from six invasive breast and six invasive prostate tumors were obtained from the Institute of Pathology tissue bank, University Hospital Lausanne (CHUV) in compliance with institutional ethical regulations. Informed written consent was obtained from all patients involved in the study and approval was obtained from the ethics committee of the CHUV and Faculty of Biology and Medicine of the University of Lausanne.

Laser capture microdissection

LCM slides were prepared from serial 6-µm-thick frozen tissue sections mounted on a polyvinyl nuclease free membrane (Molecular Machine&Industries, Glattbrugg, CH).

Tissue sections were fixed in ethanol 70% (30 sec), stained with Mayer's hematoxylin (10 sec) and eosin (30 sec), dehydrated in graded ethanol, treated with xylene and air-dried in a sterile laminar flow hood. Slides were microdissected immediately following staining using a µCut Laser Microdissector system (Nikon Eclipse TE200).

All steps and solutions were performed under RNase free conditions. All samples were subjected to histological examination in order to identify stromal regions free of tumor cells prior to microdissection.

RNA extraction, amplification and microarray

Total RNA was extracted immediately following microdissection using the PicoPure RNA isolation kit (Arcturus, Mountain View, CA, USA) according to the manufacturer's instructions. RNA was quantified using a NanoDrop spectrophotometer (NanoDrop Technologies, Wilmington, Delaware, USA), and the concentration ranged between 20–100 ng/sample.

RNA quality was assessed using an Agilent RNA 6000 Pico Kit (Agilent Technologies, Germany). Only high quality RNA was subjected to two rounds of linear amplification using the MessageAmp II aRNA Amplification Kit (Ambion, USA) according to the manufacturer's instructions and amplified RNA (aRNA) was quantified using the RNA 6000 Pico Assay Kit. During the second round of amplification, biotin-labeled nucleotides were incorporat-

ed to obtain biotin-labeled aRNA required for Affymetrix microarray hybridization. GeneChip Human Genome U133 plus 2.0 Arrays (Affymetrix, UK) representing 47,000 different RNAs were used and the following steps performed by the DNA Array Facility of Lausanne (DAFL, http://www.unil.ch/dafl): fragmentation of aRNA, hybridization on the arrays, washing and scanning of the microarrays. The outputs of the scanning were CEL files containing a value representing the level of expression for each probesets from which expression measures in log2 were computed before subsequent statistical analysis.

Statistical analysis

The RMA (Robust Multichip Average) algorithm was first applied to the microarray raw data to obtain gene expression data. All statistical analyses were performed using R and the Bioconductor suite (http://www.r-project.org/).

PCA was performed using the *prcomp* R function with default parameters.

Hierarchical cluster analysis was based on Pearson correlation between the samples. Differentially expressed genes between tumor and normal samples were identified with the *limma* package of Bioconductor, which applies empirical-based methods to a moderated t-statistic and takes multiple testing into account by providing an estimate of the false discovery rate (FDR). This analysis was performed in a paired way, .i.e. comparing tumor and normal samples from the same patient.

For the pairwise correlation analysis, the Pearson correlation was calculated in the ExpO breast and prostate subsets. Gene expression and annotation data from the ExpO consortium (http://www.intgen.org/expo/) were downloaded from GEO (GSE2109) in December 2008, including batches 1–16. The breast and prostate cancer subsets (354, respectively 83 samples) were extracted and processed separately with the RMA procedure (quantile normalization at probe-level data).

For comparison with published stromal signatures, multiple testing correction was done with the Bonferroni procedure. We re-analyzed the expression data of Ma *et al.* [13] to obtain a list of differentially expressed genes comparing invasive breast ductal carcinoma stroma versus normal stroma. For that we used the expression data deposited in GEO (series GSE14548) and performed a paired analysis of differential expression using *limma*. The probesets with FDR$<$1% were then selected and used for the comparison. We compared our upregulated stromal genes with the ones found upregulated in breast carcinoma-associated fibroblasts compared to normal mammary fibroblasts in Bauer *et al.* [22] We compared our data with the pancreatic cancer stroma genes set identified in Binkley *et al.* [15] For the comparison with the mouse study from Bacac *et al.* [16] we considered the list containing the mouse genes found to be upregulated in invasive compared to pre-invasive prostate tumor stroma. These genes were converted into human genes using HomoloGene (build 62) and taking into account only the mouse genes with a unique homologene human ortholog.

Survival analysis of publicly available data

Publicly available gene expression data together with corresponding survival data for breast cancer and prostate cancer were obtained on-line. The breast data were directly downloaded from http://www.rii.com/publications/2002/nejm.html whereas the prostate data were provided by the authors as raw CEL files and normalized with the RMA algorithm. Hierarchical clustering of the patients was performed using Pearson correlation coefficient to define dissimilarity between patient expression profiles using only the probes associated with the genes included in the signature to be tested, obtaining two clusters of patients in each case. Kaplan-Meier curves were constructed for the two clusters of patients and the statistical significance of differences in survival probability between the two clusters was computed with the log-rank test. Univariate Cox analysis was performed to determine significant correlations between the expression profile of each individual gene represented on the chips and survival time.

Quantitative real-time RT-PCR validation of microarray results

cDNA was obtained using random hexamers (Invitrogen, USA), dNTPs (Clontech, USA) and the reverse transcriptase Superscript II (Invitrogen) starting from totRNA extracted from microdissected material. Real-time PCR amplification was performed using a Syber green mix or a TaqMan primers and probes mix when available, in an ABI Prism 7700 instrument (Applied Biosystems, Foster City, CA, USA). Relative quantitation of target, normalized with an endogenous control 18s rRNA (Hs99999901_s1) was done using a comparative (Ct) method according to the manufacturer's instructions. For EGFR (Hs00193306_m1), TaqMan probes (Applied Biosystems) were used. ProbeFinder software (www.roche-applied-science.com) was used to design primers for the Syber green method. The sequences of the forward (Fw) and reverse (Rev) primers were: INHBA Fw (ctcggagatcatcacgtttg), Rev (ccttggaaatctcgaagtgc); RUNX1 Fw (tgcctccctgaaccactc), Rev (gatggttggatctgccttgta); TGFBR3 Fw (gatttcatcttcggcttgaaa), Rev (gctcaggaggaatagtgtgga); NOVA1 Fw (gggttcccatagacctggac), Rev (gaaaatactggccgtcttcg); ENPP2 Fw (tgatggcttacatgacacagaa), Rev (agtgagttggaacaggaatgg); POSTN Fw (gaaccaaaaattaaagtgattgaagg), Rev (tgacttttgttagtgtgggtcct); ESR1 Fw (ttactgaccaacctggcaga), Rev (atcatggagggtcaaatcca); NKX3-1 Fw (ctcagtccctactgagtactctttctc), Rev (cagtgaaatgtgtaacccttgc); HOXB13 Fw (aacccaccaggtcccttt), Rev (tgtacggaatgcgtttcttg); SFRP1 Fw (gctggagcacgagaccat), Rev (tggcagttcttgttgagcag); ERG Fw (gccaggtgaatggctcaa), Rev (agttcatcccaacggtgtct); NELL2 Fw (aagaactgcacatgcctgaa), Rev (tcaggatttgggcagattaga); BMP5 Fw (gcaataaatccagctctcatca), Rev (tgtttttgctcacttgtgttataatct); HOXD13 Fw (ggaacagccaggtgtactgc), Rev (cggctgatttagagccaca).

Immunohistochemistry

Paraffin-embedded tissue sections were deparaffinized and hydrated according to standard procedures. Sections were subjected to antigen retrieval by boiling in EDTA (1 mM, pH 7.5) for 10 min, cooled, washed, and blocked in normal serum (from the same species from which the secondary antibody was produced). Frozen tissue sections were acetone-fixed and rehydrated prior to immunostaining and blocked in normal serum. The sections were then incubated with the primary antibody (for 1 hour at room temperature), followed by the incubation with the horse radish peroxidase (HRP)-conjugated secondary antibody for additional 30 minutes at room temperature. Diaminobenzidine (DAB) was used as a chromogene resulting in brown staining of positive cells. The nuclei were counterstained in blue using Harris hematoxylin. The antibodies were purchased as follows: NCL-C11 anti-multi-cytokeratin (Novocastra, UK), Keratin-903 anti-cytokeratin (cat. M 0630, Dako, USA), anti-human vimentin (cat. M 0725, Dako, USA), anti-periostin (cat. ab14041, Abcam, UK). For routine histopathological examination, 4-µm-thick frozen tissue sections were H&E stained according to standard procedures.

Supporting Information

Figure S1 Identification of tumor and stromal compartments. Representative images of A, breast carcinoma and B, prostate carcinoma sections stained with multi-cytokeratin anti-

body, with tumor cells appearing in brown. C, representative image of breast carcinoma with the stromal compartment identified by brown staining using anti-vimentin antibody. Magnification: 400×.
(TIF)

Figure S2 Laser capture microdissection. Examples of stroma microdissection using LCM from A, normal breast tissue, B, breast carcinoma, C, normal prostate tissue and D, prostate carcinoma. Arrows indicate the epithelial compartment whereas arrowheads point to the stroma. Staining: H&E, magnification: 200×.
(TIF)

Figure S3 Validation of gene expression. qReal-time RT-PCR validation of genes identified by microarray analysis. A–B, breast cancer stromal genes, C–E, prostate cancer stromal genes. The strong induction of ESR1 is represented on a separate panel for graphical reason.
(TIF)

Table S1 Histopathological classification of A, infiltrating breast ductal carcinoma and B, invasive prostate carcinoma patients used in the present study.
(DOC)

Table S2 Complete list of differentially expressed breast genes between tumor and normal stroma (FDR = 0.05).
(XLS)

Table S3 Complete list of differentially expressed prostate genes between tumor and normal stroma (FDR = 0.10).
(XLS)

Acknowledgments

We thank the DNA Array Facility (DAF) of Lausanne for their expert support.

Author Contributions

Conceived and designed the experiments: AP MB IS. Performed the experiments: AP JCS. Analyzed the data: AP MB PP MD. Contributed reagents/materials/analysis tools: PP MD CF. Wrote the paper: AP MB IS.

References

1. Hotary K, Li XY, Allen E, Stevens SL, Weiss SJ (2006) A cancer cell metalloprotease triad regulates the basement membrane transmigration program. Genes Dev 20: 2673–2686.
2. Bacac M, Stamenkovic I (2008) Metastatic cancer cell. Annu Rev Pathol 3: 221–247.
3. Bhowmick NA, Neilson EG, Moses HL (2004) Stromal fibroblasts in cancer initiation and progression. Nature 432: 332–337.
4. Olumi AF, Grossfeld GD, Hayward SW, Carroll PR, Tlsty TD, et al. (1999) Carcinoma-associated fibroblasts direct tumor progression of initiated human prostatic epithelium. Cancer Res 59: 5002–5011.
5. Bhowmick NA, Chytil A, Plieth D, Gorska AE, Dumont N, et al. (2004) TGF-beta signaling in fibroblasts modulates the oncogenic potential of adjacent epithelia. Science 303: 848–851.
6. Bierie B, Moses HL (2006) Tumour microenvironment: TGFbeta: the molecular Jekyll and Hyde of cancer. Nat Rev Cancer 6: 506–520.
7. Coussens LM, Werb Z (2002) Inflammation and cancer. Nature 420: 860–867.
8. Le Bitoux MA, Stamenkovic I (2008) Tumor-host interactions: the role of inflammation. Histochem Cell Biol 130: 1079–1090.
9. Saranac L, Bjelakovic B, Stamenkovic H, Kamenov B (2007) Orexitropic signaling proteins in obese children. ScientificWorldJournal 7: 1263–1271.
10. Chang HY, Sneddon JB, Alizadeh AA, Sood R, West RB, et al. (2004) Gene expression signature of fibroblast serum response predicts human cancer progression: similarities between tumors and wounds. PLoS Biol 2: E7.
11. Dvorak HF (1986) Tumors: wounds that do not heal. Similarities between tumor stroma generation and wound healing. N Engl J Med 315: 1650–1659.
12. Liotta LA, Kohn EC (2001) The microenvironment of the tumour-host interface. Nature 411: 375–379.
13. Ma XJ, Dahiya S, Richardson E, Erlander M, Sgroi DC (2009) Gene expression profiling of the tumor microenvironment during breast cancer progression. Breast Cancer Res 11: R7.
14. Finak G, Bertos N, Pepin F, Sadekova S, Souleimanova M, et al. (2008) Stromal gene expression predicts clinical outcome in breast cancer. Nat Med 14: 518–527.
15. Binkley CE, Zhang L, Greenson JK, Giordano TJ, Kuick R, et al. (2004) The molecular basis of pancreatic fibrosis: common stromal gene expression in chronic pancreatitis and pancreatic adenocarcinoma. Pancreas 29: 254–263.
16. Bacac M, Provero P, Mayran N, Stehle JC, Fusco C, et al. (2006) A mouse stromal response to tumor invasion predicts prostate and breast cancer patient survival. PLoS ONE 1: e32.
17. Allinen M, Beroukhim R, Cai L, Brennan C, Lahti-Domenici J, et al. (2004) Molecular characterization of the tumor microenvironment in breast cancer. Cancer Cell 6: 17–32.
18. Farmer P, Bonnefoi H, Anderle P, Cameron D, Wirapati P, et al. (2009) A stroma-related gene signature predicts resistance to neoadjuvant chemotherapy in breast cancer. Nat Med 15: 68–74.
19. Ramaswamy S, Ross KN, Lander ES, Golub TR (2003) A molecular signature of metastasis in primary solid tumors. Nat Genet 33: 49–54.
20. Levanon D, Groner Y (2004) Structure and regulated expression of mammalian RUNX genes. Oncogene 23: 4211–4219.
21. Levanon D, Brenner O, Negreanu V, Bettoun D, Woolf E, et al. (2001) Spatial and temporal expression pattern of Runx3 (Aml2) and Runx1 (Aml1) indicates non-redundant functions during mouse embryogenesis. Mech Dev 109: 413–417.
22. Bauer M, Su G, Casper C, He R, Rehrauer W, et al. Heterogeneity of gene expression in stromal fibroblasts of human breast carcinomas and normal breast. Oncogene 29: 1732–1740.
23. van de Vijver MJ, He YD, van't Veer LJ, Dai H, Hart AA, et al. (2002) A gene-expression signature as a predictor of survival in breast cancer. N Engl J Med 347: 1999–2009.
24. Glinsky GV, Berezovska O, Glinskii AB (2005) Microarray analysis identifies a death-from-cancer signature predicting therapy failure in patients with multiple types of cancer. J Clin Invest 115: 1503–1521.
25. Erkan M, Kleeff J, Gorbachevski A, Reiser C, Mitkus T, et al. (2007) Periostin creates a tumor-supportive microenvironment in the pancreas by sustaining fibrogenic stellate cell activity. Gastroenterology 132: 1447–1464.
26. Horiuchi K, Amizuka N, Takeshita S, Takamatsu H, Katsuura M, et al. (1999) Identification and characterization of a novel protein, periostin, with restricted expression to periosteum and periodontal ligament and increased expression by transforming growth factor beta. J Bone Miner Res 14: 1239–1249.
27. Baril P, Gangeswaran R, Mahon PC, Caulee K, Kocher HM, et al. (2007) Periostin promotes invasiveness and resistance of pancreatic cancer cells to hypoxia-induced cell death: role of the beta4 integrin and the PI3k pathway. Oncogene 26: 2082–2094.
28. Gillan L, Matei D, Fishman DA, Gerbin CS, Karlan BY, et al. (2002) Periostin secreted by epithelial ovarian carcinoma is a ligand for alpha(V)beta(3) and alpha(V)beta(5) integrins and promotes cell motility. Cancer Res 62: 5358–5364.
29. Bao S, Ouyang G, Bai X, Huang Z, Ma C, et al. (2004) Periostin potently promotes metastatic growth of colon cancer by augmenting cell survival via the Akt/PKB pathway. Cancer Cell 5: 329–339.
30. Ismail RS, Baldwin RL, Fang J, Browning D, Karlan BY, et al. (2000) Differential gene expression between normal and tumor-derived ovarian epithelial cells. Cancer Res 60: 6744–6749.
31. Sasaki H, Yu CY, Dai M, Tam C, Loda M, et al. (2003) Elevated serum periostin levels in patients with bone metastases from breast but not lung cancer. Breast Cancer Res Treat 77: 245–252.
32. Shao R, Bao S, Bai X, Blanchette C, Anderson RM, et al. (2004) Acquired expression of periostin by human breast cancers promotes tumor angiogenesis through up-regulation of vascular endothelial growth factor receptor 2 expression. Mol Cell Biol 24: 3992–4003.
33. Yoshioka N, Fuji S, Shimakage M, Kodama K, Hakura A, et al. (2002) Suppression of anchorage-independent growth of human cancer cell lines by the TRIF52/periostin/OSF-2 gene. Exp Cell Res 279: 91–99.
34. Tilman G, Mattiussi M, Brasseur F, van Baren N, Decottignies A (2007) Human periostin gene expression in normal tissues, tumors and melanoma: evidences for periostin production by both stromal and melanoma cells. Mol Cancer 6: 80.
35. Michaylira CZ, Wong GS, Miller CG, Gutierrez CM, Nakagawa H, et al. Periostin, a cell adhesion molecule, facilitates invasion in the tumor microenvironment and annotates a novel tumor-invasive signature in esophageal cancer. Cancer Res 70: 5281–5292.

Figure S1

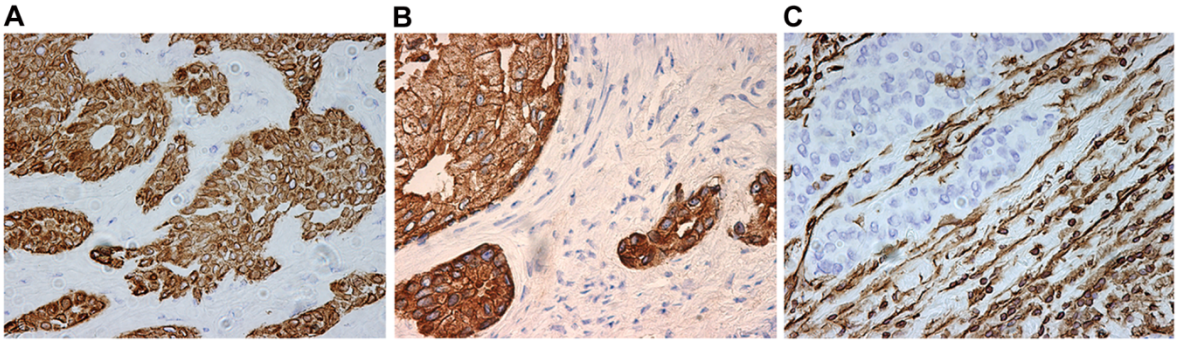

Figure S2

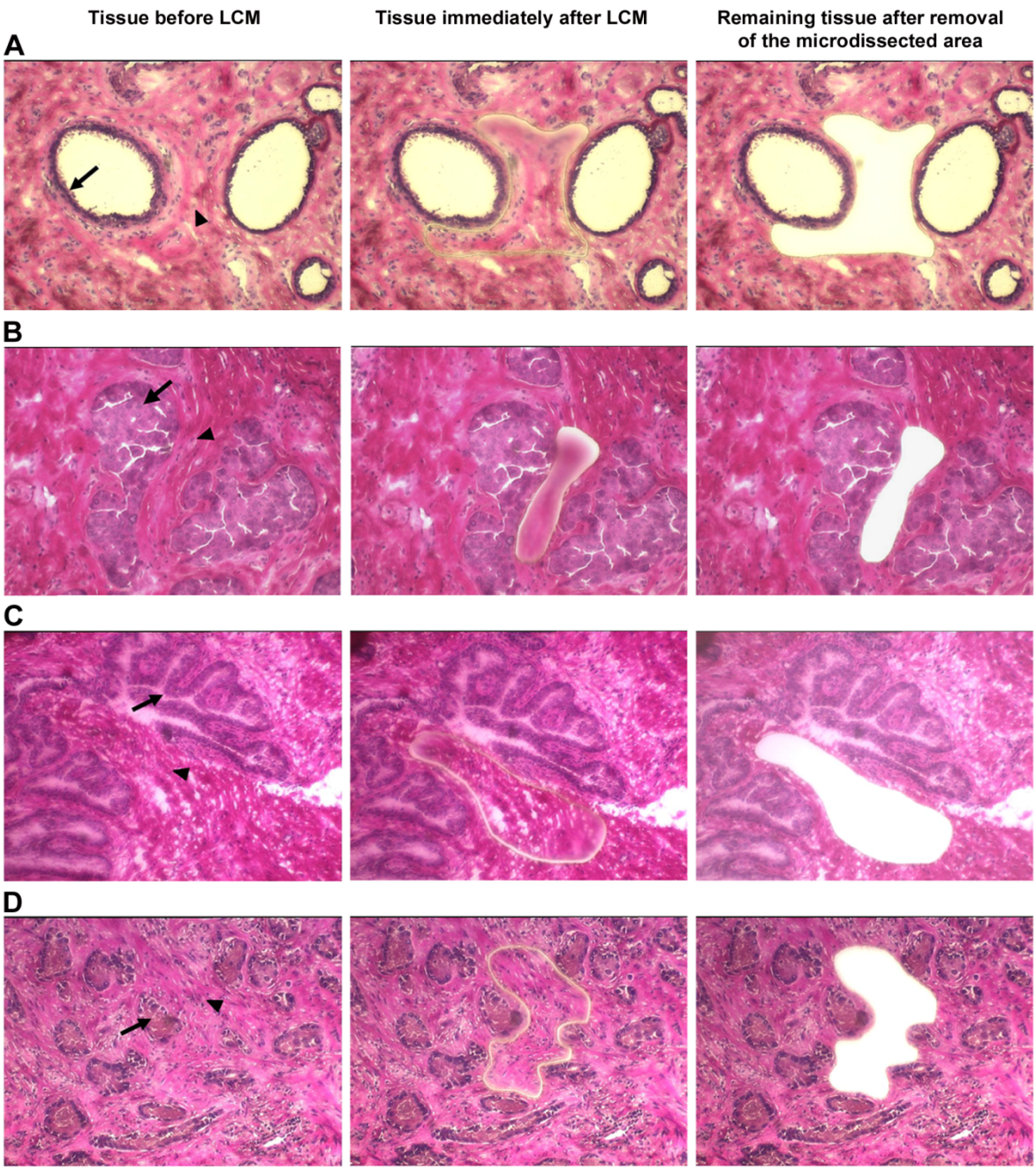
Tissue before LCM
Tissue immediately after LCM
Remaining tissue after removal of the microdissected area
A
B
C
D

Figure S3

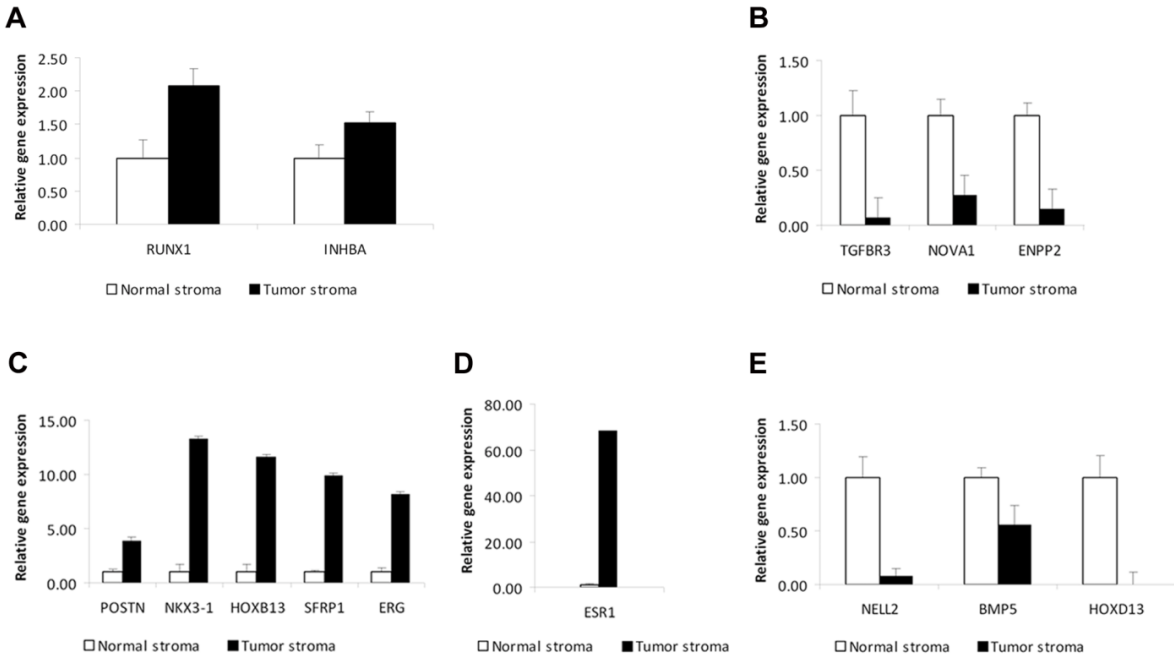
A
Relative gene expression
2.50
2.00
1.50
1.00
0.50
0.00
RUNX1
INHBA
Normal stroma
Tumor stroma
B
Relative gene expression
1.50
1.00
0.50
0.00
TGFBR3
NOVA1
ENPP2
Normal stroma
Tumor stroma
C
Relative gene expression
15.00
10.00
5.00
0.00
POSTN
NKX3-1
HOXB13
SFRP1
ERG
Normal stroma
Tumor stroma
D
Relative gene expression
80.00
60.00
40.00
20.00
0.00
ESR1
Normal stroma
Tumor stroma
E
Relative gene expression
1.50
1.00
0.50
0.00
NELL2
BMP5
HOXD13
Normal stroma
Tumor stroma

Table S1. Histopathological classification of **A**, infiltrating breast ductal carcinoma and **B**, invasive prostate carcinoma patients used in the present study.

A

Tumor stage	Patient age	ER	PR	HER-2
pT1b, pN1 mi (sn), Mx	51	100%	100%	0
pT1c, pN2, Mx, R0, G2	56	90%	95%	0
pT1c, pN1a (1/9), Mx, G2, R0	70	90%	70%	1+
pT3, pN1a (1/9), Mx, G2, R0	90	100%	0%	2+
pT2, pN1a (3/14), Mx	57	0%	0%	0
pT2, pN0, pMx	47	100%	100%	0

B

Tumor stage	Patient age	Gleason
pT2c, pN0	56	7
pT3a, pN0, Mx	58	4+4=8
pT2c, pN0 (0/7), Mx, R1	60	7
pT3a, pN0 (0/6), Mx	74	7
pT2c, pN0 (0/8), Mx, R1	62	7
pT3a, pN0, Mx	75	4+4=8

PART 2: GLG1 AND THE CONTROL OF THE SECRETORY PATHWAY IN TUMOR CELLS

Introduction

The first tumor-associated microenvironment study conducted in our laboratory was performed on mouse microdissected stroma at the primary tumor site and highlighted a mouse stromal signature with predictive value for patient outcome [15]. Particular attention was subsequently paid to one such identified gene called securin (*PTTG1*). Securin is primarily known as an anaphase inhibitor that regulates normal chromosome segregation by recruiting and controlling the proteolytic activity of separase (ESPL1). Interestingly, both molecules were observed to be abundantly expressed within the cytoplasm of human tumor cell lines, with a localization that outlines the biosynthetic/secretory pathways. Further investigation showed that securin and separase depletion impairs constitutive protein secretion and endocytic degradative and recycling pathways, uncovering an unexpected implication of securin and separase in membrane trafficking control in mammalian cells, including tumor cells [52].

Large-scale co-immunoprecipitation was then performed to uncover new binding partners of separase, and identified many non-nuclear proteins as candidate interactors of separase. Among them was the Golgi apparatus protein 1 (GLG1), a type I transmembrane protein, that caught our attention. GLG1 was first identified as a conserved membrane sialoglycoprotein of the rat Golgi apparatus and called MG-160 [53]. MG-160 was subsequently found to be homologous to two apparently unrelated molecules [54, 55], the E-selectin ligand 1 (ESL-1), a glycoprotein identified on mouse myeloid cells [56], and the avian cysteine-rich fibroblast growth factor (FGF) receptor (CFR) [57]. Divergent data have been reported concerning the subcellular localization and function of GLG1. As an E-selectin ligand, GLG1 is predicted to be expressed at the cell surface of leukocytes to mediate rolling on endothelial cells that express E-selectin. In non-myeloid cells such as fibroblast-like COS cells or chinese hamster ovary (CHO) cells, GLG1 was observed to be primarily located in the Golgi complex [58], with some studies reporting that it might be secreted as well [59, 60]. Suggested functions of GLG1 related to its Golgi localization include a role in the secretion of various FGFs [58, 59] and in the processing and secretion of TGF-β [61, 62]. These data suggest that GLG1 is a multifunctional and bitopic protein of the Golgi apparatus and the

plasma membrane whose definitive function and localization are probably cell type- and context-dependent.

Based on these observations, GLG1 was proposed to play a role in tumor progression by regulating intracellular FGF levels [63, 64] or through its selectin binding activity [65]. Others, however, suggested that GLG1 is not associated with prostate tumor progression and metastasis [66]. To validate GLG1 as a relevant candidate for further analysis, an experimental metastasis assay was performed in our laboratory to investigate the ability of cells depleted in GLG1 to colonize lungs after their injection into the blood circulation of NOD/SCID mice. This pilot experiment showed that silencing of GLG1 in MDA-MB-231 breast cancer cells and HT-1080 fibrosarcoma cells led to a reduced number of lung metastases. The metastatic lesions derived from GLG1-depleted cells were confined to blood vessels with less infiltration of the parenchyma than those derived from control cells. These observations correlated with impaired migratory capacity of GLG1-depleted cells observed in wounding experiments *in vitro*. Surprisingly, staining of lymph nodes adjacent to the lungs revealed frequent infiltration by tumor cells depleted of GLG1 but almost never by control cells.

These preliminary data prompted us to investigate the functional role of GLG1 in tumor cells that remains largely unknown. As a cell surface protein, GLG1 could play a direct role in mediating tumor cell adhesion to endothelium, as it appears to do in leukocytes [56, 67]. By contrast, an intracellular, Golgi localization would argue in favor of an indirect, but no less important, role of GLG1 in tumor progression by affecting trafficking of key molecules implicated in cell migration. Therefore, the first aim of the study was to define the subcellular localization of GLG1 in tumor cells. Immunofluorescence microscopy analysis was performed in several diverse tumor cell lines (the cervical carcinoma cell line HeLa, HT-1080, MDA-MB-231 and the osteosarcoma cell line MNNG/HOS) in each of which GLG1 displayed Golgi localization. This observation was further supported by immunohistochemical analysis of human cancer samples that revealed a similar pattern of GLG1 expression. These observations suggested that the main function of GLG1 in tumor cells is likely to be Golgi related.

The Golgi apparatus, a polarized complex that is central to the biosynthetic/secretory pathways (Figure 6 A), serves as a processing (mainly glycosylation) and sorting station in the transport of most transmembrane and soluble proteins. The sorting and packaging of cargo

molecules to their final destination, including the endosomes, the plasma membrane, the preceding Golgi cisternae or the endoplasmic reticulum (ER), take place in the last compartment of the Golgi, the *trans*-Golgi network (TGN) [68, 69]. Cargo packaging into budding transport carriers and dissociation of these carriers from TGN by membrane fission require complex machinery of which ADP-ribosylation factor (ARF) proteins as well as their regulators and effectors are part. There are six mammalian ARF proteins divided into Class I (ARF1-3), Class II (ARF4-5) and Class III (ARF6), each displaying a distinct cellular distribution that may be an important determinant for dictating unique function. ARF proteins regulate membrane trafficking and organelle structure by recruiting cargo-sorting coat proteins, modulating membrane lipid composition and interacting with cytoskeletal factors. Inactive, GDP-bound ARFs are recruited to specific membrane domains. In their GDP-bound state, ARF membrane association is reversible but may be stabilized upon exchange of GDP for GTP (Figure 6 B). The resulting activation is mediated by guanine nucleotide-exchange factors (GEFs) (Figure 6 C) that are also recruited to specific sites through as yet unknown mechanisms. Tight spatial and temporal control of the interactions of ARF proteins with their many GEFs, GTPase-activating proteins (GAPs) and effectors is required for proper coordination of membrane trafficking (Figure 6 A) [70, 71].

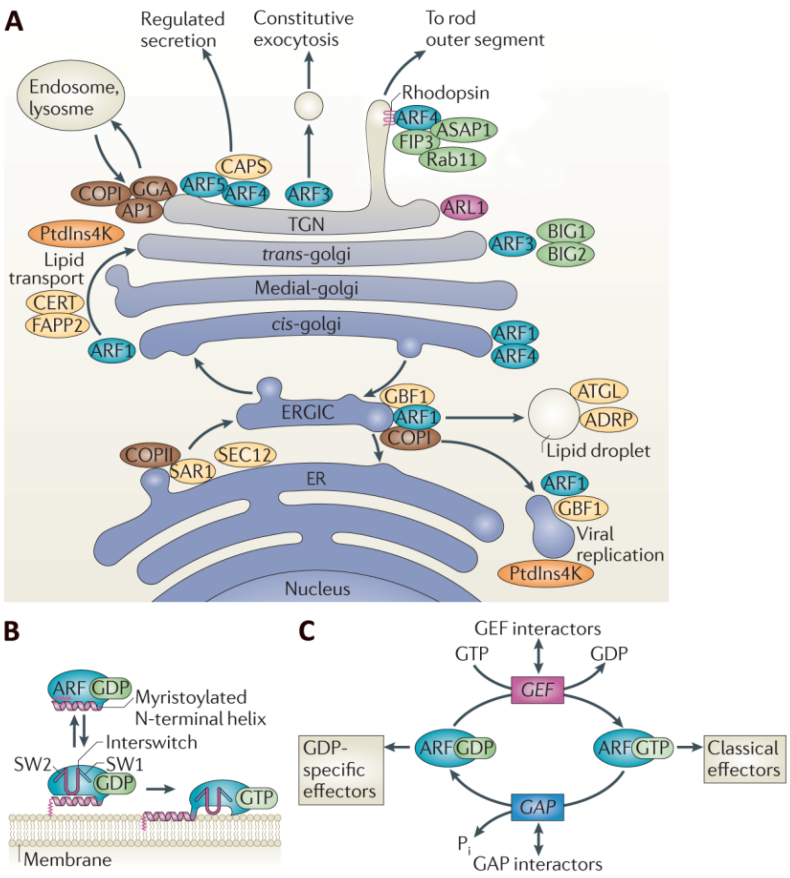

Figure 6. ARFs and the biosynthetic/secretory pathways. (A) ARF proteins display distinct localizations and functions in the ER-Golgi system. (B) The nature of ARF association with the membrane depends on its activation status. (C) ARF GTP exchange and hydrolysis are mediated by guanine nucleotide-exchange factors (GEFs) and GTPase-activating proteins (GAPs), respectively. Adapted from [70].

Increasing evidence suggests that intracellular trafficking is deregulated in cancer cells. Accelerated receptor recycling and increased secretion of growth factors, adhesion receptors and matrix components are believed to be required for malignant cell survival, growth and dissemination. In light of our preliminary observations and because of its privileged position in the secretory pathway of tumor cells, we put forth the hypothesis that GLG1 may be involved in the trafficking of molecules implicated in tumor cell migration and set out to identify the underlying molecular mechanism.

Results summary

In order to address the function of GLG1 in tumor cells, its localization was assessed in a panel of human tumor samples as well as in different tumor cell lines. Immunohistochemical analysis of human breast and prostate carcinoma, Ewing's sarcoma and glioblastoma showed a peri-nuclear staining pattern by anti-GLG1 antibody consistent with Golgi localization (Figure 7 A-D). Immunofluorescence analysis of three unrelated tumor cell lines (HeLa, HT1080 and MDA-MB-231 cell lines) confirmed this assumption by revealing an exclusively intracellular GLG1 signal that co-localized with that of the Golgi marker TGN46 (Figure 7 E-G for HeLa cells). To explore its intracellular function, GLG1 expression was silenced using two different GLG1-specific siRNA oligonucleotides. Effective GLG1 silencing using one or the other siRNA induced statistically significant fragmentation of the Golgi as quantified from TGN46 immunofluorescence labeling images (Figure 7 H-J).

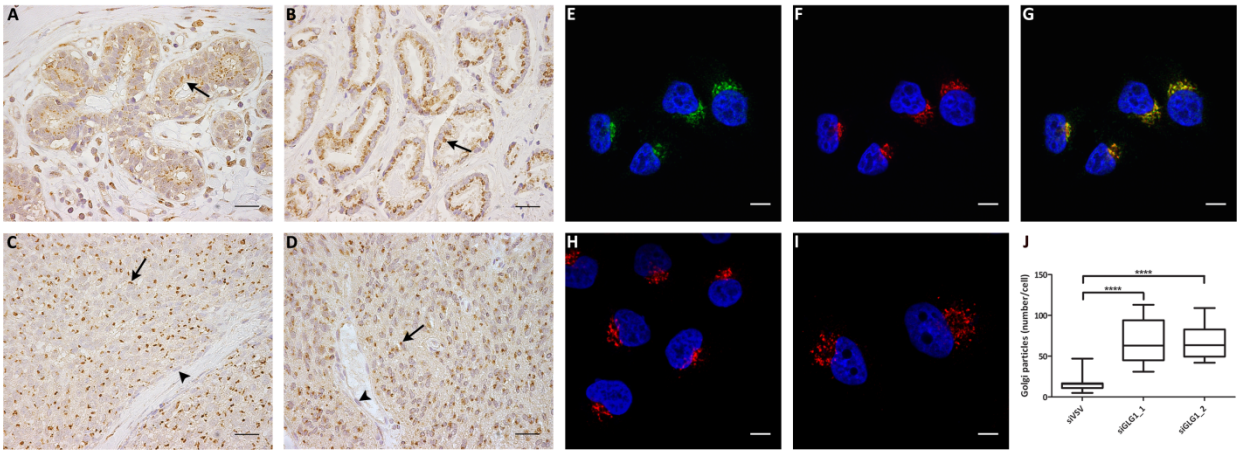

Figure 7. GLG1 and the Golgi apparatus. (A-D) Immunohistochemistry of human (A) breast and (B) prostate carcinoma, (C) Ewing's sarcoma and (D) glioblastoma using anti-human GLG1 antibody (brown) shows a staining pattern consistent with the Golgi complex in tumor cells in all samples (arrows) but not in endothelial cells of Ewing's sarcoma and glioblastoma where staining is absent (arrowheads). (E-G) Representative confocal micrographs of HeLa cells stained with antibodies against GLG1 (green, E) and the Golgi marker TGN46 (red, F) showing predominant Golgi localization of GLG1 as highlighted by colocalization of both signals (yellow) in merged images (G). (H-I) Representative confocal micrographs of HeLa cells stained with anti-TGN46 antibody showing markedly altered Golgi architecture upon GLG1 depletion (I) compared to siVSV control cells (H). DNA is stained by DAPI (blue). Scale bars: 20 µm (A-D), 8 µm (E-I). (J) Quantitative analysis of Golgi fragmentation revealing highly significant increase of the number of TGN46-positive particles when GLG1 is depleted using two different siRNAs ($n \geq 155$ cells, ****$P < 0.0001$ by Student's t-test).

As perturbation of the Golgi morphology observed upon GLG1 silencing is reminiscent of that induced by Brefeldin A-inhibited guanine nucleotide-exchange protein 1 (BIG1) silencing [72] and by expression of a dominant negative mutant of ARF3, [N126I]ARF3 [73], the putative functional relationship between GLG1 and the cytosolic proteins BIG1 and ARF3 was investigated. Analysis of protein-protein interaction by co-immunoprecipitation

revealed that the cytosolic tail of GLG1 is necessary and sufficient to mediate interaction with BIG1 (Figure 8 A). Proximity ligation assay (PLA) confirmed the interaction between GLG1 and BIG1 in an *in vivo* setting and localized it to the Golgi apparatus (Figure 8 B-C). These observations suggested that GLG1 might act as a docking site for BIG1 at the Golgi membrane. They were supported by cell fractionation experiments that showed a decrease of the BIG1 protein in the membrane fraction upon GLG1 depletion and its concomitant increase in the cytosolic fraction (Figure 8 D-E). In addition, expression of a GLG1 mutant composed of the transmembrane and cytoplasmic domains only (GLG1_CT) was shown to be sufficient to rescue the siRNA-induced phenotype (Figure 8 D-E), underscoring the importance of the cytosolic domain of GLG1 for the recruitment of BIG1 to the membrane.

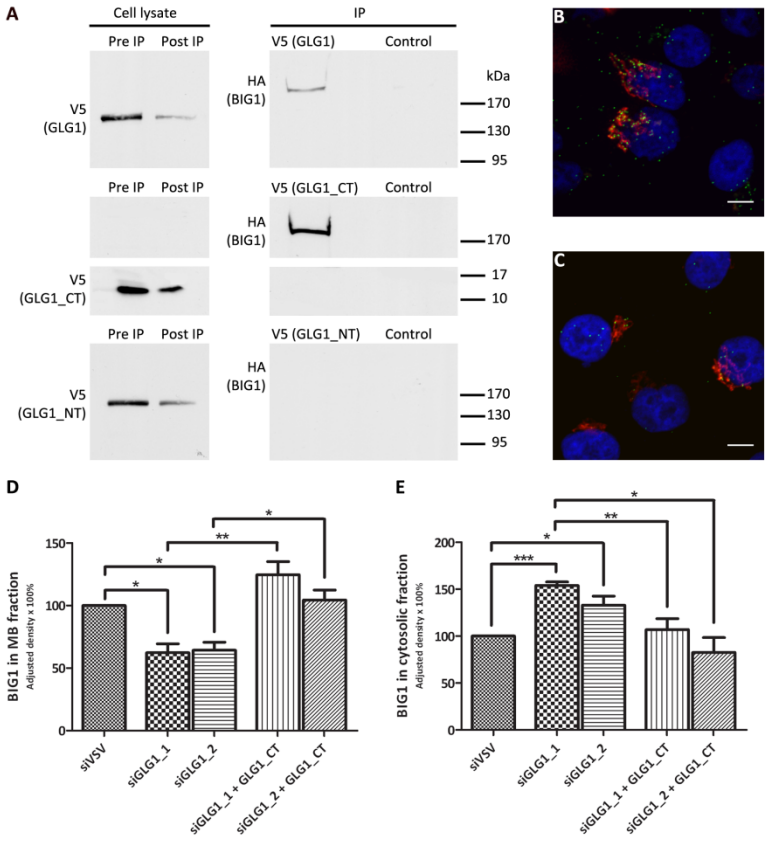

Figure 8. GLG1 interacts with and recruits BIG1 to membranes via its cytosolic tail. (A) V5-tagged full-length GLG1, and GLG1 deletion mutants composed of the transmembrane and cytoplasmic domains only (GLG1_CT) or transmembrane and luminal domains only (GLG1_NT) were co-expressed with wild type HA-tagged BIG1 in HEK293T cells. Anti-V5 immunoprecipitation of V5-tagged wild type GLG1 (top panels), GLG1_CT (middle panels) and GLG1_NT (bottom panels) followed by Western blotting using anti-HA antibody revealing interaction of wild type GLG1 and GLG1_CT, but not of GLG1_NT with BIG1 (right panels). Left panels show successful depletion of GLG1 in the post immunoprecipitation (Post IP) lysates compared to input lysates. As control, Flag-tagged wild type or mutant GLG1 were co-expressed with HA-tagged BIG1 and samples were subsequently processed as above using anti-V5 antibody coated beads. (B-C) Representative confocal micrographs of PLA showing Golgi localized (red staining) interactions (green dots) between GLG1 and BIG1 in HeLa cells transfected with V5-tagged (B) or Flag-tagged (D, control) GLG1 and HA-tagged BIG1 and infected with CellLight Golgi-RFP BacMam. PLA was performed using mouse anti-V5 and rabbit anti-BIG1 antibody. DNA is stained by DAPI (blue). Scale bars: 8 µm. (D-E) Cell fractionation experiment showing decreased BIG1 in the membrane fraction (D) and simultaneous increase in the cytosolic fraction (E) of HeLa cells upon GLG1 silencing using two different siRNAs (siGLG1_1

and siGLG1_2) compared to control (siVSV). The siGLG1-induced phenotype could be rescued by expression of GLG1_CT (D-E, siGLG1_1/_2 + GLG1_CT). Data were normalized to transferrin receptor (TfR) for the membrane fraction and to tubulin for the cytosolic fraction. Results represent mean values ± s.e.m. ($n \geq 3$, *P<0.05, **P<0.01, ***P<0.001 by Student's *t*-test).

To analyze the relationship between GLG1 and ARF3, cell fractionation was performed and depletion of GLG1 or BIG1 using two different siRNAs for each was observed to redistribute ARF3 from the membrane to the cytosolic fraction (Figure 9 A-B). Given the established role of BIG1 as an ARF3 GEF at the Golgi membrane [74], activation status of ARF3 was examined upon GLG1 or BIG1 silencing. Depletion of BIG1 or GLG1 was shown to significantly decrease the amount of active, GTP-bound ARF3 (Figure 9 C). Expression of the GLG1_CT mutant in endogenous GLG1-depleted cells was shown to be sufficient to restore a level of active ARF3 similar to that in control cells (Figure 9 C).

Because ARF proteins are important for vesicular trafficking, the impact of GLG1 depletion on constitutive secretion was addressed. Whereas neither the integral membrane protein VSV-G nor the soluble protein ss-HRP was affected by GLG1 silencing, reduction of MMP-9 secretion was observed in siGLG1-treated HT-1080 cells (Figure 9 D).

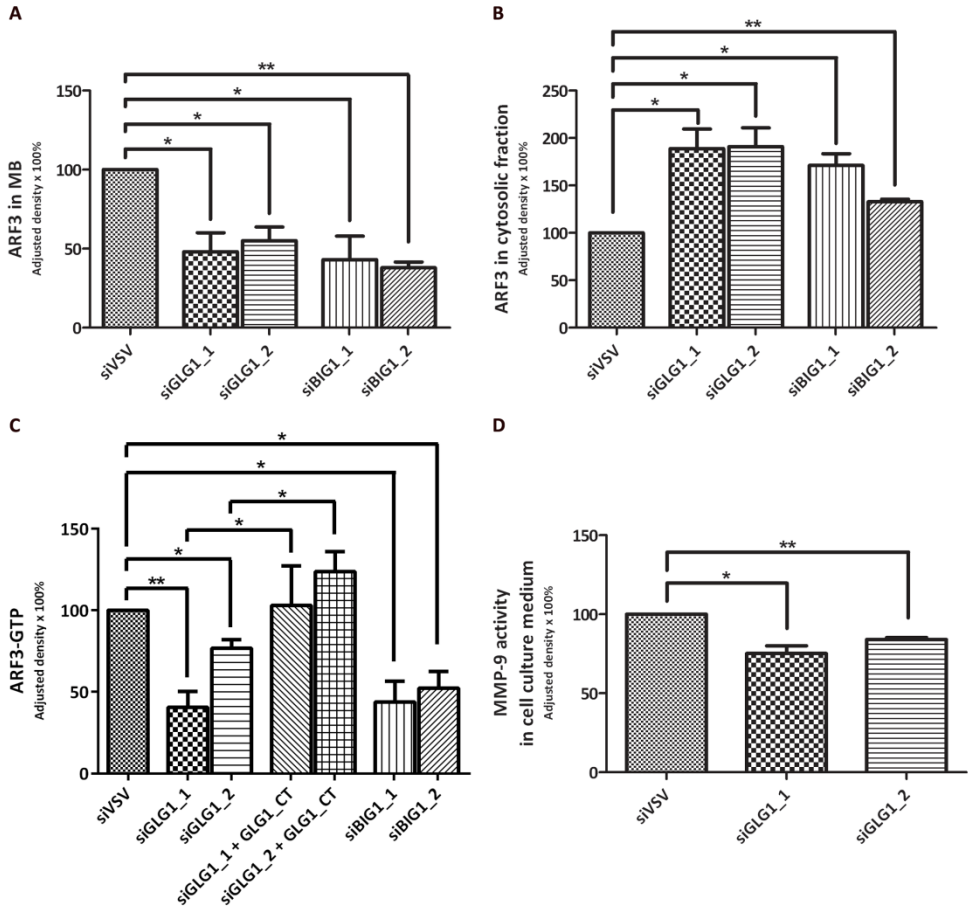

Figure 9. GLG1 is implicated in stable ARF3 binding to the membrane and its activation, and in MMP-9 secretion. (A-B) Cell fractionation experiment showing decreased ARF3 in the membrane fraction (A) and simultaneous increase in the cytosolic fraction (B) upon GLG1 or BIG1 silencing using two different siRNAs (siGLG1_1, siGLG1_2 and siBIG1_1, siBIG1_2) in HeLa cells transiently transfected with ARF3. Data were normalized to transferrin receptor (TfR) for the membrane fraction and to tubulin for the cytosolic fraction and subsequently adjusted to total ARF3. Results represent mean values ± s.e.m. ($n \geq 3$, *P<0.05, **P<0.01 by Student's *t*-test). (C) ARF3-GTP pull-down using HeLa cells transiently transfected with ARF3 showing significant decrease of GTP-bound ARF3 in GLG1- (siGLG1_1/_2) and BIG1- (siBIG1_1/_2) depleted cells compared to control cells (siVSV). The siGLG1-induced phenotype can be rescued by expression of GLG1_CT (siGLG1_1/_2 + GLG1_CT). Data were normalized to total ARF3. Results represent mean values ± s.e.m. ($n \geq 3$, *P<0.05, **P<0.01 by Student's *t*-test). (D) 48 h post siRNA transfection, HT-1080 cells were incubated overnight in fresh DMEM containing 0.1% BSA and 5 nM PMA. Conditioned media were collected and MMP-9 secretion quantitated by its enzymatic activity on zymogram gels, showing reduced MMP-9 secretion upon GLG1-silencing. Data were normalized to total protein content of cell lysates. Results represent mean values ± s.e.m. ($n \geq 3$, *P<0.05, **P<0.01 by Student's *t*-test).

The key findings of this work were that:

- GLG1 is localized to the Golgi apparatus of tumor cells
- GLG1 participates in BIG1 and ARF3 recruitment to the Golgi membrane and subsequent ARF3 activation
- Depletion of GLG1 decreases MMP-9 secretion in HT-1080 cells

Discussion and perspectives

During progression, tumor and associated stromal cells undergo important genetic, metabolic and morphological modifications that further sustain tumor growth and dissemination. Major features of cancer cells include increased and sustained division capacity, evasion from growth suppressors, resistance to cell death and subversion of the microenvironment to their own advantage. To fulfill the requirements inherent to these traits, tumor cells need to boost intrinsic cellular mechanisms and can also reactivate dormant developmental programs. Tumor cells thus display enhanced recycling of adhesion molecules, including integrins, and increased secretion of growth factors, adhesion receptors and matrix components, as mentioned before. Often neglected is the notion that all these processes require efficient, and probably enhanced, membrane trafficking.

In the present work, the investigation of the specific role played by GLG1 in tumor cells led us to enter the field of membrane trafficking. Indeed, GLG1 was shown to be mostly Golgi localized in diverse tumor cells, suggesting a role in processing and/or secretion of proteins. Further analysis uncovered interaction between GLG1 and the ARF GEF BIG1 that was previously shown to specifically activate ARF3 [74]. The main function of GEFs is to ensure precise temporal and spatial activation of small GTP-binding proteins, including ARFs. ARFs, especially ARF1-5, have long been thought to display overlapping and redundant functions. However, increasing evidence suggests only partial functional overlap among ARFs of Class I and II in membrane trafficking within the Golgi, with different ARFs fulfilling distinct roles [73]. Individual ARFs may also display multiple functions depending on the context and the associated regulatory network. Appropriate ARF function thus requires tight regulation, which is mediated at several levels by ARF GEFs, ARF GAPs and downstream effectors that contribute to specific ARF activation [75]. For instance, recruitment of selected ARF GEFs to specific membrane locations through defined, as yet unknown membrane receptors, is a key regulatory event [74]. The capacity of individual ARF proteins to assume multiple functions and the redundancy, although restricted, observed among ARFs limit the impact of a defect that affects a single ARF through compensatory mechanisms. However, deletion or knock-down of single ARF family member can also result in pronounced phenotypes as illustrated by several ARF and ARF-like (ARFL) gene homozygous or heterozygous knock-out mouse models. ARF4 was shown to regulate dendritic spine development [76], a process that

involves membrane trafficking, whereas *ARF6*$^{-/-}$ mouse embryos exhibit abnormal liver with reduced size and aberrant structure [77]. In addition, absence of an ARF-like protein, ARL3, was shown to affect the transport of photopigments in photoreceptors, among other defects [78]. These data underline the importance of single ARF proteins whose loss may severely impair specific cellular processes. Interestingly, two ARF GEFs have been associated with neuronal diseases. Mutations in BIG2 are linked to autosomal recessive periventricular heterotopia (ARPH), a disease in which neurons fail to migrate to the cortex because of impairment in vesicular trafficking that affects their adhesive properties [79, 80]. Mutations in the members of the BRAG family of ARF6 GEFs are implicated in mental retardation [81] and long-term depression [82] by affecting ARF6 activation and related endocytosis process.

The phenotypes observed in ARF knock-out mouse models and in ARF GEF-related diseases underscore the significance of efficient and tightly regulated membrane trafficking to maintain homeostasis. Whereas deletions or mutations of ARF or ARF-GEF proteins seem to result in a loss of function in membrane trafficking, membrane traffic deregulation in tumor cells is more likely to consist of a gain of function. Indeed, enhanced secretion of growth factors and proteases as well as increased recycling of adhesion molecules have already been implicated in tumor progression [6, 16, 83]. In addition, recent studies showed that tumor cells might also display quantitative and qualitative alterations in released exosomes, a class of extracellular vesicles that are derived from the endomembrane system and that support tumor growth and metastasis. These tumor-derived exosomes were shown to induce a pro-angiogenic signaling program in the microenvironment [84], to educate the bone marrow toward a pro-metastatic phenotype [85] and to condition lymph nodes [86]. These observations reveal the capacity of tumor-excreted material to subvert and educate the tumor environment toward a pro-tumorigenic state, underscoring the relevance of the secretion pathways in the mediation of tumor-host interactions.

Our observations support the notion that GLG1 may be a Golgi membrane receptor, implicated in the recruitment of BIG1 to membranes of specific Golgi compartments. Depletion of GLG1 was shown to decrease membrane association of BIG1 and to reduce the pool of active, GTP-bound ARF3 resulting in impairment of MMP-9 secretion. No general effect on constitutive secretion was observed suggesting that GLG1 may be involved in the secretion of a specific subset of molecules that includes MMP-9. It would therefore be of

interest to identify other molecules whose secretion requires GLG1 and to determine whether these proteins are unrelated or whether, on the contrary, they are functionally related. To help identify these molecules, proteomic analysis of the secretome of tumor cells depleted of GLG1 is currently being pursued.

The data presented here describe a functional mechanism associated with the small cytosolic tail of GLG1. However, the functions associated with the large intraluminal domain of GLG1 remain unidentified and will require further investigation. One hypothesis may be that GLG1 serves as a link between the biosynthetic and secretory pathways. Newly synthesized proteins that arrived from the ER and passed through the Golgi stacks may come into contact with the intraluminal domain of GLG1. GLG1 may thus help trap specific proteins at a defined location where it can simultaneously recruit, via its C-terminal tail, the cytosolic machinery necessary for vesicle formation and subsequent secretion. GLG1 may thus be important to coordinate the physical segregation of given cargo molecules at a specific membrane domain and vesicle budding initiation.

The novel role of GLG1 presented here was uncovered in tumor cells. The expression level of GLG1 was observed to vary considerably between different tumor cell lines. Further analysis of GLG1 mRNA expression level within a number of malignancies using Oncomine[2] database identified Ewing's sarcoma (later referred as ESFT for Ewing's sarcoma family tumors) as one tumor type that display elevated expression of GLG1. Interestingly, GLG1 was observed to be selectively overexpressed in ESFT compared to other sarcomas. This observation correlates with the work of Baird *et al*. that identified GLG1 in a list of genes that discriminate ESFT form other sarcomas [87]. ESFT contain a specific chromosomal translocation that leads to the expression of the oncogenic EWS-FLI1 fusion protein. Interestingly, in the work published by Kauer *et al.*, a decrease of GLG1 expression is observed upon EWS-FLI1 knock-down [88], suggesting that GLG1 could be a candidate EWS-FLI1 target gene. In addition, another microarray analysis showed that GLG1 is overexpressed in ESFT metastatic tumors versus ESFT localized tumors and that it is involved in neither response of primary tumors to polychemotherapy nor to *in vitro* toxicity [89].

Previously, our group focused on the identification of the primary cell from which ESFT originates. Primary data revealed that expression in human mesenchymal stem cells (MSC)

[2] http://www.oncomine.org

of EWS-FLI1 can be stably maintained and resulted in transformation with the emergence of morphological and gene expression hallmarks of ESFT. The similarities were further highlighted by expressing the fusion gene in human pediatric MSC (hpMSC) and by maintaining these cells under reprogramming medium culture conditions [90]. Interestingly, analysis of the microarray data revealed that hpMSC expressing EWS-FLI1 overexpress GLG1 under reprogramming medium compared to serum-supplemented culture conditions. In addition, GLG1 overexpression is dependent on the expression of EWS-FLI1 because it is not observed in the absence of the fusion gene in reprogramming compared to normal medium culture conditions. Again, these observations show that GLG1 behave like an EWS-FLI1 target gene. If GLG1 turns out to be functionally related to Ewing sarcomagenesis, it will be interesting to determine whether its implication is also related to membrane trafficking or to some other functions. Preliminary immunohistochemical and immunofluorescence analyses of ESFT samples and cell lines, respectively, revealed a Golgi localization of GLG1, suggesting a role related to its newly identified Golgi function. But the possibility cannot be excluded that in response to specific stimuli, GLG1 may be translocated to the cell surface of ESFT cells where it could display distinct functions, including cell adhesion-related properties. ESFT cells are described as small round blue cells, a morphological appearance reminiscent of that of leukocytes in which GLG1 presents E-selectin ligand activity. Leukocytes travel in the blood stream and extravasate at sites of inflammation with the help of selectin-ligand interactions. Similarly, in ESFT cells, which present the particularity to preferentially disseminate through hematogenous routes, a pool of GLG1 may be present at the cell surface under certain circumstances and therefore may participate in tumor dissemination as a selectin ligand.

Finally, this work provides novel data regarding GLG1 while opening several avenues of investigations.

Original article

The Golgi protein GLG1 coordinates ARF3 activation by recruiting the guanine nucleotide-exchange factor BIG1 to the Golgi membrane

Anne Planche and Ivan Stamenkovic

Institute of Pathology, CHUV
and
Faculty of Biology and Medicine, University of Lausanne
Lausanne, Switzerland

Correspondence to Ivan Stamenkovic:

Tel : +41 21 314 7136
Fax : +41 21 314 7110
Email : Ivan.Stamenkovic@chuv.ch

The Golgi protein 1 (GLG1) is suggested to be an E-selectin ligand at the cell surface of leukocytes and an intracellular FGF receptor. Here we addressed the function of GLG1 in tumor cells where it is localized primarily in the Golgi. We show that GLG1 recruits the Brefeldin A-inhibited guanine nucleotide-exchange protein 1 (BIG1) to the Golgi membrane. GLG1-recruited BIG1 can then participate in the tethering of ADP-ribosylation factor 3 (ARF3) to the Golgi membrane and its activation. Depletion of GLG1 or BIG1 markedly reduced ARF3 membrane localization and activation and altered the Golgi structure. Interestingly, the observed morphological perturbation of the Golgi apparatus, a central component of intracellular trafficking, did not affect the secretory pathway in general, but rather seemed to impair secretion of selected molecules including gelatinase B, MMP-9. Our observations demonstrate that GLG1 is a membrane receptor for BIG1 and elucidate a GLG1-dependent mechanism of ARF3 activation.

Current opinion holds that GLG1, also known as E-selectin ligand 1 (ESL-1), cysteine-rich fibroblast growth factor receptor (CFR) and Golgi sialoglycoprotein MG-160, is a bitopic protein of the Golgi apparatus and the plasma membrane that fulfils distinct functions in each cellular compartment. GLG1 was described as a Golgi-localized fibroblast growth factor receptor (FGFR) [1] and MG-160 membrane protein [2], as well as a selectin ligand on surface of murine leukocytes [3]. Based on these observations, GLG1 was proposed to play a role in tumor progression by regulating intracellular trafficking of FGFs [4, 5] or through its selectin binding activity [6]. We therefore addressed the function of GLG1 in tumor cells by assessing its localization and identifying its putative molecular partners.

GLG1 localization was examined in a panel of human tumor samples and tumor cell lines. Immunohistochemical analysis of human breast and prostate carcinoma, as well as Ewing's sarcoma and glioblastoma cells showed peri-nuclear staining of the anti-GLG1 antibody, consistent with localization in the Golgi apparatus (Figure 1 A-D). This observation was further supported by immunofluorescence analysis that revealed co-localization of the GLG1 signal with that of the Golgi marker TGN46 in three unrelated tumor cell lines, including the cervical carcinoma HeLa (Figure 1 E-G), the fibrosarcoma HT1080 (Figure 1 H-J) and the breast carcinoma MDA-MB-231 cell lines (Figure 1 K-M). Interestingly, no plasma membrane staining was detected in any of the human tumor samples or the three cell lines analyzed, suggesting that the main function of GLG1 in tumor cells is likely to be Golgi related. To

obtain clues regarding its intracellular function, GLG1 expression was silenced using two different GLG1-specific siRNA oligonucleotide sequences. All experiments were performed 72 h following siRNA transfection, as endogenous GLG1 depletion was found to be maximal at this time point (Figure 2 H). Transient silencing of GLG1 using both siRNAs was observed to induce marked fragmentation the Golgi, as illustrated by TGN46 immunofluorescence labeling in all three cell lines (Figure 2 A-C, Supplemental Figure 1 A-F) and image quantification that revealed a significant increase in the number of TGN46-positive particles in GLG1-depleted compared to control HeLa cells (Figure 2 D). The Golgi ribbon is known to undergo disassembly during mitosis, with a fragmented and dispersed pattern appearing during metaphase that resembles, in part, the siGLG1-induced phenotype [7]. However, based on DAPI staining, the possibility that Golgi dispersion in response to GLG1 silencing was cell cycle dependent could be excluded, given that it was mainly observed in non-mitotic cells. We therefore investigated the functional role of GLG1 in the Golgi apparatus of tumor cells. As the location of GLG1 and the effect of its depletion were comparable in several diverse tumor cell lines, we conducted our experiments on HeLa cells that express an elevated level of GLG1 and are convenient for a broad range of *in vitro* experiments.

The Golgi fragmentation observed upon GLG1 depletion is reminiscent of that induced by silencing of BIG1 [8] and by expression of the dominant negative mutant of ARF3, [N126I]ARF3 [9]. To assess the effect of BIG1 depletion and dominant negative ARF3 expression in HeLa cells, transient transfection with BIG1 siRNA for 72 h, that lead to a greater than 85% reduction of BIG1 expression (Figure 2 H), or with [N126I]ARF3 for 48 h was performed followed by staining for TGN46. Depletion of BIG1 induced pronounced dispersion of the Golgi (Figure 2 E-G), whereas [N126I]ARF3 expression resulted in a more heterogeneous phenotype ranging from fragmentation (Figure 2 L-M) to almost complete disappearance of TGN46 staining (data not shown). This was probably due to variable expression of the mutant ARF3 in different cells. Perturbation of the Golgi morphology induced by [N126I]ARF3 expression was related to reduced ARF3 activity given that no incidence on the Golgi architecture could be observed when wild type ARF3 was overexpressed (Figure 2 I-K).

These observations prompted us to explore whether GLG1 may be functionally related to BIG1 and/or ARF3. HEK293T cells were used to transiently co-express proteins with high

efficiency for analysis of protein-protein interactions by co-immunoprecipitation. V5-tagged full-length GLG1, and GLG1 mutants composed of the transmembrane and cytoplasmic domains only (GLG1_CT) or transmembrane and luminal domains only (GLG1_NT) (Figure 3 A) were expressed along with HA-tagged BIG1, immunoprecipitated with anti-V5 antibody and immunoblotted with anti-HA antibody. Full-length GLG1 as well as GLG1_CT were observed to interact with BIG1, whereas no interaction was observed between BIG1 and GLG1_NT (Figure 3 B), indicating that the cytosolic domain of GLG1 is necessary and sufficient to mediate GLG1-BIG1 complex formation. The interaction was confirmed by immunoprecipitation with anti-HA antibody and immunoblotting with anti-V5 antibody (Supplemental Figure 2 A). We then used the proximity ligation assay (PLA) to validate and localize the interaction between GLG1 and BIG1 *in vivo*. GLG1 and BIG1 were transiently co-expressed in HeLa cells and BacMam technology was used simultaneously to specifically label the Golgi apparatus. PLA was performed immediately after fixation that preserved cellular morphology, sub-cellular organelles partitioning and correct protein location throughout the experiment. The results clearly revealed the Golgi localization of GLG1-BIG1 interaction (Figure 3 C-D), and given that BIG1 is a cytosolic protein, these observations suggest that GLG1 may act as a docking site for BIG1 at the Golgi membrane. This notion implies that the depletion of GLG1 should prevent translocation of BIG1 to membranes, keeping it cytosolic. To assess this hypothesis, cell fractionation experiments were performed. Post nuclear supernatants of GLG1-depleted cells were subjected to high-speed ultracentrifugation to separate the membranes from the cytosolic fraction. BIG1 was then quantified by Western blot analysis in each fraction. Consistent with our hypothesis, we observed that membrane association of BIG1 decreased upon GLG1 depletion (Figure 3 E) while its cytosolic level increased (Figure 3 F). In addition, the siRNA-induced phenotype could be rescued by expression of the GLG1_CT mutant that was not targeted by any of the GLG1 siRNAs (Figure 3 E-F), underscoring the notion that the cytosolic tail of GLG1 is responsible for the recruitment of BIG1 to the membrane.

Given the established role of BIG1 as a specific ARF3 guanine nucleotide-exchange factor (GEF) [10], we examined the possible functional relationship between BIG1, GLG1 and ARF3. Co-immunoprecipitation revealed interaction between GLG1 and ARF3 confirmed by immunoprecipitating GLG1 and blotting for ARF3 and vice-versa (Figure 4 A, Supplemental

Figure 2 B), as well as by PLA (Figure 4 B-C). The GLG1_CT mutant was found to be sufficient to mediate interaction with ARF3 (Figure 4 A, Supplemental Figure 2 B). However, no interaction could be observed between BIG1 and ARF3 by immunoprecipitation (Figure 4 A, Supplemental Figure 2 B), whereas PLA analysis was consistent with an interaction *in vivo* (Figure 4 D-E). This discrepancy may be explained by the nature of the interaction between BIG1 and ARF3 compared to that between GLG1 and ARF3. The principal function of BIG1 is to promote ARF3 activation by catalyzing the exchange of GDP for GTP, a process that requires transient interaction between the two molecules [11]. This interaction could thus be easily disrupted during immunoprecipitation, whereas it may be detected by PLA that works on intact cells and preserves weak interactions. Furthermore, ARF3 undergoes conformational changes upon GTP loading that is suggested to reinforce its contact with the membrane. This stabilized anchorage to the membrane may explain the interaction with the integral membrane protein GLG1 observed both by immunoprecipitation and PLA. These observations therefore uncover physical proximity between GLG1, BIG1 and ARF3, consistent with the concept of a complex whose formation may be initiated by GLG1-mediated recruitment of BIG1.

To gain further insight onto the relationship among GLG1, BIG1 and ARF3, cell fractionation was performed on siGLG1- and siBIG1-treated HeLa cells in which HA-tagged ARF3 was transiently expressed. Consistent with previous studies [10], BIG1 silencing was observed to redistribute ARF3 from the membrane to the cytosolic fraction. Similar results were obtained upon GLG1 silencing (Figure 4 F-G), implicating GLG1 in the regulation of ARF3 membrane recruitment as well. Together these data suggest that presence of BIG1 at the membrane, via its recruitment by GLG1, is needed for stable ARF3 binding to the membrane.

As already mentioned, tight membrane association requires ARF3 to be in its activated, GTP-bound state. We therefore examined the activation status of ARF3 upon silencing of GLG1 or BIG1 using two different siRNAs in each case. HeLa cells transiently silenced for GLG1 or BIG1 expression were transfected with HA-tagged ARF3 and a specific ARF-GTP pull-down was performed using the protein-binding domain (PDB) of ADP-ribosylation factor-binding protein GGA3 as bait. A significant decrease of GTP-bound ARF3 in GLG1- and BIG1-depleted cells was observed compared to control cells (Figure 4 H). Interestingly, in

agreement with previously published data [10], no decrease of ARF1 activity was observed upon either BIG1 or GLG1 depletion (Supplemental Figure 3), supporting the notion of a mechanism specific to ARF3. Requirement of GLG1 expression for the biological activity of ARF3 was validated by showing that expression of the GLG1_CT mutant in endogenous GLG1-depleted cells was sufficient to restore a level of active ARF3 similar to that in control cells (Figure 4 H).

ARF proteins are important for vesicular trafficking principally through the regulation of coated carrier vesicle formation, recruitment and activation of phosphatidylinositol (PtdIns) kinases and interaction with cytoskeletal factors [12]. Perturbation of their function would therefore be predicted to have an impact on the secretory pathway. To test whether the absence of GLG1, by decreasing ARF3 activity, may perturb constitutive secretion, we addressed the requirement of GLG1 for the transport of the integral membrane protein VSV-G and a soluble protein, horseradish peroxidase fused to a signal sequence (ss-HRP). HeLa cells expressing the GFP-tagged temperature-sensitive mutant (ts045)VSV-G were transfected with GLG1 or control siRNA. Cells were incubated at the non-permissive temperature to block the protein in the ER, and then shifted to permissive temperatures to monitor its trafficking along the secretory pathway. Transport of VSV-G was tracked by immunofluorescence and images were compared to those obtained with control cells. Trafficking of VSV-G protein to the cell surface was unaffected by any of the GLG1 siRNAs. Thus, VSV-G was first similarly arrested in the ER under all conditions after overnight incubation at 40°C, as assessed by co-staining with the ER marker KDEL (Figure 5 A). More remarkably, the protein was shown to accumulate in and be exported out of the dispersed TGN46-positive fragments resulting from GLG1 silencing as effectively as out of the conserved Golgi structure of control cells (Figure 5 B), reaching the plasma membrane with the same kinetics (Figure 5 C).

In parallel, ss-HRP expressing HeLa and HepG2 cells, that display high secretory properties, were transfected with a pool of GLG1 or control siRNA and release of ss-HRP into the medium was quantitated by its enzymatic activity. A pool of the two GLG1 siRNAs was used in this experiment to minimize off-target effects. No change in the quantity of ss-HRP activity was measured between cells transfected with GLG1 or control siRNA (Figure 5 D). Consistent with these observations, we observed that the *cis-trans* Golgi polarity was

maintained upon GLG1 silencing, despite the scattering of the Golgi apparatus. This was highlighted by immunofluorescence experiments in which cells were double-labeled with antibodies against a marker of the *cis*-Golgi (GM130) and a marker of the *trans*-Golgi network (TGN46). The two compartments were shown to remain clearly distinct even when the Golgi was fragmented due to the GLG1 depletion (Supplemental Figure 4), indicating that the Golgi polarity remained unaffected.

Although it is not yet clearly established, there is evidence that, despite some redundancy, each member of the ARF family may perform unique functions contrary to what was previously believed, in particular for ARF1 and ARF3 [9, 10]. Spatial and temporal ARF regulation by GEFs, GTPase-activating proteins (GAPs) and effectors may allow control of specific cargo sorting. According to this scenario, perturbation of ARF3 activity would most probably affect the secretion of a restricted and defined set of proteins rather than the overall secretory process as suggested by the absence of disruption of constitutive VSV-G and ss-HRP protein secretion. Previous data have shown that ARFs are implicated in MMP-9 secretion [13] and the work of Ho and colleagues [14] provided evidence of the specific role of ARF3 in the regulation of MMP-9 secretion in HT-1080 cells. We therefore assessed whether GLG1 silencing may impact MMP-9 secretion. HT-1080 cells were used instead of HeLa cells because of their higher MMP-9 expression level and secretion rate. HT-1080 cells were stimulated with phorbol 12-myristate 13-acetate (PMA) to enhance MMP-9 secretion that was then quantitated by its enzymatic activity on zymogram gels. Silencing of GLG1 using any of the siRNA oligonucleotides was observed to reduce MMP-9 secretion by 15% (siGLG1_2) to 25% (siGLG1_1) (Figure 5 E), whereas MMP-9 level in cell lysates was not affected (data not shown).

Increasing evidence suggests that endocytosis and membrane trafficking are deregulated in cancer cells. Because of their dependence on selected signaling pathways, tumor cells may need to rely on accelerated receptor recycling and increased secretion of a variety of molecules including matrix components, adhesion receptors and growth factors. This deregulated intracellular trafficking could strongly contribute to the malignant phenotype by conferring self-sufficiency and highly dynamic features to the tumor cells. To address the possible clinical relevance of GLG1 expression in tumor cells, GLG1 mRNA expression level was assessed within a number of malignancies using the Oncomine database. GLG1 was

found to be highly expressed in head and neck squamous cell carcinoma [15], melanoma [16] as well as in bladder carcinoma [17] compared to corresponding normal tissue (Supplemental Figure 5 A-C). Interestingly, a correlation was observed between GLG1 expression and tumor grade for melanoma (Supplemental Figure 5 B) and bladder carcinoma (Supplemental Figure 5 C). GLG1 was also shown to be highly expressed in sarcoma cell lines (Supplemental Figure 5 D) [18]. In addition, further analysis revealed that GLG1 is selectively elevated in Ewing's sarcoma compared to other sarcomas (Supplemental Figure 5 E) [19]. These observations are consistent with the possibility that GLG1 may be relevant for tumor progression *in vivo*, and more precisely for sarcomagenesis.

The results presented here provide insight into a novel and specific role of GLG1 in intracellular trafficking of tumor cells. Because of its privileged localization in the secretory pathway, we speculate that GLG1 may influence tumor progression by affecting trafficking of key molecules implicated in cell migration.

ACKNOWLEDGMENTS

We thank Jean-Christophe Stehle from Mouse Pathology Facility, Faculty of Biology and Medicine, University of Lausanne, Switzerland for immunohistochemistry. We also thank Marie-Aude Le Bitoux, Cynthia Dayer, Aurélie Formey de Saint Louvent and Phil Shaw for insightful discussions.

METHODS

Antibodies

Antibody concentrations were as follows. Immunohistochemistry: rabbit serum anti-GLG1 (1:2000, kindly provided by C. J. Dimitroff). Immunofluorescence: rabbit serum anti-GLG1 (1:2000), rabbit anti-TGN46 (1:200, Novus Biologicals), sheep anti-TGN46 (1:200, Novus Biologicals), mouse anti-GM130 (1:250, BD Biosciences), mouse anti-KDEL (1:100, Abcam); Alexa Fluor 488- and 594-conjugated secondary antibodies were used at 1:1,500 (Molecular Probes). Western blots: rabbit serum anti-GLG1 (1:3,000), rabbit anti-BIG1 (1:2,000, Abcam), mouse anti-V5 (1:5,000, Invitrogen), mouse anti-HA (1:1,000, Covance), mouse anti-Transferrin Receptor (TfR) (1:1,000, Invitrogen), mouse anti-tubulin (1:4,000, Calbiochem), mouse anti-GFP (1:1,000, Roche), rabbit anti-MMP-9 (1:5,000, Chemicon International), rabbit anti-CD81 (1:1000, Abcam); anti-rabbit and anti-mouse peroxidase-conjugated secondary antibodies were used at 1:10,000 (Dako) and 1:25,000 (GE Healthcare Life Sciences), respectively. PLA: Mouse anti-V5 (1:2,500), rabbit anti-BIG1 (1:3,500), rabbit anti-GLG1 (1:3,500), rabbit anti-GFP (1:2,000).

Plasmid construction

pLiVC vector was derived from pLVTHM lentiviral vector (Addgene) by removal of the shRNA cassette and GFP gene and insertion of a PGK-puromycin cassette. C-terminal V5- and Flag-tagged full-length GLG1 as well as the V5-tagged mutants lacking the cytosolic domain (GLG1_NT) or consisting of the transmembrane and cytosolic domains of GLG1 (GLG1_CT) were generated by PCR and inserted into pLiVC vector. ss-HRP and ts045-VSV-G-GFP plasmids were obtained from V. Malhotra, V5-tagged ARF1 from J. Gruenberg and GFP- and HA-tagged ARF3 from P. Melançon, and were all subcloned into the pLiVC vector. Dominant negative [N126I]ARF3 was created by site-directed mutagenesis (QuickChange Site-Directed Mutagenesis Kit, Stratagene). HA-tagged BIG1 construct was obtained from M. Vaughan.

Cell culture, transfection and infection

HeLa, HT-1080 and MDA-MB-231 cell lines were maintained in DMEM with 4.5 mg/ml of glucose (Invitrogen), supplemented with 10% fetal calf serum (FCS, PAA Laboratories) at 37°C in a 5% CO2 incubator. The medium was supplemented with 1% non-essential amino acids (NEAA, Invitrogen) for the HepG2 and HEK293T cell lines. Transient transfections were performed using Fugene (Roche) according to manufacturer's instructions. HeLa and HepG2

cells were infected using lentiviral particles produced by HEK293T cells transfected with ss-HRP or ts045-VSV-G-GFP constructs, followed by selection with 3.3 µg/ml and 2 µg/ml of puromycin, respectively.

siRNA oligonucleotide transfection

siRNA oligonucleotides (Qiagen) were transfected using INTERFERin (Polyplus-transfection). Transient GLG1 and BIG1 downregulation was achieved using two different oligonucleotides. siRNA oligonucleotides targeting GLG1 were GGCCAAGGATGATTCAGAA (siGLG1_1) and AGCTGACATTCCTAAATTC (siGLG1_2), and for BIG1 CCATGATTGTGAGGAAAAG (siBIG1_1) and AGCTGAATGGATGACAACA (siBIG1_2). siRNA oligonucleotide targeting VSV-G (siVSV, AAAGGAAACTGGAAAAATG) and AllStars Negative Control siRNA (Qiagen) were used as negative controls. Cells were transfected with siRNA oligonucleotides at a final concentration of 20 nM. When two siRNA oligonucleotides were pooled (siGLG1_pool), each oligonucleotide was used at a final concentration of 10 nM, giving a final total concentration of 20 nM.

Immunohistochemistry

Paraffin-embedded sections of human breast and prostate carcinoma, Ewing's sarcoma and glioblastoma were stained after citrate antigen retrieval with rabbit anti-GLG1 (1:2000) for 1 h. Horseradish peroxidase (HRP) staining was performed using EnVision Rabbit HRP (DAKO) and revealed with a DAKO DAB kit (DAKO).

Immunofluorescence microscopy

Cells grown on coverslips were fixed between 24 h and 72 h post transfection or infection with paraformaldehyde (PFA) 4% for 20 min at room temperature, washed and permeabilized with 0.3% Triton X-100 (Fluka) in blocking buffer (PBS–FCS 10%) for 3 min. Fixed cells were incubated with primary antibodies diluted in blocking buffer for 45 min at room temperature, washed, incubated with secondary antibodies for 45 min, washed, and mounted using Immu-Mount (ThermoShandon). DAPI (Roche) was used to visualize the nuclei. All images were acquired with a Zeiss LSM 710 Quasar confocal microscope using the ZEN 2009 software at the Core Imaging Facility of the University of Lausanne. The acquisition was performed in sequential mode to avoid the dye crosstalk.

Co-immunoprecipitation

48 h post transfection of plasmids encoded the tagged form of the proteins of interest, HEK293T cells were cooled down on ice and washed twice with cold PBS. Proteins were extracted in modified RIPA lysis buffer (50 mM Tris-HCl pH 7.4, 150 mM NaCl, 1 mM EDTA, 1% Triton X-100, protease inhibitor cocktail (Roche), 5 mM NaF, 5 mM β-glycerophosphate, 1 mM NaVO3) 10 min on ice and resulting extracts were centrifuged. Agarose or sepharose beads were added to the supernatants and discarded after 1 h of pre-clearing. Supernatants were quantified and equal amounts of lysates were used for immunoprecipitation with anti-V5 agarose beads (Sigma), anti-HA agarose beads (Roche) or with anti-GFP antibody bound to Protein G Sepharose (GE Healthcare). After overnight incubation at 4°C, beads were washed and proteins were eluted by boiling the beads for 5 min in sample buffer. Purified complexes were analysed by Western blotting.

Proximity ligation assay (PLA)

HeLa cells were transfected with plasmids encoded the tagged form of the proteins of interest. 48 h after transfection, cells were transferred to 16-well glass chamber slides (Lab-Tek). When indicated, cells were infected with CellLight Golgi-RFP BacMam (Life Technologies) at the time they were plated in the glass chamber slides. 24 h later, cells were fixed with 4% PFA, permeabilized with 0.3% Triton X-100 in PBS, and processed according to the Duolink In Situ PLA assay protocol (Olink Biosciences). Samples were analyzed with a confocal microscope.

Cell fractionation

HeLa cells were either transfected with siRNA for 72 h, or transfected with siRNA for 52 h and then transfected with HA-tagged ARF3 for an additional 20 h, or transfected with siRNA for 24 h and then infected with lentivirus carrying V5-tagged GLG1_CT cDNA for an additional 48 h. In all cases, 72 h after initial siRNA transfection, cells were cooled on ice for 5 min, rinsed twice with cold PBS, scraped, centrifuged for 5 min at 300g and resuspended in homogenization buffer (HB, 250 mM sucrose, 3 mM imidazole, pH 7.4). Post nuclear supernatant (PNS) was obtained by mechanical disruption of cells with a 22-G needle and centrifugation at 600g for 10 min. Membrane (MB) and cytosol were obtained from PNS subjected to high-speed ultracentrifugation (100,000g for 45 min) in a TLA-120.2 rotor (Beckmann Coulter Ultracentrifuge). All steps were performed at 4°C. Equal amounts of

proteins for all fractions were resolved on SDS-PAGE gradient gels an immunoblotting was performed using anti-BIG1, anti-HA (for ARF3), anti-TfR and anti-tubulin antibody. ImageJ program was used for bands quantitation. Density of the band of each condition was expressed relative to the band of the control sample (siVSV). Adjusted density values were then calculated by dividing the relative densities obtained for each condition by the relative densities for the corresponding TfR (for the MB) or tubulin (for the cytosol). For ARF3, the results were subsequently normalized to the relative density obtained for ARF3 in the PNS (total ARF3).

Active ARF pull-down

HeLa cells were either transfected with siRNA only for 72 h, or transfected with siRNA for 24 h and then infected with lentivirus carrying V5-tagged GLG1_CT cDNA for an additional 48 h. 52 h after initial siRNA transfection, cells were transfected with V5-tagged ARF1 or HA-tagged ARF3 for 20 h. As both active ARF1 and ARF3 can be pulled down with the protein-binding domain (PBD) of GGA3, active ARF1 as well as active ARF3 pull-down were carried out using the Active ARF1 Pull-down and Detection Kit (Thermo Scientific) according to the manufacturer's instructions. Whole cell lysates and pull-down samples were resolved on SDS-PAGE gel. Immunoblotting was conducted using anti-V5 or anti-HA antibody and ImageJ program was used for quantitation. Density of the band of each condition was expressed relative to the band of the control sample (siVSV). Adjusted density values were then calculated by dividing the relative densities obtained for each pull-down by the relative densities obtained for ARF1 or ARF3 in the corresponding whole cell lysate samples.

ts045VSV-G-GFP transport assay

Temperature-sensitive mutant (ts045)VSV-G-GFP expressing HeLa cells were grown on coverslips and transfect with siRNA. 48 h after transfection, cells were incubated overnight at 40°C, leading to the retention of the ts045VSV-G-GFP protein in the ER. After the addition of 100 µg/ml of cycloheximide, the temperature was shifted to 20°C and the cells incubated for 2 h, allowing the protein to be exported out of the ER and to concentrate in the Golgi apparatus. The temperature was then raised to 31.5°C for 1 h 20 min to let the protein exit the Golgi and reach the cell surface. The cells were fixed at the indicated time points and then processed for confocal microscopy.

ss-HRP secretion assay

Activity of horseradish peroxidase fused to a signal sequence (ss-HRP) was measured from supernatants of ss-HRP expressing HeLa and HepG2 cells 72 h after siRNA transfection in 12-well plates. Briefly, the culture medium was replaced by 500 µl of fresh medium and the cells were incubated for 6 h. 5 µl of supernatant was then collected and added to 100 µl of ECL reagent (Western Lightning Ultra Extreme Sensitivity Chemiluminescence substrate, PerkinElmer). Luminescence was measured with a microplate reader and normalized to total protein content.

MMP-9 secretion and activity assay

48 h after siRNA transfection, HT-1080 cells were washed with PBS and incubated overnight in DMEM supplemented with 0.1% BSA (Sigma) and containing phorbol 12-myristate 13-acetate (PMA) at a final concentration of 5 nM. Conditioned media were collected and loaded with non-reducing sample buffer (10% SDS, 4% sucrose, 1.5 M Tris-HCl pH 8.8, Bromophenol Blue) on zymogram gels. After running, gels were incubated 30 min at room temperature in zymogram renaturing buffer (2.5% Triton X-100 (v:v) in water) and then 30 min in developing buffer. Gels were incubated overnight in fresh developing buffer at 37°C. Finally, gels were fixed (40% ethanol, 10% acetic acid) and stain with EZBlue Gel Staining Reagent (Sigma). Gels were scanned and ImageJ program was used for quantitation. Density of the band of each condition was expressed relative to the band of the control sample (siVSV) and results were adjusted to total protein content. In parallel, cells were lysed using EDTA-free lysis buffer and MMP-9 level assessed by Western blotting.

Statistical analysis

All experiments were performed at least three times, independently. Statistical analysis was carried out using GraphPad Prism 5 software. For cell fractionation, active ARF3 pull-down and MMP-9 secretion experiments, two-tailed, paired Student's t-test was used to test the difference between control (siVSV) and siRNA data, while two-tailed unpaired Student's t-test was applied when comparing siRNA and rescue (GLG1_CT) data. For quantitative analysis of the Golgi fragmentation, the same threshold was applied to all images and the number of Golgi-derived particles per cell was determined using the Analyze Particles function of ImageJ software. Statistical analysis was performed by two-tailed unpaired Student's t-test.

REFERENCES

1. Burrus, L.W., et al., Identification of a cysteine-rich receptor for fibroblast growth factors. Mol Cell Biol, 1992. 12(12): p. 5600-9.
2. Gonatas, J.O., et al., MG-160. A novel sialoglycoprotein of the medial cisternae of the Golgi apparatus [published eeratum appears in J Biol Chem 1989 Mar 5;264(7):4264]. J Biol Chem, 1989. 264(1): p. 646-53.
3. Levinovitz, A., et al., Identification of a glycoprotein ligand for E-selectin on mouse myeloid cells. J Cell Biol, 1993. 121(2): p. 449-59.
4. Yamaguchi, F., et al., Identification of MG-160, a FGF binding medial Golgi sialoglycoprotein, in brain tumors: an index of malignancy in astrocytomas. Int J Oncol, 2003. 22(5): p. 1045-9.
5. Crnogorac-Jurcevic, T., et al., *Gene expression profiles of pancreatic cancer and stromal desmoplasia.* Oncogene, 2001. 20(50): p. 7437-46.
6. Antoine, M., et al., Expression of E-selectin ligand-1 (CFR/ESL-1) on hepatic stellate cells: implications for leukocyte extravasation and liver metastasis. Oncol Rep, 2009. 21(2): p. 357-62.
7. Colanzi, A. and D. Corda, *Mitosis controls the Golgi and the Golgi controls mitosis.* Curr Opin Cell Biol, 2007. 19(4): p. 386-93.
8. Boal, F. and D.J. Stephens, Specific functions of BIG1 and BIG2 in endomembrane organization. PLoS One, 2010. 5(3): p. e9898.
9. Volpicelli-Daley, L.A., et al., Isoform-selective effects of the depletion of ADP-ribosylation factors 1-5 on membrane traffic. Mol Biol Cell, 2005. 16(10): p. 4495-508.
10. Manolea, F., et al., Arf3 is activated uniquely at the trans-Golgi network by brefeldin A-inhibited guanine nucleotide exchange factors. Mol Biol Cell, 2010. 21(11): p. 1836-49.
11. Cherfils, J. and P. Melancon, On the action of Brefeldin A on Sec7-stimulated membrane-recruitment and GDP/GTP exchange of Arf proteins. Biochem Soc Trans, 2005. 33(Pt 4): p. 635-8.
12. Donaldson, J.G. and C.L. Jackson, ARF family G proteins and their regulators: roles in membrane transport, development and disease. Nat Rev Mol Cell Biol, 2011. 12(6): p. 362-75.
13. Williger, B.T., W.T. Ho, and J.H. Exton, Phospholipase D mediates matrix metalloproteinase-9 secretion in phorbol ester-stimulated human fibrosarcoma cells. J Biol Chem, 1999. 274(2): p. 735-8.
14. Ho, W.T., J.H. Exton, and B.T. Williger, Arfaptin 1 inhibits ADP-ribosylation factor-dependent matrix metalloproteinase-9 secretion induced by phorbol ester in HT 1080 fibrosarcoma cells. FEBS Lett, 2003. 537(1-3): p. 91-5.
15. Cromer, A., et al., Identification of genes associated with tumorigenesis and metastatic potential of hypopharyngeal cancer by microarray analysis. Oncogene, 2004. 23(14): p. 2484-98.
16. Talantov, D., et al., Novel genes associated with malignant melanoma but not benign melanocytic lesions. Clin Cancer Res, 2005. 11(20): p. 7234-42.

17. Dyrskjot, L., et al., Gene expression in the urinary bladder: a common carcinoma in situ gene expression signature exists disregarding histopathological classification. Cancer Res, 2004. 64(11): p. 4040-8.
18. Garnett, M.J., et al., Systematic identification of genomic markers of drug sensitivity in cancer cells. Nature, 2012. 483(7391): p. 570-5.
19. Baird, K., et al., Gene expression profiling of human sarcomas: insights into sarcoma biology. Cancer Res, 2005. 65(20): p. 9226-35.

FIGURE LEGENDS

Figure 1.

Golgi localization of GLG1 in human tumor samples and tumor cell lines. (A-D) Immunohistochemistry of human (A) breast and (B) prostate carcinoma, (C) Ewing's sarcoma and (D) glioblastoma using anti-human GLG1 antibody (brown) shows a staining pattern consistent with the Golgi complex in tumor cells in all samples (arrows) but not in endothelial cells of Ewing's sarcoma and glioblastoma where staining is absent (arrowheads). (E-M) Representative confocal micrographs of (E-G) HeLa, (H-J) HT-1080 and (K-M) MDA-MB-231 cells stained with antibodies against GLG1 (green) and the Golgi marker TGN46 (red) showing predominant Golgi localization of GLG1 as highlighted by colocalization of both signals (yellow) in merged images (G, J, M). DNA is stained by DAPI (blue). Scale bars: 20 µm (A-D), 8 µm (E-M).

Figure 2.

Absence of GLG1 profoundly affects Golgi morphology mimicking the effect of BIG1 silencing and ARF3 dominant negative expression. (A-C) Representative confocal micrographs of HeLa cells stained with anti-TGN46 antibody showing markedly altered Golgi architecture upon GLG1 depletion using two different siRNAs, namely siGLG1_1 (B) and siGLG1_2 (C) compared to siVSV control cells (A). (D) Quantitative analysis of Golgi fragmentation revealing highly significant increase of the number of TGN46-positive particles when GLG1 is depleted using two different siRNAs ($n \geq 155$ cells, $^{****}P < 0.0001$ by Student's *t*-test). (E-G) Representative confocal micrographs showing similar Golgi scattering phenotype in HeLa cells upon silencing of BIG1 with two different siRNAs (F-G) compared to control cells (E). (H) Western blot analysis showing GLG1 and BIG1 depletion 72 h after transfection of two different siRNAs compared to the control siVSV. Anti-tubulin immunoblots were used as loading controls. Arrow denotes GLG1 while the asterisk indicates an unspecific band due to cross-reactivity of anti-GLG1 antibody with an unidentified protein. (I-M) Representative confocal micrographs of HeLa cells transfected with (I) empty vector, (J-K) GFP-tagged wild type ARF3 or (L-M) GFP-tagged dominant negative [N126I]ARF3. Staining with anti-TGN46 antibody shows Golgi dispersion when dominant negative ARF3 is expressed (M). Wild type ARF3 (K) or empty vector (I) have no effect. DNA is stained by DAPI (blue). Scale bars: 8 µm.

Figure 3.

GLG1 interacts with and recruits BIG1 to membranes via its cytosolic tail. (A) Constructs encoding full-length GLG1, a GLG1 deletion mutant lacking the cytosolic tail (GLG1_NT) and a GLG1 deletion mutant lacking the intraluminal domain (GLG1_CT). All constructs are C-terminally tagged. (B) Wild type and mutant V5-tagged GLG1 were co-expressed with wild type HA-tagged BIG1 in HEK293T cells. Anti-V5 immunoprecipitation of V5-tagged wild type GLG1 (top panels), GLG1_CT (middle panels) and GLG1_NT (bottom panels) followed by Western blotting using anti-HA antibody revealing interaction of wild type GLG1 and GLG1_CT, but not of GLG1_NT with BIG1 (right panels). Left panels show successful depletion of GLG1 in the post immunoprecipitation (Post IP) lysates compared to input lysates. As control, Flag-tagged wild type or mutant GLG1 were co-expressed with HA-tagged BIG1 and samples were subsequently processed as above using anti-V5 antibody coated beads. (C-D) Representative confocal micrographs of PLA showing Golgi localized (red staining) interactions (green dots) between GLG1 and BIG1 in HeLa cells transfected with V5-tagged (C) or Flag-tagged (D, control) GLG1 and HA-tagged BIG1 and infected with CellLight Golgi-RFP BacMam. PLA was performed using mouse anti-V5 and rabbit anti-BIG1 antibody. DNA is stained by DAPI (blue). Scale bars: 8 μm. (E-F) Cell fractionation experiment showing decreased BIG1 in the membrane fraction (E) and simultaneous increase in the cytosolic fraction (F) of HeLa cells upon GLG1 silencing using two different siRNAs (siGLG1_1 and siGLG1_2) compared to control (siVSV). The siGLG1-induced phenotype could be rescued by expression of GLG1_CT (E-F, siGLG1_1/_2 + GLG1_CT). Data were normalized to transferrin receptor (TfR) for the membrane fraction and to tubulin for the cytosolic fraction. Results represent mean values ± s.e.m. ($n \geq 3$, *P<0.05, **P<0.01, ***P<0.001 by Student's *t*-test).

Figure 4.

GLG1 and BIG1 form a complex with ARF3 and are both necessary for ARF3 activation and stable binding to the membrane. (A) V5-tagged GLG1 or GLG1_CT were co-expressed with HA-tagged ARF3 and HA-tagged BIG1 was co-expressed with GFP-tagged ARF3 in HEK293T cells. Anti-V5 immunoprecipitation of V5-tagged GLG1 (top panels) and V5-tagged GLG1_CT (middle panels) followed by Western blotting using anti-HA antibody revealing interaction of GLG1 and GLG1_CT with ARF3. Anti-HA antibody immunoprecipitation of HA-tagged BIG1 (bottom panels) followed by Western blotting using anti-GFP antibody showing

absence of interaction between BIG1 and ARF3. Left panels show successful depletion of GLG1 or BIG1 in the post immunoprecipitation (Post IP) lysates compared to input lysates. As control, Flag-tagged GLG1 and BIG1 were co-expressed with ARF3 and samples were subsequently processed as above using anti-V5 beads (GLG1, GLG1_CT) or anti-HA beads (BIG1). (B-E) Representative confocal micrographs of PLA showing interaction (red dots) between GLG1 and ARF3 (B-C) and between BIG1 and ARF3 (D-E) in HeLa cells transfected with GFP-tagged (B) or HA-tagged (C, control) ARF3 and V5-tagged GLG1, and with GFP-tagged (D) or HA-tagged (E, control) ARF3 and HA-tagged BIG1. PLA was performed using mouse anti-GFP and rabbit anti-GLG1 or anti-BIG1 antibody. DNA is stained by DAPI (blue). Scale bars: 8 µm. (F-G) Cell fractionation experiment showing decreased ARF3 in the membrane fraction (F) and simultaneous increase in the cytosolic fraction (G) upon GLG1 or BIG1 silencing using two different siRNAs (siGLG1_1, siGLG1_2 and siBIG1_1, siBIG1_2) in HeLa cells transiently transfected with ARF3. Data were normalized to transferrin receptor (TfR) for the membrane fraction and to tubulin for the cytosolic fraction and subsequently adjusted to total ARF3. Results represent mean values ± s.e.m. ($n \geq 3$, *P<0.05, **P<0.01 by Student's *t*-test). (H) ARF3-GTP pull-down using HeLa cells transiently transfected with ARF3 showing significant decrease of GTP-bound ARF3 in GLG1- (siGLG1_1/_2) and BIG1- (siBIG1_1/_2) depleted cells compared to control cells (siVSV). The siGLG1-induced phenotype can be rescued by expression of GLG1_CT (siGLG1_1/_2 + GLG1_CT). Data were normalized to total ARF3. Results represent mean values ± s.e.m. ($n \geq 3$, *P<0.05, **P<0.01 by Student's *t*-test).

Figure 5.

GLG1 depletion does not impair overall constitutive protein secretion but specifically perturb MMP-9 secretion. (A-C) Representative confocal micrographs showing VSV-G transport from ER to plasma membrane. 48 h after siRNA transfection (top panels: ALL STAR control, middle panels: siGLG1_1, bottom panels: siGLG1_2), cells were incubated overnight at 40°C (A) and then cultivated 2 h at 20°C in the presence of cycloheximide (B) and finally shifted to 31.5°C for 1 h 20 (C). Following each incubation time, some cells were fixed, permeabilized and labelled with antibody to the ER (anti-KDEL antibody, A, red) or the *trans*-Golgi network (anti-TGN46 antibody, B, red) showing colocalization of VSV-G with the different markers in all conditions, as well as same plasma membrane pattern (C), indicating

normal VSV-G transport. Scale bars: 8 µm. (D) ss-HRP expressing HeLa and HepG2 cells were transfected with a pool of GLG1 (siGLG1_pool) or control siRNA (siVSV) for 72 h after what medium was replaced and cells further incubated for 6 h. Release of ss-HRP into the medium was quantitated by its enzymatic activity showing no difference between cells transfected with GLG1 or control siRNA. Data were normalized to total protein content of cell lysates. Results represent mean values ± s.e.m. (E) 48 h post siRNA transfection, HT-1080 cells were incubated overnight in fresh DMEM containing 0.1% BSA and 5 nM PMA. Conditioned media were collected and MMP-9 secretion quantitated by its enzymatic activity on zymogram gels, showing reduced MMP-9 secretion upon GLG1-silencing. Data were normalized to total protein content of cell lysates. Results represent mean values ± s.e.m. ($n \geq 3$, *P<0.05, **P<0.01 by Student's *t*-test).

Supplemental Figure 1.

Absence of GLG1 profoundly affects Golgi morphology in unrelated tumor cell lines. (A-F) Representative confocal micrographs of HT-1080 (A-C) and MDA-MB-231 (D-F) stained with anti-TGN46 antibody showing markedly altered Golgi architecture upon GLG1 depletion using two different siRNAs, namely siGLG1_1 and siGLG1_2 (B-C and E-F) compared to siVSV control cells (A and D). DNA is stained by DAPI (blue). Scale bars: 8 µm.

Supplemental Figure 2.

The relationship between GLG1, BIG1 and ARF3 as assessed by co-immunoprecipitation. (A) Wild type HA-tagged BIG1 was co-expressed with wild type and mutant V5-tagged GLG1 in HEK293T cells. Anti-HA immunoprecipitation of wild type HA-tagged BIG1 followed by Western blotting using anti-V5 antibody confirming interaction of BIG1 with wild type GLG1 (top panels) and GLG1_CT (middle panels) but not with GLG1_NT (bottom panels). Left panels show successful depletion of BIG1 in the post immunoprecipitation (Post IP) lysates compared to input lysates. As control, irrelevant HA-tagged protein was co-expressed with wild type or mutant GLG1 and samples were subsequently processed in the same way using anti-HA beads. (B) For co-immunoprecipitation, HA-tagged ARF3 was co-expressed with V5-tagged GLG1 or GLG1_CT and GFP-tagged ARF3 was co-expressed with HA-tagged BIG1 in HEK293T cells. Anti-HA immunoprecipitation of HA-tagged ARF3 followed by Western blotting using anti-V5 antibody confirmed interaction of ARF3 with GLG1 (top panels) and GLG1_CT (middle panels). Anti-GFP immunoprecipitation of GFP-tagged ARF3 (bottom

panels) followed by Western blotting using anti-HA antibody showing absence of interaction between ARF3 and BIG1. Left panels show successful depletion of ARF3 in the post immunoprecipitation (Post IP) lysates compared to input lysates. As control, ARF3 presenting irrelevant, GFP (top and middle panels) or HA (bottom panels) tag were co-expressed with GLG1 or BIG1 and samples were subsequently processed in the same way using anti-HA beads (GLG1, GLG1_CT) or anti-GFP beads (BIG1).

Supplemental Figure 3.

Absence of GLG1 or BIG1 does not induce a decrease of ARF1 activity. ARF1-GTP pull-down using HeLa cells transiently transfected with ARF1 showing no decrease of GTP-bound ARF1 in GLG1- (siGLG1_1/_2) and BIG1- (siBIG1_1/_2) depleted cells compared to control cells (siVSV). Data were normalized to total ARF1. Results represent mean values ± s.e.m.

Supplemental Figure 4.

***Cis-trans* polarity is maintained in Golgi fragments induced by GLG1 silencing.** Representative confocal micrographs of control (left) and GLG1-depleted (right) HeLa cells double-labeled with antibodies against a marker of the *cis*-Golgi (GM130, green) and a marker of the *trans*-Golgi network (TGN46, red). The two compartments are clearly distinct indicating an unaffected Golgi polarity. Zoom on details are shown in insets. DNA is stained by DAPI (blue). Scale bars: 5 µm.

Supplemental Figure 5.

Oncomine data regarding GLG1 gene expression level in normal human tissues, tumor samples and tumor cell lines. GLG1 expression is higher in head and neck squamous cell carcinoma (A), cutaneous melanoma (B) and bladder carcinoma (C) than in corresponding normal tissues. (D) GLG1 is more strongly expressed in sarcoma cell lines compared to other non-sarcoma cell lines and (E) more highly expressed in Ewing's sarcoma than in other sarcomas.

FIGURES

Figure 1.

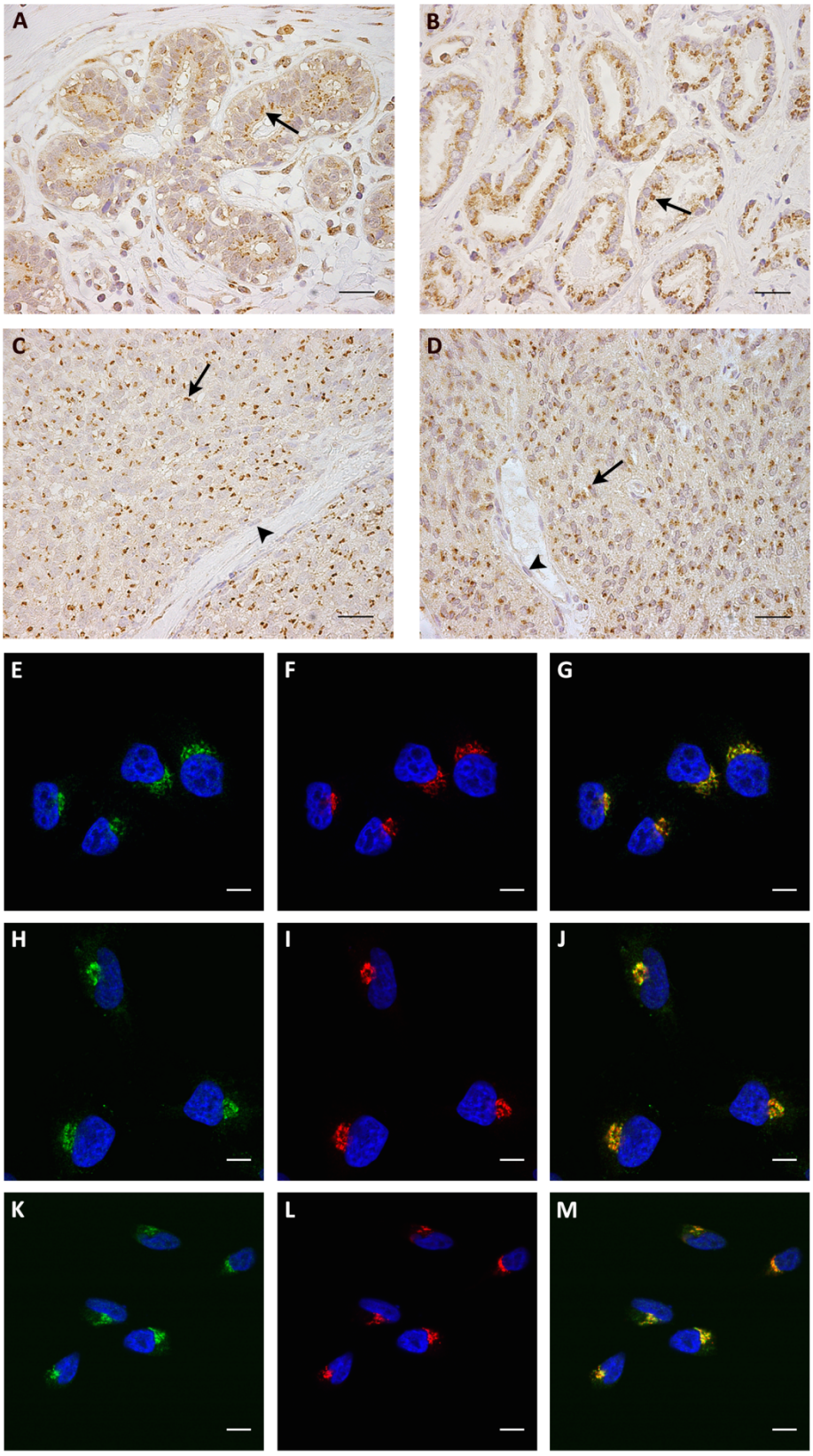

Figure 2.

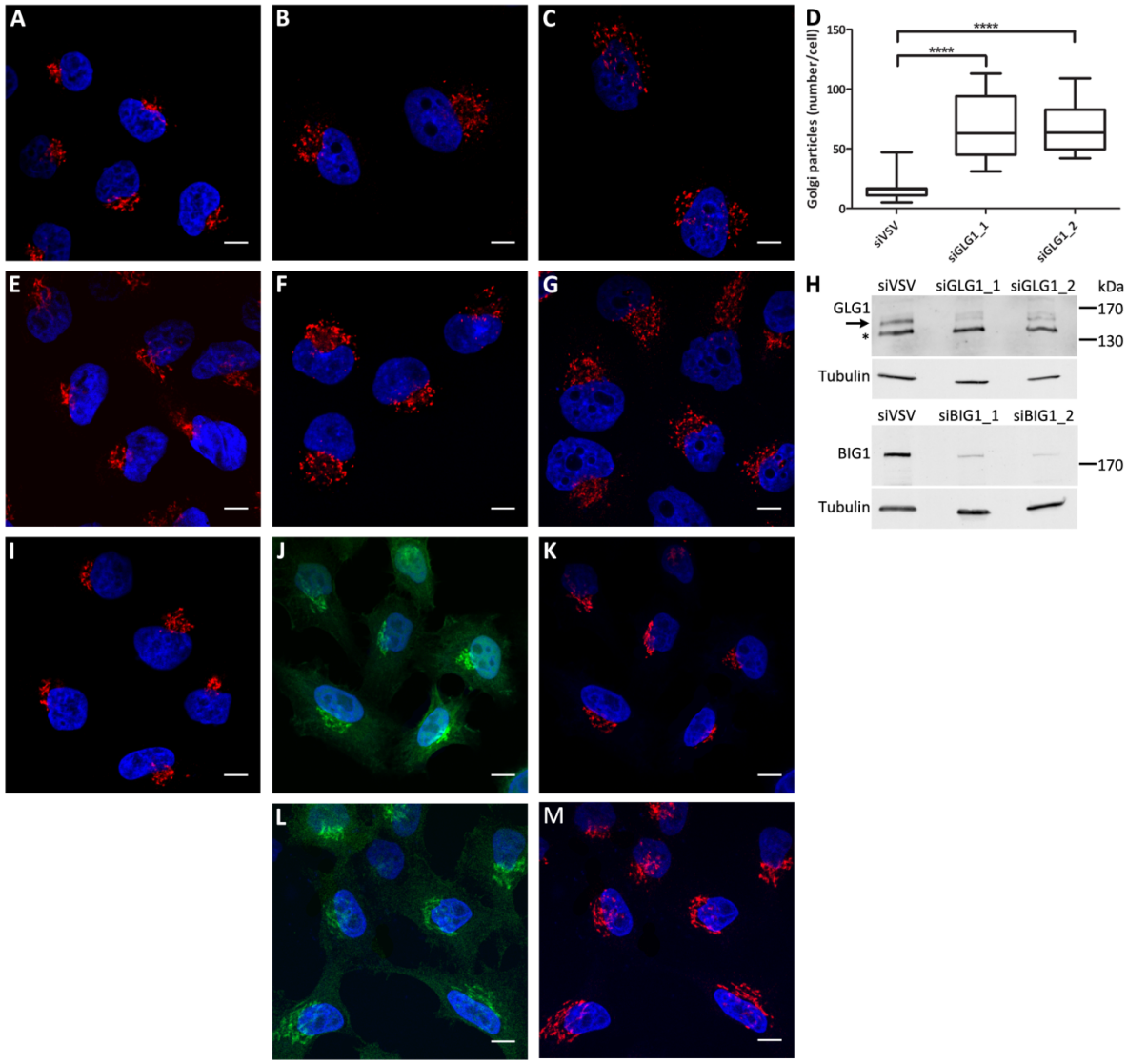
A
B
C
D
Golgi particles (number/cell)
150
100
50
0
****
****
siVSV
siGLG1_1
siGLG1_2
E
F
G
H
siVSV
siGLG1_1
siGLG1_2
kDa
GLG1
*
170
130
Tubulin
siVSV
siBIG1_1
siBIG1_2
BIG1
170
Tubulin
I
J
K
L
M

Figure 3.

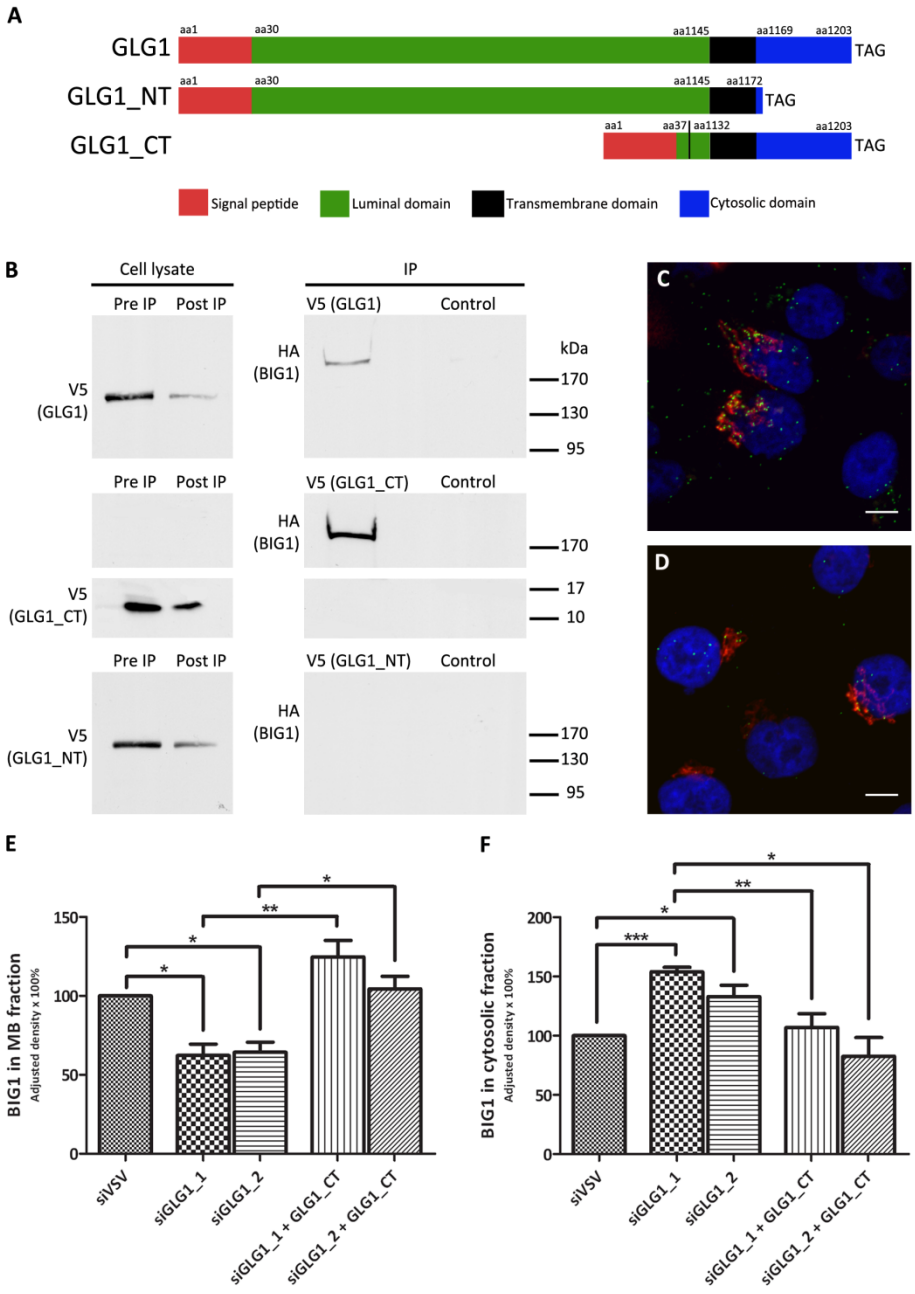
A
GLG1
GLG1_NT
GLG1_CT
aa1
aa30
aa1145
aa1169
aa1203
aa1172
aa37
aa1132
TAG
Signal peptide
Luminal domain
Transmembrane domain
Cytosolic domain
B
Cell lysate
IP
Pre IP
Post IP
V5 (GLG1)
Control
HA (BIG1)
kDa
170
130
95
V5 (GLG1_CT)
17
10
V5 (GLG1_NT)
C
D
E
BIG1 in MB fraction
Adjusted density x 100%
siVSV
siGLG1_1
siGLG1_2
siGLG1_1 + GLG1_CT
siGLG1_2 + GLG1_CT
F
BIG1 in cytosolic fraction

Figure 4.

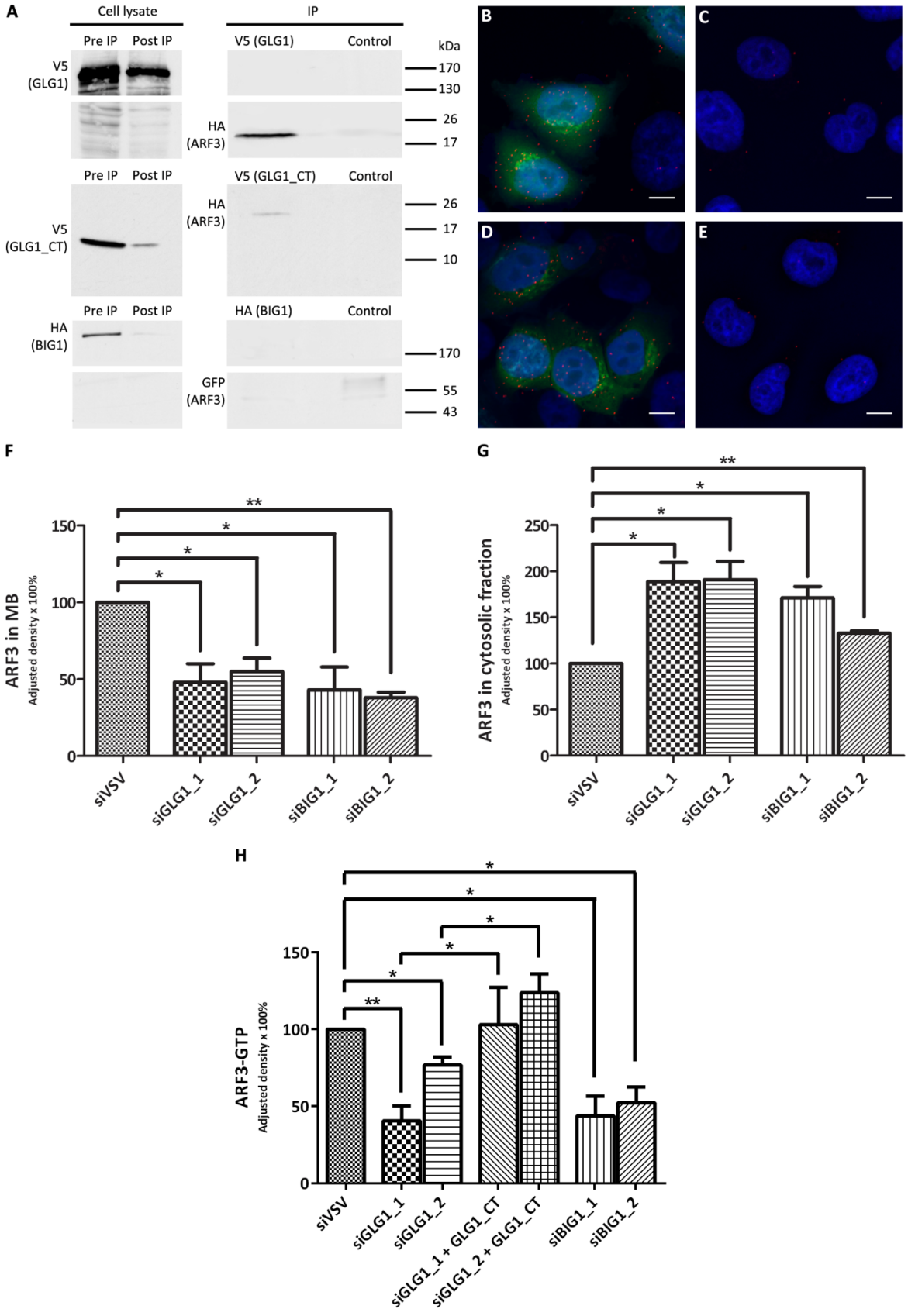
A
Cell lysate
IP
Pre IP
Post IP
V5 (GLG1)
Control
kDa
170
130
HA (ARF3)
26
17
V5 (GLG1_CT)
10
HA (BIG1)
GFP (ARF3)
55
43
B
C
D
E
F
ARF3 in MB
Adjusted density x 100%
siVSV
siGLG1_1
siGLG1_2
siBIG1_1
siBIG1_2
G
ARF3 in cytosolic fraction
H
ARF3-GTP
siGLG1_1 + GLG1_CT
siGLG1_2 + GLG1_CT

Figure 5.

A
40°C, overnight
B
20°C, 2 h
C
31.5°C, 1 h 20
ts045VSV-G-GFP
KDEL
merge
TGN46
ALL STAR
siGLG1_1
siGLG1_2
D
Secreted HRP activity (A.U.)
HeLa
HepG2
ns
siVSV
siGLG1_pool
E
MMP-9 activity
in cell culture medium
Adjusted density x 100%
*
**

Supplemental Figure 1.

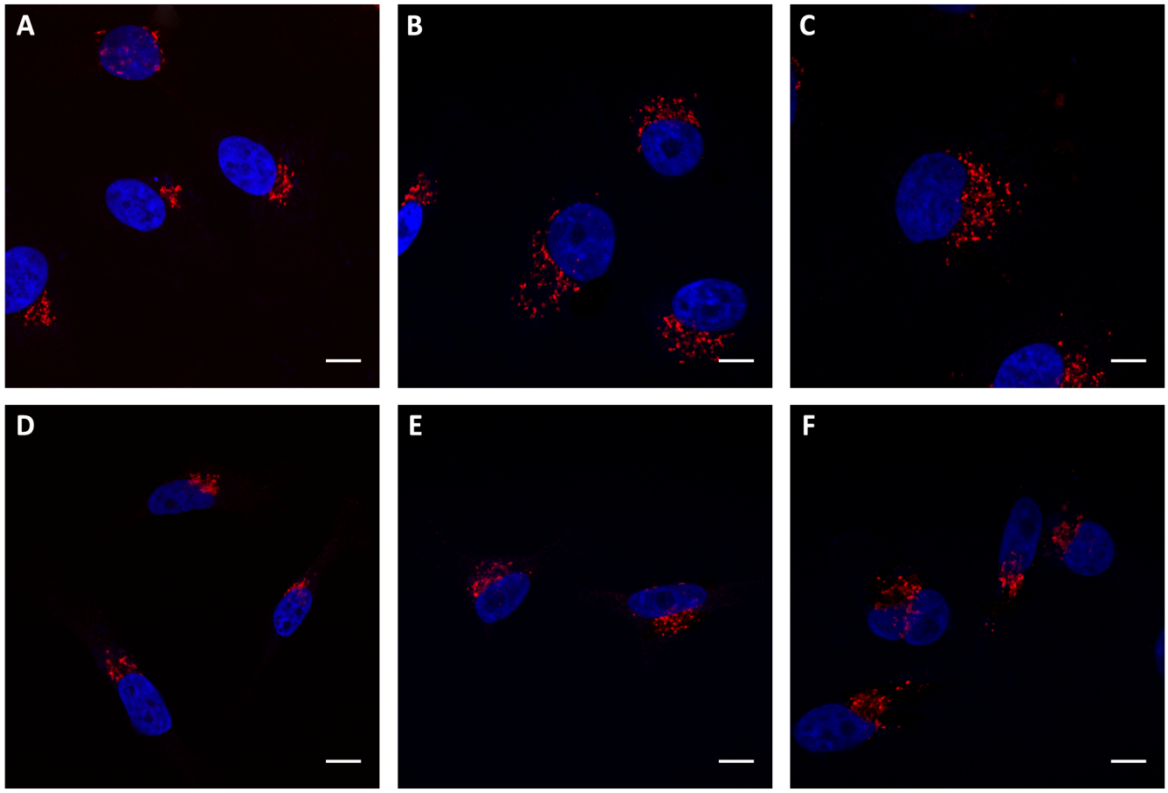

Supplemental Figure 2.

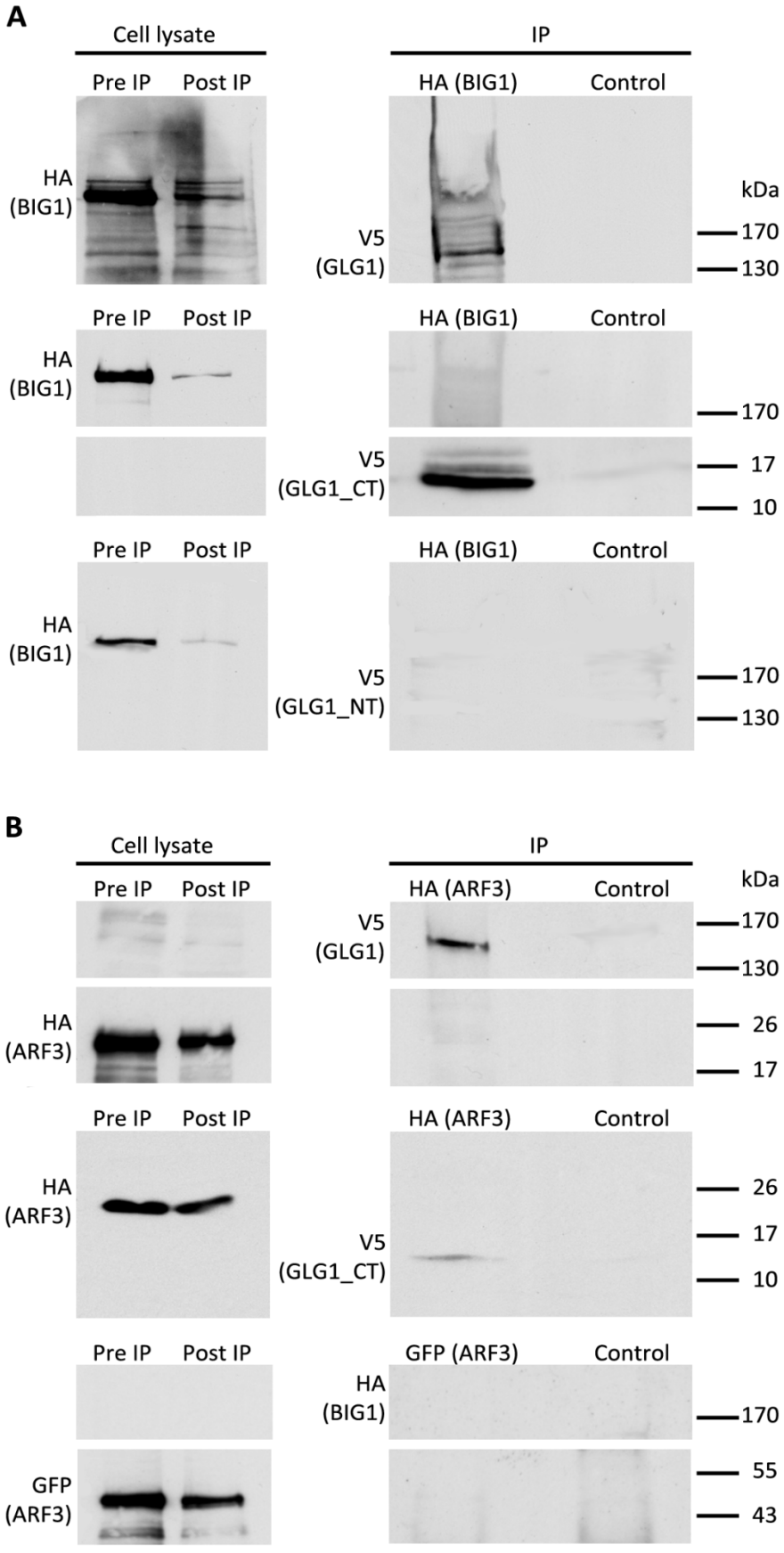

Supplemental Figure 3.

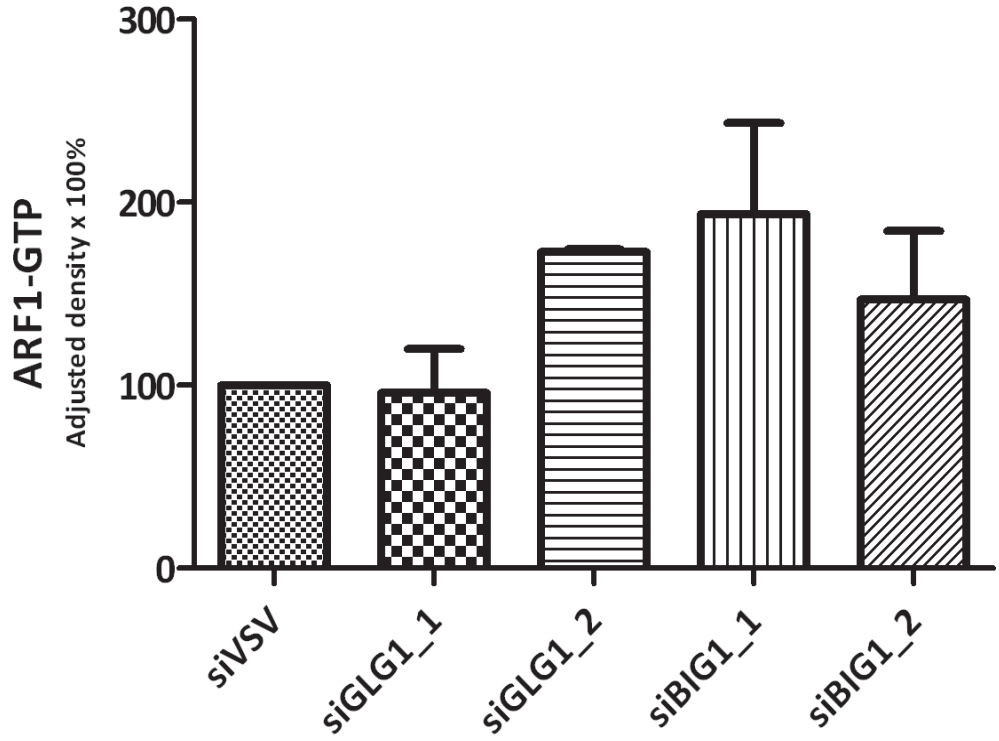

Supplemental Figure 4.

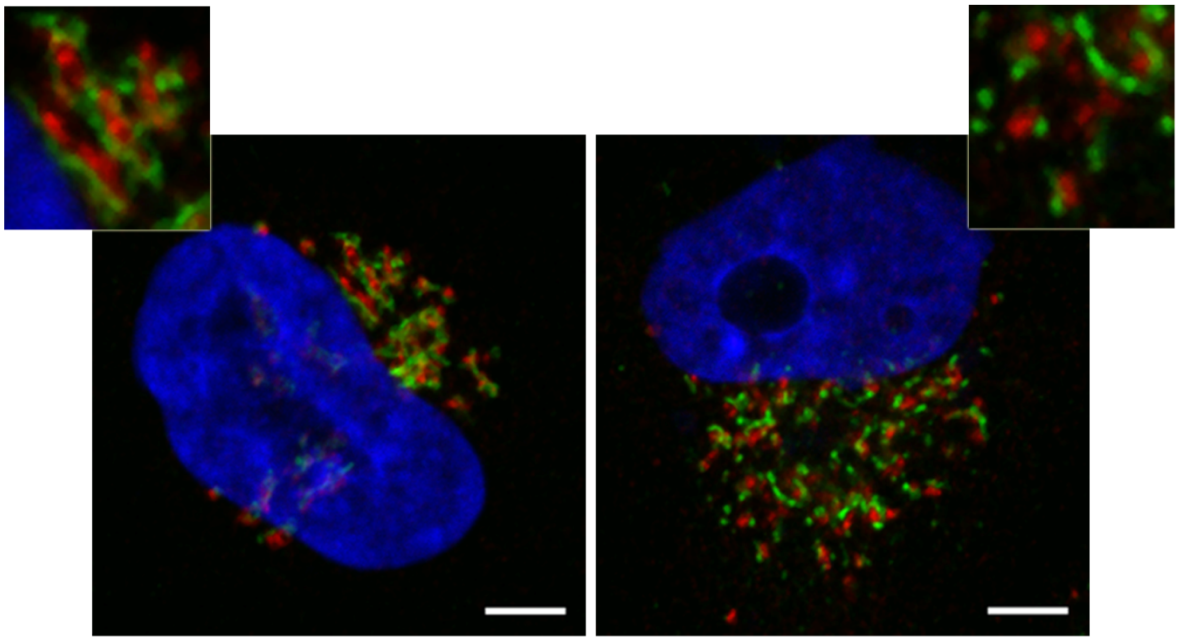

Supplemental Figure 5.

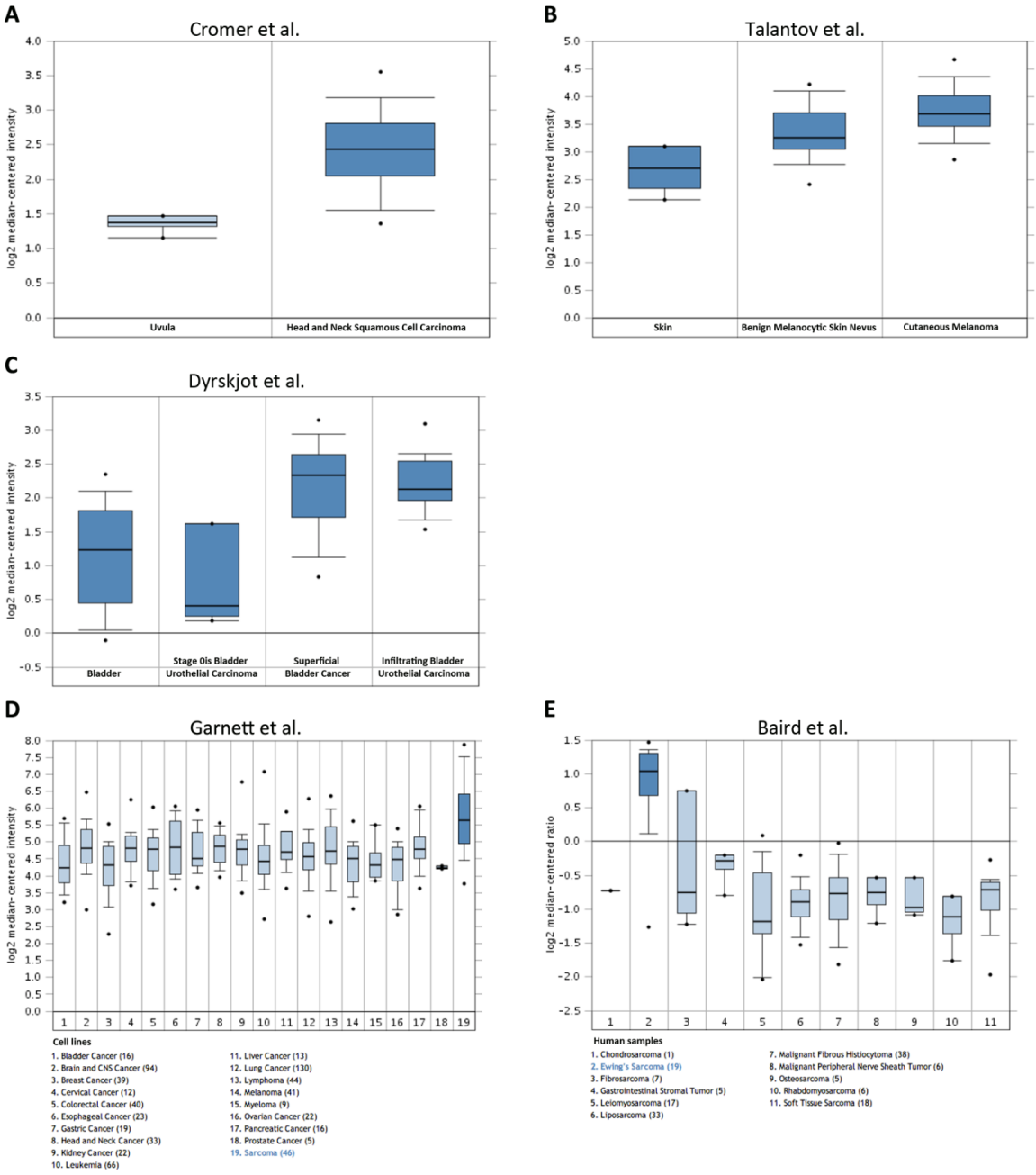

EPILOGUE

Mutations of oncogenes and tumor suppressor genes in tumor cells have long been viewed as the only cause of cancer initiation and progression, supporting reductionist cancer-cell- and genome-centered models. However, over the past decade, increasing interest for the stroma surrounding tumors emerged. Tumors behave like normal, complex organs that cannot survive and function appropriately on their own but need to rely on a supportive microenvironment. Whereas the dynamic interplay between epithelial cells of a healthy organ and the associated stroma maintains tissue homeostasis and physiological function, pathological crosstalk between tumor cells and their microenvironment sustains tumor growth, invasion and dissemination. Identifying and understanding the molecular mechanisms implicated in tumor-host interactions could help control tumor progression by developing new mechanism-based therapeutic approaches that take into account not only the tumor cells themselves but also their microenvironment.

Selective gene expression profiling of tumor-associated stroma is one approach to identify potential therapeutic targets within the stroma. Ideally, a valid stromal target should be specific for tumor-associated tissue and should not be expressed elsewhere in normal tissues to avoid undesired side effects. The accessibility of the target by therapeutic agents is also important. The first part of the present work proposes such a stromal target, POSTN, which is exclusively expressed in the stroma of breast and prostate cancer patients. In addition, POSTN is secreted, and thus easily accessible, and was recently found to be implicated in metastatic colonization, offering attractive therapeutic possibilities.

Previous studies on stromal reactions conducted in the laboratory have led us, for the second part of this thesis, to focus our attention on a somewhat neglected subject in the cancer-related field, namely membrane trafficking. Membrane trafficking and protein secretion are important for both normal cell physiology and oncogenesis by supporting intercellular communication. Altered trafficking and secretion of key molecules may help tumor cells proliferate and subvert their microenvironment to their own advantage. Identifying the molecules and mechanisms implicated in these alterations may improve our understanding of tumor-host interactions during tumorigenesis. In this work, GLG1 was shown to be implicated in membrane trafficking of tumor cells. Gene expression level analysis across publicly available datasets revealed elevated GLG1 expression in some

tumors including Ewing's sarcoma, reinforcing the notion that membrane trafficking-related proteins may be relevant for tumor progression.

Ultimately, the two projects described in this work, the identification of the molecular features of stromal reactions to tumor progression and an analysis of membrane trafficking, as a mechanism underlying intercellular interactions, represent two different approaches with a common purpose: to provide further insight into tumor-host interactions that may have therapeutic relevance.

REFERENCES

1. Weinberg, R.A., *Preface*, in *The biology of cancer*. 2007, Garland Science: New York. p. vii.
2. Hanahan, D. and R.A. Weinberg, *Hallmarks of cancer: the next generation.* Cell, 2011. **144**(5): p. 646-74.
3. Bacac, M. and I. Stamenkovic, *Metastatic cancer cell.* Annu Rev Pathol, 2008. **3**: p. 221-47.
4. Kalluri, R. and M. Zeisberg, *Fibroblasts in cancer.* Nat Rev Cancer, 2006. **6**(5): p. 392-401.
5. Bhowmick, N.A., E.G. Neilson, and H.L. Moses, *Stromal fibroblasts in cancer initiation and progression.* Nature, 2004. **432**(7015): p. 332-7.
6. Mueller, M.M. and N.E. Fusenig, *Friends or foes - bipolar effects of the tumour stroma in cancer.* Nat Rev Cancer, 2004. **4**(11): p. 839-49.
7. Elenbaas, B. and R.A. Weinberg, *Heterotypic signaling between epithelial tumor cells and fibroblasts in carcinoma formation.* Exp Cell Res, 2001. **264**(1): p. 169-84.
8. Fukino, K., et al., Genomic instability within tumor stroma and clinicopathological characteristics of sporadic primary invasive breast carcinoma. JAMA, 2007. **297**(19): p. 2103-11.
9. Pelham, R.J., et al., Identification of alterations in DNA copy number in host stromal cells during tumor progression. Proc Natl Acad Sci U S A, 2006. **103**(52): p. 19848-53.
10. Moinfar, F., et al., Concurrent and independent genetic alterations in the stromal and epithelial cells of mammary carcinoma: implications for tumorigenesis. Cancer Res, 2000. **60**(9): p. 2562-6.
11. Hu, M., et al., Distinct epigenetic changes in the stromal cells of breast cancers. Nat Genet, 2005. **37**(8): p. 899-905.
12. Finak, G., et al., Stromal gene expression predicts clinical outcome in breast cancer. Nat Med, 2008. **14**(5): p. 518-27.
13. Binkley, C.E., et al., The molecular basis of pancreatic fibrosis: common stromal gene expression in chronic pancreatitis and pancreatic adenocarcinoma. Pancreas, 2004. **29**(4): p. 254-63.
14. Ma, X.J., et al., Gene expression profiling of the tumor microenvironment during breast cancer progression. Breast Cancer Res, 2009. **11**(1): p. R7.
15. Bacac, M., et al., A mouse stromal response to tumor invasion predicts prostate and breast cancer patient survival. PLoS One, 2006. **1**: p. e32.
16. Mosesson, Y., G.B. Mills, and Y. Yarden, Derailed endocytosis: an emerging feature of cancer. Nat Rev Cancer, 2008. **8**(11): p. 835-50.
17. D'Souza-Schorey, C. and J.W. Clancy, Tumor-derived microvesicles: shedding light on novel microenvironment modulators and prospective cancer biomarkers. Genes Dev, 2012. **26**(12): p. 1287-99.
18. Muralidharan-Chari, V., et al., Microvesicles: mediators of extracellular communication during cancer progression. J Cell Sci, 2010. **123**(Pt 10): p. 1603-11.

19. Lee, T.H., et al., Microvesicles as mediators of intercellular communication in cancer--the emerging science of cellular 'debris'. Semin Immunopathol, 2011. **33**(5): p. 455-67.
20. Bobrie, A., et al., Exosome secretion: molecular mechanisms and roles in immune responses. Traffic, 2011. **12**(12): p. 1659-68.
21. Mathivanan, S., H. Ji, and R.J. Simpson, Exosomes: extracellular organelles important in intercellular communication. J Proteomics, 2010. **73**(10): p. 1907-20.
22. Dombkowski, A.A., D. Cukovic, and R.F. Novak, Secretome analysis of microarray data reveals extracellular events associated with proliferative potential in a cell line model of breast disease. Cancer Lett, 2006. **241**(1): p. 49-58.
23. Shi, Y., et al., Quantitative proteomes and in vivo secretomes of progressive and regressive UV-induced fibrosarcoma tumor cells: mimicking tumor microenvironment using a dermis-based cell-trapped system linked to tissue chamber. Proteomics, 2007. **7**(24): p. 4589-600.
24. Xue, H., B. Lu, and M. Lai, The cancer secretome: a reservoir of biomarkers. J Transl Med, 2008. **6**: p. 52.
25. Dvorak, H.F., Tumors: wounds that do not heal. Similarities between tumor stroma generation and wound healing. N Engl J Med, 1986. **315**(26): p. 1650-9.
26. Liotta, L.A. and E.C. Kohn, The microenvironment of the tumour-host interface. Nature, 2001. **411**(6835): p. 375-9.
27. De Wever, O. and M. Mareel, Role of tissue stroma in cancer cell invasion. J Pathol, 2003. **200**(4): p. 429-47.
28. Kuperwasser, C., et al., Reconstruction of functionally normal and malignant human breast tissues in mice. Proc Natl Acad Sci U S A, 2004. **101**(14): p. 4966-71.
29. Olumi, A.F., et al., Carcinoma-associated fibroblasts direct tumor progression of initiated human prostatic epithelium. Cancer Res, 1999. **59**(19): p. 5002-11.
30. Orimo, A., et al., Stromal fibroblasts present in invasive human breast carcinomas promote tumor growth and angiogenesis through elevated SDF-1/CXCL12 secretion. Cell, 2005. **121**(3): p. 335-48.
31. Joyce, J.A., Therapeutic targeting of the tumor microenvironment. Cancer Cell, 2005. **7**(6): p. 513-20.
32. Farmer, P., et al., A stroma-related gene signature predicts resistance to neoadjuvant chemotherapy in breast cancer. Nat Med, 2009. **15**(1): p. 68-74.
33. Sangle, N.A. and S.L. Perkins, Core-binding factor acute myeloid leukemia. Arch Pathol Lab Med, 2011. **135**(11): p. 1504-9.
34. Scheitz, C.J., et al., Defining a tissue stem cell-driven Runx1/Stat3 signalling axis in epithelial cancer. EMBO J, 2012. **31**(21): p. 4124-39.
35. Pradhan, M.P., N.K. Prasad, and M.J. Palakal, A systems biology approach to the global analysis of transcription factors in colorectal cancer. BMC Cancer, 2012. **12**(1): p. 331.
36. Fijneman, R.J., et al., Runx1 is a tumor suppressor gene in the mouse gastrointestinal tract. Cancer Sci, 2012. **103**(3): p. 593-9.

37. Wang, L., J.S. Brugge, and K.A. Janes, Intersection of FOXO- and RUNX1-mediated gene expression programs in single breast epithelial cells during morphogenesis and tumor progression. Proc Natl Acad Sci U S A, 2011. **108**(40): p. E803-12.

38. Banerji, S., et al., Sequence analysis of mutations and translocations across breast cancer subtypes. Nature, 2012. **486**(7403): p. 405-9.

39. Hoi, C.S., et al., Runx1 directly promotes proliferation of hair follicle stem cells and epithelial tumor formation in mouse skin. Mol Cell Biol, 2010. **30**(10): p. 2518-36.

40. Scheitz, C.J. and T. Tumbar, New insights into the role of Runx1 in epithelial stem cell biology and pathology. J Cell Biochem, 2012.

41. Planaguma, J., et al., Matrix metalloproteinase-2 and matrix metalloproteinase-9 codistribute with transcription factors RUNX1/AML1 and ETV5/ERM at the invasive front of endometrial and ovarian carcinoma. Hum Pathol, 2011. **42**(1): p. 57-67.

42. Mangan, J.K. and N.A. Speck, RUNX1 mutations in clonal myeloid disorders: from conventional cytogenetics to next generation sequencing, a story 40 years in the making. Crit Rev Oncog, 2011. **16**(1-2): p. 77-91.

43. Baril, P., et al., Periostin promotes invasiveness and resistance of pancreatic cancer cells to hypoxia-induced cell death: role of the beta4 integrin and the PI3k pathway. Oncogene, 2007. **26**(14): p. 2082-94.

44. Gillan, L., et al., Periostin secreted by epithelial ovarian carcinoma is a ligand for alpha(V)beta(3) and alpha(V)beta(5) integrins and promotes cell motility. Cancer Res, 2002. **62**(18): p. 5358-64.

45. Bao, S., et al., Periostin potently promotes metastatic growth of colon cancer by augmenting cell survival via the Akt/PKB pathway. Cancer Cell, 2004. **5**(4): p. 329-39.

46. Ismail, R.S., et al., Differential gene expression between normal and tumor-derived ovarian epithelial cells. Cancer Res, 2000. **60**(23): p. 6744-9.

47. Shao, R., et al., Acquired expression of periostin by human breast cancers promotes tumor angiogenesis through up-regulation of vascular endothelial growth factor receptor 2 expression. Mol Cell Biol, 2004. **24**(9): p. 3992-4003.

48. Yoshioka, N., et al., Suppression of anchorage-independent growth of human cancer cell lines by the TRIF52/periostin/OSF-2 gene. Exp Cell Res, 2002. **279**(1): p. 91-9.

49. Tilman, G., et al., Human periostin gene expression in normal tissues, tumors and melanoma: evidences for periostin production by both stromal and melanoma cells. Mol Cancer, 2007. **6**: p. 80.

50. Erkan, M., et al., Periostin creates a tumor-supportive microenvironment in the pancreas by sustaining fibrogenic stellate cell activity. Gastroenterology, 2007. **132**(4): p. 1447-64.

51. Malanchi, I., et al., Interactions between cancer stem cells and their niche govern metastatic colonization. Nature, 2012. **481**(7379): p. 85-9.

52. Bacac, M., et al., Securin and separase modulate membrane traffic by affecting endosomal acidification. Traffic, 2011. **12**(5): p. 615-26.

53. Gonatas, J.O., et al., MG-160. A novel sialoglycoprotein of the medial cisternae of the Golgi apparatus [published eeratum appears in J Biol Chem 1989 Mar 5;264(7):4264]. J Biol Chem, 1989. **264**(1): p. 646-53.

54. Gonatas, J.O., et al., MG-160, a membrane sialoglycoprotein of the medial cisternae of the rat Golgi apparatus, binds basic fibroblast growth factor and exhibits a high level of sequence identity to a chicken fibroblast growth factor receptor. J Cell Sci, 1995. **108 (Pt 2)**: p. 457-67.

55. Steegmaier, M., et al., The E-selectin-ligand ESL-1 is a variant of a receptor for fibroblast growth factor. Nature, 1995. **373**(6515): p. 615-20.

56. Levinovitz, A., et al., Identification of a glycoprotein ligand for E-selectin on mouse myeloid cells. J Cell Biol, 1993. **121**(2): p. 449-59.

57. Burrus, L.W., et al., Identification of a cysteine-rich receptor for fibroblast growth factors. Mol Cell Biol, 1992. **12**(12): p. 5600-9.

58. Zuber, M.E., et al., Cysteine-rich FGF receptor regulates intracellular FGF-1 and FGF-2 levels. J Cell Physiol, 1997. **170**(3): p. 217-27.

59. Kohl, R., et al., Cysteine-rich fibroblast growth factor receptor alters secretion and intracellular routing of fibroblast growth factor 3. J Biol Chem, 2000. **275**(21): p. 15741-8.

60. Antoine, M., et al., Secreted cysteine-rich FGF receptor derives from posttranslational processing by furin-like prohormone convertases. Biochem Biophys Res Commun, 2009. **382**(2): p. 359-64.

61. Olofsson, A., et al., Latent transforming growth factor-beta complex in Chinese hamster ovary cells contains the multifunctional cysteine-rich fibroblast growth factor receptor, also termed E-selectin-ligand or MG-160. Biochem J, 1997. **324 (Pt 2)**: p. 427-34.

62. Yang, T., et al., E-selectin ligand-1 regulates growth plate homeostasis in mice by inhibiting the intracellular processing and secretion of mature TGF-beta. J Clin Invest, 2010. **120**(7): p. 2474-85.

63. Yamaguchi, F., et al., Identification of MG-160, a FGF binding medial Golgi sialoglycoprotein, in brain tumors: an index of malignancy in astrocytomas. Int J Oncol, 2003. **22**(5): p. 1045-9.

64. Crnogorac-Jurcevic, T., et al., Gene expression profiles of pancreatic cancer and stromal desmoplasia. Oncogene, 2001. **20**(50): p. 7437-46.

65. Antoine, M., et al., Expression of E-selectin ligand-1 (CFR/ESL-1) on hepatic stellate cells: implications for leukocyte extravasation and liver metastasis. Oncol Rep, 2009. **21**(2): p. 357-62.

66. Dimitroff, C.J., et al., Identification of leukocyte E-selectin ligands, P-selectin glycoprotein ligand-1 and E-selectin ligand-1, on human metastatic prostate tumor cells. Cancer Res, 2005. **65**(13): p. 5750-60.

67. Wild, M.K., et al., Affinity, kinetics, and thermodynamics of E-selectin binding to E-selectin ligand-1. J Biol Chem, 2001. **276**(34): p. 31602-12.

68. Bard, F. and V. Malhotra, The formation of TGN-to-plasma-membrane transport carriers. Annu Rev Cell Dev Biol, 2006. **22**: p. 439-55.

69. Wilson, C., et al., The Golgi apparatus: an organelle with multiple complex functions. Biochem J, 2011. **433**(1): p. 1-9.

70. Donaldson, J.G. and C.L. Jackson, ARF family G proteins and their regulators: roles in membrane transport, development and disease. Nat Rev Mol Cell Biol, 2011. **12**(6): p. 362-75.
71. D'Souza-Schorey, C. and P. Chavrier, ARF proteins: roles in membrane traffic and beyond. Nat Rev Mol Cell Biol, 2006. **7**(5): p. 347-58.
72. Boal, F. and D.J. Stephens, Specific functions of BIG1 and BIG2 in endomembrane organization. PLoS One, 2010. **5**(3): p. e9898.
73. Volpicelli-Daley, L.A., et al., Isoform-selective effects of the depletion of ADP-ribosylation factors 1-5 on membrane traffic. Mol Biol Cell, 2005. **16**(10): p. 4495-508.
74. Manolea, F., et al., Arf3 is activated uniquely at the trans-Golgi network by brefeldin A-inhibited guanine nucleotide exchange factors. Mol Biol Cell, 2010. **21**(11): p. 1836-49.
75. Kahn, R.A., Toward a model for Arf GTPases as regulators of traffic at the Golgi. FEBS Lett, 2009. **583**(23): p. 3872-9.
76. Jain, S., et al., Arf4 determines dentate gyrus-mediated pattern separation by regulating dendritic spine development. PLoS One, 2012. **7**(9): p. e46340.
77. Suzuki, T., et al., Crucial role of the small GTPase ARF6 in hepatic cord formation during liver development. Mol Cell Biol, 2006. **26**(16): p. 6149-56.
78. Schrick, J.J., et al., ADP-ribosylation factor-like 3 is involved in kidney and photoreceptor development. Am J Pathol, 2006. **168**(4): p. 1288-98.
79. Sheen, V.L., et al., Mutations in ARFGEF2 implicate vesicle trafficking in neural progenitor proliferation and migration in the human cerebral cortex. Nat Genet, 2004. **36**(1): p. 69-76.
80. Ferland, R.J., et al., Disruption of neural progenitors along the ventricular and subventricular zones in periventricular heterotopia. Hum Mol Genet, 2009. **18**(3): p. 497-516.
81. Shoubridge, C., et al., Mutations in the guanine nucleotide exchange factor gene IQSEC2 cause nonsyndromic intellectual disability. Nat Genet, 2010. **42**(6): p. 486-8.
82. Scholz, R., et al., AMPA receptor signaling through BRAG2 and Arf6 critical for long-term synaptic depression. Neuron, 2010. **66**(5): p. 768-80.
83. Parachoniak, C.A. and M. Park, Dynamics of receptor trafficking in tumorigenicity. Trends Cell Biol, 2012. **22**(5): p. 231-40.
84. Hood, J.L., et al., Paracrine induction of endothelium by tumor exosomes. Lab Invest, 2009. **89**(11): p. 1317-28.
85. Peinado, H., et al., Melanoma exosomes educate bone marrow progenitor cells toward a pro-metastatic phenotype through MET. Nat Med, 2012. **18**(6): p. 883-91.
86. Hood, J.L., R.S. San, and S.A. Wickline, Exosomes released by melanoma cells prepare sentinel lymph nodes for tumor metastasis. Cancer Res, 2011. **71**(11): p. 3792-801.
87. Baird, K., et al., Gene expression profiling of human sarcomas: insights into sarcoma biology. Cancer Res, 2005. **65**(20): p. 9226-35.
88. Kauer, M., et al., A molecular function map of Ewing's sarcoma. PLoS One, 2009. **4**(4): p. e5415.

89. Schaefer, K.L., et al., Microarray analysis of Ewing's sarcoma family of tumours reveals characteristic gene expression signatures associated with metastasis and resistance to chemotherapy. Eur J Cancer, 2008. **44**(5): p. 699-709.

90. Maherali, N. and K. Hochedlinger, Guidelines and techniques for the generation of induced pluripotent stem cells. Cell Stem Cell, 2008. **3**(6): p. 595-605.